2022

DISTRIBUTION NETWORK OPERATION WITH SOLAR PHOTOVOLTAIC AND ENERGY STORAGE TECHNOLOGY

Mohammad Ramin Feizi
faizi.m.r@gmail.com

DISTRIBUTION NETWORK OPERATION WITH SOLAR PHOTOVOLTAIC AND ENERGY STORAGE TECHNOLOGY

Approved by:

Dr. Mohammad E. Khodayar
Electrical and Computer Engineering
Dissertation Committee Chairperson

Dr. Jianhui Wang
Electrical and Computer Engineering

Dr. Behrouz Peikari
Electrical and Computer Engineering

Dr. Khaled Abdelghany
Civil Engineering

Dr. Eli Olinick
Engineering Management, Information and System

DISTRIBUTION NETWORK OPERATION WITH SOLAR PHOTOVOLTAIC AND ENERGY STORAGE TECHNOLOGY

A Dissertation Presented to the Graduate Faculty of the

Lyle School of Engineering

Southern Methodist University

in

Partial Fulfillment of the Requirements

for the degree of

Doctor of Philosophy

with a

Major in Electrical Engineering

by

Mohammad Ramin Feizi

M.S., Electrical Engineering, University of Kurdistan
B.S., Electrical Engineering, Sahand University of Technology

December 17, 2022

ACKNOWLEDGMENTS

I dedicate my sincerest gratitude to my academic advisor, Prof. Mohammad Khodayar, for his patience and guidance in my Ph.D. career. This dissertaion would not have been complete without his invaluable wisdom, encouragement and constructive advice. I always feel privileged and honored to work with him and advance my career. Appreciation further extends to the respected advisory committee memeber, Prof. Behrouz Peikari, Prof. Jianhui Wang, Prof. Eli Olinick and Prof. Khaled Abdelghany, who have provided suggestions of value and endless support.

During my Ph.D. studies, I was fortunate to work with wonderful friends who support me on many occasions. I would like to acknowledge the support from Dr. Saeed Manshadi, Dr. Ali Vafamehr, Dr. Shengfei Yin, Dr. Bardia Heidari and Dr. Ying Zhang for their genuine help. Furthermore, my fellow friends, Tau Wu, Bin Huang, Seyed Saeed Fazlhashemmi, Abduraheem Alobaidi, You Lin, Yanling Lin and Anping Zhou have my gratitude for their company, friendship and helpful discussions of research.

Last but not least, I dedicate my greatest gratitude to my mother Khadijeh Faramarzpour, in loving memories of my father Abdollah Feizi, and my siblings, Adel, Erfan, Fatemeh Fanoos and Shamsollah.

Feizi, Mohammad Ramin M.S., Electrical Engineering, University of Kurdistan, 10/2014
B.S., Electrical Engineering, Sahand University of Technology,10/2012

Distribution Network Operation with Solar Photovoltaic and Energy Storage Technology

Advisor: Dr. Mohammad E. Khodayar

Doctor of Philosophy conferred December 17, 2022

Dissertation completed August 9, 2022

Among distributed energy resources, solar photovoltaic (PV) generation has the largest penetration in the distribution networks. Serving electric vehicles (EV) with renewable resource generation would further reduce the carbon footprint of the energy supply chain for electric vehicles. However, the integration of solar PV and EVs in the unbalanced distribution network introduces several challenges including voltage fluctuations, voltage imbalances, reverse power flow, and protection devices' malfunctions. The uncertainties associated with solar PV integration and electric vehicles operation require significant effort to develop accurate optimization methodologies in the unbalanced distribution systems operation. In this thesis, in order to cope with the uncertainties, we first developed a two-stage optimization problem, to identify the feasible dispatch margins of photovoltaic generation considering the distribution network operation constraints. The dispatch margins of photovoltaic generation are quantified considering the worst-case realization of demand in the distribution network. The linear and the second-order cone mathematical problem formulation is procured to solve the optimal power flow problem. Second, a data-driven distributionally robust optimization framework is proposed for the operation of the unbalanced distribution network considering the uncertainties associated with the interconnected EV fleets and solar PV generation, and the proposed framework leverages the column-and-constraint generation approach. Moreover, to minimize the operation cost and improve the ramping flexibility, a continuous-time optimization problem, is developed and reformulated to a linear programming problem using Bernstein polynomials. Here, a generalized exact linear reformulation of the data-driven distributionally

robust optimization is used to capture the worst-case probability distribution of the net demand uncertainties. Furthermore, in this thesis, an interconnection of multi microgrids (MGs) technology is considered a promising solution to handle the variability of the distributed renewable energy resources and improve the energy resilience in the distribution network. The coordination among the microgrids in the distribution network could improve the operation cost, reliability, and security of the distribution network. Therefore, an adaptive robust distributed optimization framework is developed for the operation of a distribution network with interconnected microgrids considering the uncertainties in the demand and solar PV generation.

TABLE OF CONTENTS

LIST OF FIGURES

LIST OF TABLES

Chapter 1

Introduction

1.1 Feasible dispatch limits of the PV generation with Uncertainties in PV, EV and demand

1.1.1 Motivations of research

Solar power generation is the fastest growing renewable resource which is expected to provide a quarter of global electricity needs and reduce the global CO_2 emission of the energy sector by 21% by 2050 [1]. Driven by regulatory policies, renewable portfolio standards, and federal tax credits, the capacity of solar power generation is increasing in the transmission and distribution sectors [2]. Solar power generation, the fastest growing technology among other renewable energy resources in the distribution networks, is expected to increase to 8.3 trillion kWh by 2050 worldwide as the manufacturing costs decrease. Such generation capacity will represent 70% of the total renewable generation and serves up to 16% of the electric demand worldwide [3].

Lowering the energy costs, reducing the carbon footprint of energy supply to electric vehicles (EVs), and mitigating the reliance on fossil fuel resources to generate the electricity required to charge EVs, are among the motivations to leverage PV generation for EV charging. The global deployment of EV technology has been growing rapidly in the last decade and the number of passenger EVs increased by 63% in 2018 compared to the previous year worldwide [4]. The increase in the installed capacity of PV generation as the power supply, and the growing market of EVs as electric loads with storage capability, introduce operational challenges to the power grid operators. Considering the uncertainties in the PV generation and EV interconnections in the distribution networks, managing the demand and supply to ensure reliability and network security is a challenging task. The increase in EV sales and improvements to the EV battery capacity will reshape the electricity demand in the

distribution networks. The changes in the distribution network demand profile stemming from integrating fast charging and commercial vehicle charging stations, and residential EV charging hubs introduce operational challenges in network security and reliability. The increase in the demand as a result of charging EVs increases the network loss, deteriorates the power quality with considerable voltage drops, and increases the stress on power distribution assets. In this context, effective coordination among the EV operators and other distributed energy resources would address the challenges imposed by EVs in the distribution networks.

Among distributed energy resources, solar PV generation has the largest penetration in the distribution networks. Rooftop solar PV panels and utility-scale solar plants improve the reliability and economics of energy supply as such energy resources could be placed close to the consumers in the distribution networks. Serving the EVs with solar PV generation would further reduce the carbon footprint of the energy supply chain for EVs. The integration of solar PV in the distribution network introduces several challenges including voltage fluctuations, voltage imbalances, reverse power flow, and protection devices' malfunctions. Coordinating the PV generation with EV charging/discharging could mitigate the adverse effects of PV generation in the distribution networks.

Given the limitations of the current assets in serving the growing EV demand and the current investment portfolio on solar PV generation resources in distribution networks, quantifying the dispatchable limits of PV generation is crucial to maintain the security of the distribution network. Quantifying the dispatchable PV generation enables the distribution system operator to gain an understanding of the feasible dispatch limits of this generation resource to avoid voltage violations and demand curtailments. The uncertainties associated with the EV integration, including the arrival and departure times and the stochasticity in energy and power capacity limits, are represented as the uncertainties in demand and available energy storage capacity in the distribution network. Motivated by such notions, this research is focused on determining the feasible dispatch limits of PV generation with the uncertain interconnection of EVs, PVs and electricity demand in the distribution network.

1.1.2 Background and related works

Recent studies were focused on various approaches to enhance the capacity of solar photovoltaic (PV) generation in transmission and distribution networks [5–7]. In [5] the hosting capacity of rooftop PV generation is quantified using Monte Carlo simulation. The impacts of the number of PV installations and their power factors, the loading of the feeders and the conductor characteristics on the PV hosting capacity were investigated. A voltage profile design algorithm is proposed in [6] to handle the variation of the demand profile and improve the hosting capacity of the PV generation in the distribution feeders. In [7] a mixed-integer nonlinear programming (MINLP) problem is formulated to maximize the PV hosting capacity by controlling the voltage regulators, PV inverters, capacitor banks as well as controllable branch switches. The power flow problem is solved using the OpenDSS simulator and the formulated MINLP problem is solved using genetic algorithm. In [8] a Nomogram-based approach is proposed to quantify the hosting capacity of low voltage distribution systems and determine the connection criteria for PV generation units. The energy storage operation set points are determined to tackle the overvoltage challenges in the distribution network with high penetration of PV generation in [9]. The PV hosting capacity is increased in [10] by providing voltage droop control in active transformers. A Monte Carlo-based framework is proposed in [11] to quantify the hosting capacity of PV generation in distribution feeder and the sensitivity of PV hosting capacity to the circuit characteristics is evaluated. The expansion planning of static VAR compensators was proposed as a two-stage stochastic programming problem in [12] to increase the installed capacity of PV generation in distribution networks. Here, the Benders decomposition technique was used to solve the formulated problem. An integrated generation and transmission expansion planning framework is proposed in [13] to maximize the large-scale solar PV penetration and minimize the investment on the dispatchable generation units and transmission lines. The formulated problem is solved using a decomposition technique. In [14] voltage regulators and reactive power resources are managed to maximize the hosting capacity of PV generation in the distribution network. The proposed management scheme captures the uncertainties associated with EVs in the network. A multi-objective volt/VAR control approach was presented in [15] in which a scenario-based stochastic operation scheme was used to minimize

energy loss, voltage deviation, as well as total emission and energy costs. The uncertainty of renewable energy resources including solar PV generation was captured in [16] by formulating a two-stage robust optimization problem for the expansion planning of distributed generation (DG) in microgrids. The objective was to minimize the operation cost of microgrids considering the revenue for providing services to the demand entities.

The variability and uncertainty in PV generation introduce significant operation challenges including unacceptable voltage fluctuations, thermal limit violation of the distribution cables, reverse power flow, fault current measurement errors, and protection malfunctions [17]. If not addressed properly, such challenges would jeopardize the stability, reliability, and security of the distribution networks. Curtailing PV generation is considered as a practical solution to partially resolve these issues [18]; however, this solution will reduce the penetration level of PV generation and the corresponding economic and environmental benefits. Effective operation strategies such as coordinating the operation of renewable energy resources with dispatchable distributed generation technologies would improve the economic and sustainability of the distribution network operation and mitigate the adverse effects of variable and volatile PV generation in these networks [19]. A two-stage optimization model was proposed in [20], to determine the real and reactive power dispatch of controllable PV generation resources with PV power output uncertainties. A stochastic optimal voltage control strategy that captures the demand and PV generation uncertainties was proposed in [21]. A chance-constrained optimization problem was formulated to address the risk of overvoltage and voltage regulator runaway conditions in the distribution networks.

The impacts of PV generation capacity on the maximum voltage of the feeder and line loading along the feeder were investigated in [22] considering various demand profiles. Voltage regulation was used in [23] to improve the hosting capacity of PV generation in the distribution network. The harmonics injected by distributed generation and demand could reduce the hosting capacity of solar PV in the distribution network. Passive filters were designed in [24] to address this challenge, minimize the loss and maximize the power factor. An approach for allocating the series and shunt voltage source converters was introduced in [25] to improve the hosting capacity of PV generation in distribution networks. In [26] the hosting capacity of PV generation was improved by regulating the heating and cooling loads of the customers

in the distribution network. A distributed framework using Dantzig-Wolfe decomposition was proposed to address the consumers' privacy. An approach to determine the PV hosting capacity of the distribution network was proposed in [27] considering the smart inverter control strategies for the PV generation and battery energy storage. PV hosting capacity is evaluated using an interval overvoltage probability-based approach to decrease the risk associated with voltage violations in [28] while considering the uncertainty in PV generation and demand.

The integration of EV in distribution system operation was addressed in [29–33]. In [29], the chargeable region for EVs was quantified by formulating a two-stage robust optimization problem with the network's technical constraints. The impacts of charging EVs on the distribution network were evaluated in [31] considering the uncertainties in the EVs' ownership, rating, and duration of charging as well as the distributed generation (DG) penetration. As high penetration of EVs in the distribution network impacts the operational and technical measures including power loss, nodal voltage profile, and operation cost; ensuring the reliability and security of the distribution network imposes capacity limits on the EV demand served in the distribution network. An approach to allocating the EV parking lots and renewable energy resources was presented in [32] that minimizes the loss in the distribution network. Meta-heuristic approaches are used to minimize the loss in the distribution network. An online adaptive EV charging strategy was proposed in [33] to minimize the voltage imbalances and violations, transformer capacity violations, and EV charging cost, while considering the EV owners' convenience.

The integration of EV in the distribution network impacts the hosting capacity of PV generation. Earlier research addressed the interactions between EV and PV technologies in the three-phase balanced [34–38] and unbalanced [39–41] distribution networks. In [34] the authors proposed a conceptual framework to investigate the large-scale integration of solar PV generation and EVs, considering the coordination among these assets with multiple EV penetration levels. To reduce the solar PV curtailment and customer costs, [35] proposed an EV charging management scheme using an auction mechanism that captured the benefit and voluntary participation of each customer. A two-stage operation framework for the EV parking stations with rooftop solar PV generation was proposed in [36] to schedule the

EV charging in the day-ahead and real-time operations, considering the uncertainties in the available solar power generation and customer parking behavior. A decision-tree-based algorithm was proposed in [37] to decrease the peak demand in the residential distribution networks by coordinating the flexible EVs with vehicle-to-grid (V2G) capability with solar PV generation and battery energy storage. Fast response power electronic compensation at load side and feeder level, was used in [38] to control the voltage in the distribution network with variable PV generation and EV loads. A coordinated scheme for EV charging and PV generation was proposed in [39] to alleviate the flow imbalances among the phases in the distribution network. The coordinated operation of PVs and EVs in an unbalanced distribution network using energy storage was proposed in [40]. An online control approach was developed based on a rolling optimization framework to ensure the security of the distribution network by regulating the power output of PV generation units, EVs, and tap changer settings. In [41], differential evolution optimization was used to determine the PV and EV outputs that minimize the power loss and improve the voltage profile in an unbalanced distribution network. The hosting capacity assessment of combined PV-EV technology is carried out in [42] ignoring the uncertainty in EV interconnection.

While extensive research works exist on the operation of the distribution networks considering the uncertainties in the EV interconnections, EV owners' preferences, and solar PV generation; limited research efforts were made to determining the dispatch limits for PV generation in distribution networks considering the unbalanced EV interconnections and the corresponding uncertainties. Quantifying the dispatch limits for PV generation provides feasible operation regions that accommodate the PV generation in the distribution network. Such solutions would help the system operator to determine the upper and lower limits of the uncertainty sets associated with the PV generation that are required for solving the risk-based distribution network operation problems. In the bulk power network, quantifying do-not-exceed limits for renewable resources was proposed in [43–45]. In [43], a robust optimization problem was formulated to determine the dispatchability limits for a renewable resource. In [44] a data-driven algorithm was presented that aims to maximize the utilization of variable renewable generation by determining the do-not-exceed limits of this resource considering the operating points of the dispatchable resources.

1.2 Data-Driven Distributionally Robust Operation of the Distribution Network with High Penetration of PV and EV

The worldwide electric vehicle registration is increased by 41% in 2020 as the vehicle sales are decreased by 16% in 2020 due to the global pandemic [46]. As the EV sales grow, the share of gasoline vehicles' sales is estimated to decline from 94% in 2019 to 81% in 2050 [47]. Incentives for EVs including sales tax reductions and exemptions as well as subsidies for the charging assets are aimed to promote the transition toward sustainable mobility, reduce greenhouse gas generation, and improve local air quality in urban areas [48]. The increase in the number and capacity of EV interconnection will increase the EV charging demand in the distribution feeder. The EV charging load increases the residential demand peak and network loss and further increases the risk of overloading, voltage drops, and power quality degradation [49, 50]. Capacity expansions, installing energy storage, and regulating the EV charging profile are among the efforts to mitigate the adverse effects of large-scale integration of EVs in the distribution networks [51].

Solar photovoltaic (PV) generation is the prominent distributed renewable energy resource (DER) that could be installed close to the customers. The reduction in the capital cost through the project lifetime, the changes in state regulation and policies to promote PV technology (e.g., 100% renewable generation in California by 2045), and the tax incentives [47] are expected to further promote this technology and increase its installed capacity in the distribution networks. The growth in capacity of the uncertain and variable PV generation may lead to excessive voltage fluctuations, voltage violations, and unbalanced loading and increase the vulnerability of the distribution networks to overloading and protection malfunctions. The vehicle-to-grid (V2G) technology with considerable power injection capacity coupled with PV generation in the distribution feeders could further increase the probability of reverse power flow and voltage variations. Coordinating the charging and discharging schedule of EV clusters with DERs including PV generation and energy storage systems (ESS) could decrease the risk of such undesirable conditions. Providing services such as peak shaving, valley filling, reduction in load curtailment by EVs further improve the energy economics and reliability in the distribution networks [52], [53]. In [54], the coordination between EVs and DERs is formulated and solved by a differential evolution optimization algorithm to mitigate

the unbalance among phases, improve the voltage profile, and decrease the distribution system loss. In [55] a hybrid optimization is proposed to reduce the EV operation cost. The scheduling of EV charging stations is coordinated with PV and battery storage systems using the real-time empirical data.

The uncertainties associated with the operation and interconnection of EVs including the uncertainties in the daily energy consumption, arrival and departure times, maximum and minimum available energy, and the number of interconnected EVs, introduce challenges to the operation of distribution networks with EVs. Stochastic programming (SP) and robust optimization (RO) problem formulations are used in the literature to address the uncertainties associated with the integration of EVs. In [56] a two-stage SP problem is formulated to determine the location and capacity of public EV charging stations considering the uncertainties in EVs' arrival and departure times and their charging patterns, as well as the preferred walking distance to the charge station. The objective function is to maximize the availability and access of EVs to the charging stations. In [57] the capacity of EV chargers, solar PV panels, and battery energy storage in the EV charging station is determined considering the uncertainty associated with the EV mobility and charging demand, PV generation, and electricity price. The problem is formulated as a SP problem using scenarios. In [58], the dispatch of EV charging stations equipped with PV generation and energy storage systems is determined using a stochastic dynamic programming approach that captures the uncertainty in electricity price, PV output, as well as electricity tariffs. In [59] a RO problem is formulated to determine the charging and discharging schedule of EV aggregators, considering the uncertainty in the available energy of EVs that is affected by mobility patterns and driver behaviors. The objective is to minimize the operation cost of the system including the operation cost of EV aggregators. In [60], the energy cost and voltage deviation are minimized while capturing the uncertainty in charging power and energy capacity, and the volatility in real and reactive demand. A RO problem is formulated to determine the real and reactive power dispatch of EVs and Benders' decomposition technique is used to solve the problem.

While in the SP approach, the probability distribution functions of the uncertain parameters are known to generate scenarios, formulating a RO problem eliminates the need for this

assumption. In the RO problem, the uncertainty is defined as a set and the worst-case realization of uncertainty is considered. In most cases, the estimated probability distribution function for uncertain variables may not be accurate. Moreover, to accurately represent the uncertainties, a large number of scenarios is required which further increases the computation burden of solving the SP problems. Compared to the solution procured by SP, the worst-case realization of the uncertainty in the RO formulation provides a more conservative solution and by regulating the budget of uncertainty, the conservativeness of the solution is adjusted [61]. In [61, 62] a hybrid stochastic and robust optimization approach is proposed to reduce the computation burden of the SP problem by considering the uncertainty sets. Distributionally robust optimization (DRO) is introduced in [63–65] to capture the worst-case realization of the probability distribution of the uncertain variables. In [63], a decomposition framework is proposed to solve a two-stage data-driven transmission expansion planning problem. The L_1 norm is used to construct the ambiguity set using the empirical data, that represents the uncertainty in wind generation. In [64] a data-driven risk-averse stochastic unit commitment problem formulation is proposed where L_1 and L_∞ norms are used to construct the ambiguity set of probability distributions for wind generation. The formulated problem is solved using Bender's decomposition technique. In [65] a DRO framework for the unit commitment problem is proposed where the Wasserstein metric is used as a measure to construct the ambiguity set and the solution to the formulated problem is compared to that of SP and RO problems. In [66] a two-stage DRO problem with the Kullback-Divergence metric is presented for the planning of EV charging stations and renewable resources in the power network. Here, the location of the charging stations is determined in the first stage and the capacities of renewable generation and energy storage are optimized in the second stage.

1.3 Data-Driven Distributionally Robust Operation of Distribution Network with Ramping Flexibility

The environmental benefits of renewable generation technologies, the technological improvements, and the reduction in manufacturing costs have increased the interest in deploying these generation resources in bulk power and distribution networks. In 2020, 3% of the US

electricity generation was solar power generation, and this share is expected to increase to 14% and 20% by 2035 and 2050, respectively [67]. Among different solar generation technologies, the potential rooftop PV generation capacity could reach 1 TW with 8 billion square meters of rooftops in the United States [68]. The increased use of renewable energy resources in bulk power networks imposes operational challenges to maintain the generation and demand balance. Deploying flexible reserve, demand response practices, and demand curtailment are among the solutions to reduce the risk of generation scarcity and maintain network security. The advancement in monitoring and intelligent control strategies and the emerging business models for energy would evolve the bulk power system and distribution network operation paradigm. In the new paradigm, distribution system operators (DSOs) contribute to providing flexibility services to bulk power systems by managing the variability of the renewable and distributed energy resources and regulating the demand using dispatchable generation resources, including energy storage units [69]. The variable solar PV generation in the distribution network imposes operational challenges to the distribution network operation. Voltage fluctuations and violations, power quality degradation, reverse power flow, and protection malfunction is among the challenges introduced by large-scale integration of solar PV generation in distribution networks. To mitigate the demand and renewable generation curtailments while providing flexibility services to the bulk power network, DSOs handle the variability and uncertainty associated with the renewable generation and demand by leveraging flexible and dispatchable generation resources and the demand-side management.

Earlier research quantified the ramping flexibility of dispatchable generation resources to handle the variation in the demand and renewable resources in the bulk power networks [70]-[71]. In [70] and [72], the stochastic and deterministic sub-hourly operation of the bulk power network with high penetration of wind generation were proposed, respectively. In [70], the unit commitment problem is solved as a two-stage optimization problem using Benders decomposition. In [72], the feasible energy delivery of the generation units is quantified in the unit commitment problem and the resulting mixed-integer nonlinear optimization problem is transformed into a tractable mixed-integer linear programming problem. A continuous-time model for the generation ramping trajectory was proposed in [73] to reduce the error in estimating the ramping flexibility of generation resources. The proposed model leverages

Bernstein polynomial to represent the generation dispatch trajectory, and the proposed model is further used in [74] to capture the interactions between the electricity and natural gas networks. In [75], De Casteljau's algorithm is used to tighten the convex hull of Bezier curves that represent the generation and demand trajectories and improve the estimation of the flexibility provided by dispatchable generation resources. A continuous-time risk-based model is proposed in [71] to minimize the risk of sub-hourly wind curtailment in the operation scheduling horizon using scenarios. A two-stage stochastic continuous-time problem is formulated to minimize the operation cost and the probability of wind curtailment.

While earlier publications addressed the uncertainty in renewable generation using stochastic programming (SP) [76], the assumptions made on the probability of scenarios require a considerable number of historical data. The solution to the SP problem provides improved economic measures once an accurate probability distribution of uncertain variables is available. Power system operation problem is formulated as robust optimization (RO) problem once limited knowledge on characteristics of the uncertain variables is available. The solution to RO captures the worst-case realization of the uncertain variables with the cost of inefficiency in economic measures.

1.4 Adaptive Robust Distributed Operation of Distribution Network with Microgrids

The microgrid (MG) technology is a promising solution to handle the variability of the distributed renewable energy resources and improve the energy resilience in the distribution network [77]. The coordination among the microgrids could improve the operation cost and reliability and security of the distribution network [78]. Microgrids exchange energy with the main distribution network in grid-connected mode to reduce the operation cost, improve the voltage profile and reduce the network loss [79]. In order to serve the demand in contingencies, microgrids are operated in island mode to serve the load using local generation assets. In grid-connected mode, the coordination among the microgrids would improve the utilization of renewable energy resources by handling the uncertainty and variability and reducing the generation curtailment [80].

To handle the uncertainties in renewable generation and demand, distribution network and microgrid operation problems were formulated as stochastic programming and robust

optimization problems in [81–84]. In the stochastic programming problems, the uncertain variables are modeled using scenarios generated by the assumed probability distribution function. However, assuming a certain probability distribution function for the uncertain variables may not be practical due to limited information about the uncertain variables. Furthermore, to capture the probability distribution functions accurately, a large number of scenarios is required which will further increase the computation burden of stochastic programming problem solutions [85]. To address these challenges, the distribution network and microgrid operation problems are formulated as robust optimization problems, in which the uncertain variables are within a closed set. Solving the robust optimization problems provide the worst-case realization of the uncertain variables [86]. Ref. [81] formulated a two-stage robust optimization problem to determine the power flow of the soft-open points that minimizes the voltage deviation and network loss in the distribution network. The formulated problem was solved using the column-and-constraint generation algorithm (C&CG) and the power flow constraints are written as second-order cone constraints. In [82], a two-stage adaptive robust optimization problem is formulate and solved using C&CG approach to represent the collaborative operation of multiple interconnected MGs in residential area considering the worst-case realization of solar PV generation. The problem is formulated as a mixed-integer linear programming (MILP) problem, where, the first-stage problem determines the status of power exchange between MGs and the distribution system as well as charging and discharging states of the EVs, while the second-stage problem aims to minimize the network operation cost by regulating the power dispatch of distributed generation units, charging/discharging power of electric vehicles, and the power output of PV generation. In [83] a day-ahead adaptive robust economic dispatch model for the integrated energy systems was proposed. Here, the first-stage problem minimizes the startup and shut down costs of the gas turbines, and the second-stage problem minimizes the operation cost, considering the worst-case realization of the uncertainties in the net demand and outdoor temperature. In [87] an adaptive robust optimization problem is formulated to minimize the voltage deviation stemming from the fluctuation of considerable solar PV generation by regulating the fast response solar PV generation and slow response capacitor banks and on-load tap changers in multiple time-scales. The first-stage of the problem minimizes the

switching of distributed generation units, capacitor bank and tap adjustments, while the second-stage minimizes the voltage deviation and power loss considering the uncertainties in the solar PV power output and the real and reactive electricity demand. Here, the power flow constraints were written as second-order conic constraints. In [84] the energy management in multiple MGs was solved considering the cooperation among the main grid and MGs in a centralized manner. The proposed two-stage stochastic programming problem did not rely on the knowledge of the probability distribution of uncertain variables and used a sequential sampling algorithm that identified the required number of samples to characterize the uncertainty.

Distributed optimization approaches based on the augmented Lagrangian decomposition, have been widely used in power system operation and planning, where, each agent communicates with their neighbors by sharing the appropriate operation and control signals [88]. In [89], the radial distribution network is divided into several areas to minimize the power loss. The power flow constraints were modeled as second-order cone constraints and the formulated problem was solved using the alternating directional method of multipliers (ADMM). The convergence was accelerated by tuning the penalty parameters. In [90], the authors proposed a distributed transactive energy management structure based on ADMM for multi-MGs in distribution networks. The independent operation of MGs is coordinated using the distributed transactive signals. Each MG exchanges the electricity price with the distribution grid to minimize the operation cost. To handle the uncertainties of the renewable energy resources, the problem was solved as a robust optimization problem. In [91] the MGs are represented as independent energy hub entities. The objective function minimizes both the electricity and heating cost. In order to coordinate the operation of interconnected MGs and distribution network, a distributed robust framework based on the ADMM algorithm was developed.

In order to solve the energy management problem with nonlinear and nonconvex AC power flow constraints in distribution network, linear approximation and convex relaxation techniques were addressed in the literature [92–95]. The Linear programming (LP) [92], second order cone programming (SOCP) [93], and semi-definite programming (SDP) [96], are common mathematical models to solve the energy management problem in distribution network.

While LP formulation features a faster computation time, the approximation may lead to inaccurate results as the power loss is ignored and voltage imbalance is marginal. In order to capture the network loss and the unbalanced operation of the distribution network, SDP relaxation of the power flow constraints was proposed in the energy management problem in [95]. However, the SDP relaxation suffers from scalability and considerable solution time. In order to address these challenges, the energy management in distribution networks is formulated as SOCP problem in [94].

Chapter 2

Dispatchability Limits for PV Generation in Unbalanced Distribution Networks with EVs

The increase in the installed capacity of small-scale photovoltaic generation and the growing demand for electric vehicles introduce operational challenges for the unbalanced distribution networks. This chapter presents a two-stage optimization problem to determine the dispatchability limits of photovoltaic generation considering the electric vehicles' interconnection to ensure the security of the distribution network. The uncertainty associated with a) the state of charge at arrival and departure times; b) the energy and power capacity of electric vehicles; c) the maximum forecasted solar radiation and demand were considered. The proposed optimization problem is solved using the column-and-constraint-generation approach. A modified IEEE 13-bus test system is used to evaluate the effectiveness of the proposed framework. While such research works addressed the dispatchability limits of renewable energy resources, limited studies were performed on the dispatchability limits of renewable energy resources in the unbalanced distribution networks. The contributions of this chapter are as follows:

- Determining the upper and lower bounds for PV generation in the unbalanced distribution network.
- Capturing the uncertainty associated with a) the EV interconnection including the state of charge at arrival and departure times as well as the maximum energy and power capacity of EVs connected to the distribution network; b) maximum PV generation and; c) electricity demand in the distribution networks.
- The proposed formulated problem is solved using the column-and-constraint-generation (C& CG) approach to determine the worst-case realization of PV generation considering the determined upper and lower bounds.

The rest of this chapter is organized as follows; the problem formulation and solution methodology are presented in Section II. The numerical analysis and conclusion are presented in Sections III and IV respectively.

2.1 Problem Formulation

The problem formulation is shown in (2.1)-(2.33). The objective function is shown in (2.1). Here, $u_{v,t}^{\varphi}$ and $l_{v,t}^{\varphi}$ are the upper and lower bounds of PV generation respectively; and $V_{v,t}^{\varphi}$ is the auxiliary binary variable. The objective is to maximize the difference between the lower and upper bounds of PV generation while minimizing the violation in nodal real and reactive power represented by positive slack variables $s_{b,t}^{(.),\varphi}$. The constraints are shown in (2.2)-(2.33). The real and reactive power balance at each bus is shown in (2.2) and (2.3) respectively. Here, the variables are $PL_{l,t}^{\varphi}$ (the real power of the distribution line l on phase φ at time t), $P_{i,t}^{\varphi}$ (the real power of DG i), $P_{n,t}^{\varphi}$ (the real power of distribution feeder n), $P_{v,t}^{\varphi}$ (the real power of PV v), and $P_{e,t}^{\varphi}$ (the real power of EV cluster e). $P_{d,t}^{\varphi}$ is a parameter which the real power demand. The matrices AL, AI, AV, AE, AN, and AD are the line-bus, distributed generation-bus, PV generation-bus, EV cluster-bus, distribution feeder-bus, and demand-bus incidence matrices respectively. A similar constraint for reactive power $Q_{(.)}^{(.)}$ is shown in (2.3). The apparent power flow $\boldsymbol{SL}_{l,t}$ satisfies (2.4) and (2.5) in which, $\boldsymbol{U}_{k,t}$ is the vector of squared voltage on phases a, b and c of bus k ($V_{k,t}^{(.)}$) as shown in (2.38); p_l^{φ} is the availability of phase φ of the line l; $\boldsymbol{Z}_l$ is the element-wise product of matrix $\boldsymbol{A}$ and the branch impedance matrix $\boldsymbol{z}_l$ shown in (2.34)-(2.36) [10]. Here, $\boldsymbol{r}_l$ is the resistance and $\boldsymbol{x}_l$ is the inductive reactance matrix of branch l. The vector of apparent power $\boldsymbol{SL}_{l,t}$ is shown in (2.37). The real and reactive power flows of branch l satisfy (2.6)-(2.9) where $\boldsymbol{SL}_l^{\varphi,max}$ is the maximum complex power transmitted through the branch [97]. Similar constraints could be written for the distribution feeder. The real and reactive powers of DG are limited by the minimum and maximum limits as shown in (2.10) and (2.11) respectively. The real and reactive powers of feeder satisfy (2.12) and (2.13) to maintain the power factor more than a certain value ($\boldsymbol{PF}_n$). The real and reactive powers of PV generation are within the limits as shown in (2.14) and (2.15). Here, $P_v^{\varphi,max}$ is the maximum nominal capacity of the PV generation. The real power dispatch of PV generation is limited by the

available solar radiation as shown in (2.16). Here, A_v^{φ} is the area of PV generation unit for phase φ and $IR_{v,t}$ is solar radiation. The lower and upper bounds for PV generation satisfy (2.17)-(2.20). In order to determine the worst-case realization of PV generation, the dispatched PV generation is equal to the lower or upper bound as enforced by (2.21). Here $\sigma_{v,t}^{\varphi}$ is an auxiliary binary variable. The hourly real power dispatch of EV cluster e ($P_{e,t}^{\varphi}$) is formulated as (2.22) where $P_{e,t}^{\varphi,ch}$ and $P_{e,t}^{\varphi,dc}$ represent the charging and discharging powers of EV cluster e respectively. The charging and discharging powers for EV fleet e are limited by the charging and discharging power capacity ($P_e^{max,ch}$, $P_e^{max,dc}$) as shown in (2.23) and (2.24) respectively. Here $IC_{e,t}$ is a binary parameter representing the connection of EV cluster e to the distribution network. If the EV cluster e is connected to the distribution network $IC_{e,t} = 1$ and otherwise, $IC_{e,t} = 0$. The relationship between the available energy in EV cluster e and the hourly power dispatch is shown in (2.25)-(2.26) using big-M method. The energy in the EV cluster is limited by the minimum and maximum values as shown in (2.27)-(2.28). The available energy in EV cluster is enforced at arrival and departure times by (2.29)-(2.32). Here, $I_{e,t}^{ar}$ and $I_{e,t}^{dep}$ are binary parameters that represent the arrival and departure at time t respectively. The slack variables are positive as shown in (2.33).

$$\min_{u_{v,t}^{\phi}, l_{v,t}^{\phi}, V_{v,t}^{\phi}} \sum_m \sum_v \sum_\phi \sum_t (V_{v,t}^{\phi} - (u_{v,t}^{\phi} - l_{v,t}^{\phi})/P_v^{\phi,max}) + \max_{\sigma_{v,t}^{\phi}} \min_{s_{(.)}^{(.)}} \sum_m \sum_b \sum_\phi \sum_t (s_{b,t}^{1,\phi} + s_{b,t}^{2,\phi} + s_{b,t}^{3,\phi} + s_{b,t}^{4,\phi}) \quad (2.1)$$

s.t.

$$\sum_l AL_{l,b} PL_{l,t}^{\phi} + \sum_i AI_{i,b} P_{i,t}^{\phi} + \sum_v AV_{v,b} P_{v,t}^{\phi} + \sum_e AE_{e,b} P_{e,t}^{\phi,dc} + \sum_n AN_{n,b} P_{n,t}^{\phi} + s_{b,t}^{1,\phi} - s_{b,t}^{2,\phi} = \sum_d AD_{d,b} P_{d,t}^{\phi} \quad (2.2)$$

$$\sum_l AL_{l,b} QL_{l,t}^{\phi} + \sum_i AI_{i,b} Q_{i,t}^{\phi} + \sum_v AV_{v,b} Q_{v,t}^{\phi} + \sum_n AN_{n,b} Q_{n,t}^{\phi} + s_{b,t}^{3,\phi} - s_{b,t}^{4,\phi} = \sum_d AD_{d,b} Q_{d,t}^{\phi} \quad (2.3)$$

$$\boldsymbol{U}_{k,t} - \boldsymbol{U}_{b,t} + \widetilde{\boldsymbol{Z}}_l \cdot (\boldsymbol{SL}_{l,t})^* + \widetilde{\boldsymbol{Z}}_l^* \cdot \boldsymbol{SL}_{l,t} \leq M \cdot (1 - \boldsymbol{p}_l^{\varphi}) \quad (2.4)$$

$$\boldsymbol{U}_{k,t} - \boldsymbol{U}_{b,t} + \widetilde{\boldsymbol{Z}}_l \cdot (\boldsymbol{SL}_{l,t})^* + \widetilde{\boldsymbol{Z}}_l^* \cdot \boldsymbol{SL}_{l,t} \geq -M \cdot (1 - \boldsymbol{p}_l^{\varphi}) \tag{2.5}$$

$$-p_l^{\phi} \cdot SL_l^{\phi,max} \leq PL_{l,t}^{\phi} \leq p_l^{\phi} \cdot SL_l^{\phi,max} \tag{2.6}$$

$$-p_l^{\phi} \cdot SL_l^{\phi,max} \leq QL_{l,t}^{\phi} \leq p_l^{\phi} \cdot SL_l^{\phi,max} \tag{2.7}$$

$$-\sqrt{2} \cdot p_l^{\phi} \cdot SL_l^{\phi,max} \leq PL_{l,t}^{\phi} + QL_{l,t}^{\phi} \leq \sqrt{2} \cdot p_l^{\phi} \cdot SL_l^{\phi,max} \tag{2.8}$$

$$-\sqrt{2} \cdot p_l^{\phi} \cdot SL_l^{\phi,max} \leq PL_{l,t}^{\phi} - QL_{l,t}^{\phi} \leq \sqrt{2} \cdot p_l^{\phi} \cdot SL_l^{\phi,max} \tag{2.9}$$

$$0 \leq P_{i,t}^{\phi} \leq P_i^{\phi,max} \tag{2.10}$$

$$-Q_i^{\phi,max} \leq Q_{i,t}^{\phi} \leq Q_i^{\phi,max} \tag{2.11}$$

$$Q_{n,t}^{\phi} \leq tan\left(\cos^{-1} PF_n\right) \cdot P_{n,t}^{\phi} \tag{2.12}$$

$$Q_{n,t}^{\phi} \geq -tan\left(\cos^{-1} PF_n\right) \cdot P_{n,t}^{\phi} \tag{2.13}$$

$$0 \leq P_{v,t}^{\phi} \leq P_v^{\phi,max} \tag{2.14}$$

$$-Q_v^{\phi,max} \leq Q_{v,t}^{\phi} \leq Q_v^{\phi,max} \tag{2.15}$$

$$P_{v,t}^{\phi} \leq A_v^{\phi}.IR_{v,t} \tag{2.16}$$

$$0 \leq l_{v,t}^{\phi} \leq u_{v,t}^{\phi} \tag{2.17}$$

$$u_{v,t}^{\phi} \leq P_v^{\phi,max} \tag{2.18}$$

$$\left(P_v^{\phi,max} - A_v^{\phi}.IR_{v,t}\right).V_{v,t}^{\phi} - l_{v,t}^{\phi} \geq -A_v^{\phi}.IR_{v,t} \tag{2.19}$$

$$A_v^{\phi}.IR_{v,t} \cdot V_{v,t}^{\phi} + u_{v,t}^{\phi} \leq A_v^{\phi} \cdot IR_{v,t} \tag{2.20}$$

$$P_{v,t}^{\phi} = l_{v,t}^{\phi} + \left(u_{v,t}^{\phi} - l_{v,t}^{\phi}\right).\sigma_{v,t}^{\phi} \tag{2.21}$$

$$P_{e,t}^{\varphi} = P_{e,t}^{\varphi,ch} - P_{e,t}^{\varphi,dc} \tag{2.22}$$

$$0 \leq P_{e,t}^{\varphi,ch} \leq IC_{e,t} \cdot P_e^{max,ch} \tag{2.23}$$

$$0 \leq P_{e,t}^{\varphi,dc} \leq IC_{e,t} \cdot P_e^{max,ch} \tag{2.24}$$

$$E_{e,t}^{\varphi} - E_{e,t-1}^{\varphi} - P_{e,t}^{\varphi} \leq M \cdot (1 - IC_{e,t}) \tag{2.25}$$

$$E_{e,t}^{\varphi} - E_{e,t-1}^{\varphi} - P_{e,t}^{\varphi} \geq -M \cdot (1 - IC_{e,t}) \tag{2.26}$$

$$E_{e,t}^{\varphi} \leq M \cdot (1 - IC_{e,t}) + E_{e}^{max} \tag{2.27}$$

$$E_{e,t}^{\varphi} \geq -M \cdot (1 - IC_{e,t}) + E_{e}^{max} \tag{2.28}$$

$$E_{e,t}^{\varphi} \leq M \cdot (1 - I_{e,t}^{ar}) + E_{e}^{max} \tag{2.29}$$

$$E_{e,t}^{\varphi} \geq -M \cdot (1 - I_{e,t}^{ar}) + E_{e}^{max} \tag{2.30}$$

$$E_{e,t}^{\varphi} \leq M \cdot (1 - I_{e,t}^{dep}) + E_{e}^{max} \tag{2.31}$$

$$E_{e,t}^{\varphi} \geq -M \cdot (1 - I_{e,t}^{dep}) + E_{e}^{max} \tag{2.32}$$

$$s_{b,t}^{1}, s_{b,t}^{2}, s_{b,t}^{3}, s_{b,t}^{4} \geq 0 \tag{2.33}$$

$$\boldsymbol{z}_l = \boldsymbol{r}_l + j\boldsymbol{x}_l \tag{2.34}$$

$$\widetilde{\boldsymbol{Z}_l} = \boldsymbol{A} \bigodot \boldsymbol{z}_l \tag{2.35}$$

$$\boldsymbol{A} = \begin{bmatrix} 1 & e^{-j2\pi/3} & e^{j2\pi/3} \\ e^{j2\pi/3} & 1 & e^{-j2\pi/3} \\ e^{-j2\pi/3} & e^{j2\pi/3} & 1 \end{bmatrix} \tag{2.36}$$

$$\boldsymbol{SL}_{l,t} = \begin{bmatrix} PL_{l,t}^{a} + jQL_{l,t}^{a} & PL_{l,t}^{b} + jQL_{l,t}^{b} & PL_{l,t}^{c} + jQL_{l,t}^{c} \end{bmatrix} \tag{2.37}$$

$$\boldsymbol{U}_{b,t} = \begin{bmatrix} (V_{b,t}^{a})^2 & (V_{b,t}^{b})^2 & (V_{b,t}^{c})^2 \end{bmatrix} \tag{2.38}$$

2.2 Solution Methodology

The proposed two-stage optimization problem is solved using the C& CG approach [86]. The problem is decomposed into a master problem (2.39)-(2.44) with decision variable x and subproblem (2.45)-(2.48) with decision variables y,s and σ.

$$\min_{\boldsymbol{x}} \ \boldsymbol{c}^{\top}\boldsymbol{x} + \eta \tag{2.39}$$

s.t.
$$\boldsymbol{A}\boldsymbol{x} \leq \boldsymbol{d} \tag{2.40}$$

$$\eta \geq \boldsymbol{b}^{\top}\boldsymbol{s}^{l} \tag{2.41}$$

$$\boldsymbol{D}\boldsymbol{y}^{l} \leq \boldsymbol{g}; \forall l \leq k \tag{2.42}$$

$$\boldsymbol{C}\boldsymbol{y}^{l} + \boldsymbol{s}^{l} = \boldsymbol{f}; \forall l \leq k \tag{2.43}$$

$$(\boldsymbol{E} + \boldsymbol{M}\boldsymbol{\sigma}_{l}^{*})\boldsymbol{x} + \boldsymbol{G}\boldsymbol{y}^{l} = \boldsymbol{h}; \forall l \leq k \tag{2.44}$$

Here x represents the vector of first-stage decision variables i.e. $[l_{v,t}^{\varphi}, u_{v,t}^{\varphi}, V_{v,t}^{\varphi}]$.

$$\underset{\boldsymbol{\sigma}_{v,t}^{\phi,m}}{max}\underset{\boldsymbol{s}}{min}\boldsymbol{b}^{\top}\boldsymbol{s} \tag{2.45}$$

s.t.
$$\boldsymbol{D}\boldsymbol{y} \leq \boldsymbol{g} \tag{2.46}$$

$$\boldsymbol{C}\boldsymbol{y} + \boldsymbol{s} = \boldsymbol{f} \tag{2.47}$$

$$\boldsymbol{G}\boldsymbol{y} = \boldsymbol{h} - (\boldsymbol{E} + \boldsymbol{M}\boldsymbol{\sigma})\boldsymbol{x}^{*} \tag{2.48}$$

Here y represents the second-stage recourse decision variables i.e. $P_{v,t}^{\varphi}$,$P_{e,t}^{\varphi}$, $P_{n,t}^{\varphi}$,$P_{i,t}^{\varphi}$, $Q_{v,t}^{\varphi}$,$Q_{n,t}^{\varphi}$, $Q_{i,t}^{\varphi}$, $PL_{l,t}^{\varphi}$ and $QL_{l,t}^{\varphi}$ as well as the voltage magnitude on the buses ($\boldsymbol{U}_{b,t}$). The dual form of the sub-problem is shown as follows:

$$Q = \underset{\boldsymbol{\sigma},\boldsymbol{\mu}s}{max}\boldsymbol{g}^{\top}\boldsymbol{\mu}_{1} + \boldsymbol{f}^{\top}\boldsymbol{\mu}_{2} + [\boldsymbol{h} - (\boldsymbol{E} + \boldsymbol{M}\boldsymbol{\sigma})\boldsymbol{x}^{*}]^{\top}\boldsymbol{\mu}_{3} \tag{2.49}$$

$$\boldsymbol{D}^{\top}\boldsymbol{\mu}_{1} + \boldsymbol{C}^{\top}\boldsymbol{\mu}_{2} + \boldsymbol{G}^{\top}\boldsymbol{\mu}_{3} \leq 0 \tag{2.50}$$

$$\boldsymbol{\mu}_{2} \leq \boldsymbol{b}, \qquad \boldsymbol{\mu}_{3} \quad free \tag{2.51}$$

The μ_1, μ_2 and mu_3 are dual variables for constraints (2.46), (2.47) and (2.48) respectively. The C&CG algorithm is described as follows:

- Step 1: Set iteration index $k = 0$, $LB = -\infty$, $UB = \infty$ and convergence index $\varepsilon = 10^{-3}$.

- Step 2: Solve the master problem and obtain the optimal solution, x_{k+1}^{*} and η_{k+1}^{*} and

update the $LB = c^\top x^*_{k+1} + \eta^*_{k+1}$

- Step 3: Solve the sub-problem and update the $UB = \min\left\{UB, c^\top x^*_{k+1} + Q^*_{k+1}\right\}$
- Step 4: Check the convergence if $UB - LB < \varepsilon$ terminate otherwise $k = k + 1$, add constraints (2.41)-(2.44) and go to step 2.

2.3 Numerical Results

In this chapter, a modified IEEE 13-bus system for which the peak demand is shown in Table 2.1. Four PV units and four dispatchable distributed generation units (DGs) are installed in the system. Tables 2.2 and 2.3 show the characteristics of the DG and PV units respectively. The PV units and DG1-DG3 are three-phase generation units and DG4 is a single-phase distributed generation unit connected to phase C. 30 single-phase EVs are connected to the system. Table 2.4 shows the characteristics of EVs. Fig. 2.1 shows the demand and total PV generation profiles in the operation horizon. The following cases are considered:

- Case 1 – Deterministic maximum PV generation and demand without EV.
- Case 2 – Deterministic maximum PV generation and demand with EV.
- Case 3 – Uncertainty in maximum PV generation, demand, state of charge (SoC) of EVs at arrival and departure times, capacity and maximum real power dispatch of EVs.

2.3.1 Case 1 – Deterministic maximum PV generation and demand without EV

In this case, the maximum PV generation and demand are considered as forecasted values. The dispatchability limits of PV generation for each phase are shown in Fig. 2.2. The dispatchability limits for the PV generation units on phase A are shown in Fig. 2.2a. In this case, the lower bound of dispatchability limit is increasing from 0 at hour 9 to 32.917 kW and 10.592 kW at hours 10 and 11 respectively. Here, the total real power demand at hour 10 is 1116.25 kW and the total dispatch of DG and main feeder, at hour 10, cannot increase beyond 1083.33 kW as the DGs reach their maximum capacity and feeder also reach the maximum apparent power capacity on this phase. Consequently, the lower dispatchability limit for the PV generation at hour 10 on phase A reaches 32.917 kW.

Table 2.1: Demand Characteristics

Node	Phase a (kW)	Phase a (kVAr)	Phase b (kW)	Phase b (kVAr)	Phase c (kW)	Phase c (kVAr)
1	0	0	0	0	0	0
2	0	0	218.5	125.4	0	0
3	0	0	161.5	118.75	0	0
4	16.15	9.5	62.7	36.1	111.15	17.1
5	0	0	0	0	0	0
6	152	104.5	114	85.5	114	85.5
7	0	0	0	0	161.5	76
8	0	0	0	0	0	0
9	365.75	209	365.75	209	365.75	209
10	0	0	0	0	161.5	143.45
11	460.75	180.5	64.6	57	275.5	201.4
12	121.6	81.7	0	0	0	0
13	0	0	0	0	0	0
Total	1116.25	585.2	987.05	631.75	1189.4	732.45

Table 2.2: Dispatchable DG Units Characteristics

DG	Bus	$P^{min}(kW)$	$P^{max}(kW)$	$Q^{min}(kVAr)$	$Q^{max}(kVAr)$
1	4	0	200	-145	145
2	6	0	200	-145	145
3	13	0	250	-180	180
4	7	0	40	-20	20

Table 2.3: PV Generation Units Characteristics

PV	Bus	$P^{min}(kW)$	$P^{max}(kW)$	$Q^{min}(kVAr)$	$Q^{max}(kVAr)$
1	13	0	200	-100	100
2	10	0	200	-100	100
3	9	0	200	-100	100
4	4	0	100	-50	50

Table 2.4: Characteristics of EV units

EV cluster	# of vehicles	Bus	$P^{max}(kW)$	$E^{min}(kWh)$	$E^{max}(kWh)$
1	15	4	45	0	450
2	15	10	45	0	450

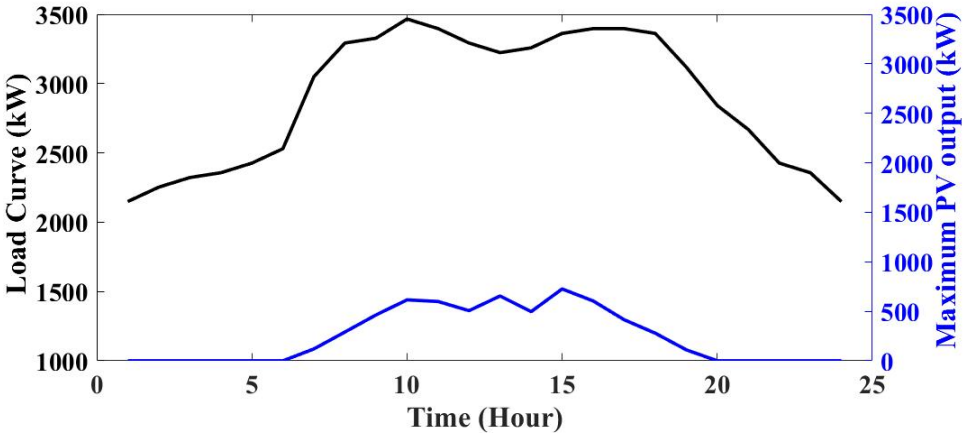

Figure 2.1: Load and PV profile

2.3.2 2) Case 2 – Deterministic maximum PV generation and demand with EV

In this case, the dispatchability limits for PV generation units are evaluated considering the EVs and forecasted maximum PV generation and demand. Five EVs are connected to each phase on buses 4 and 10. All EVs in each cluster, are considered as the same type. The maximum charging and discharging power for each EV is 3kW and maximum energy capacity is 30kWh. The arrival and departure times for EVs are 10:00 and 19:00 respectively. It is assumed that the EVs remain connected to the network within the arrival and departure times and EVs have bi-directional power capability (V2G enabled). The EVs are assumed to have 20% SoC at arrival time. The state of charge (in percent) is defined as the ratio between the available energy in EV clusters and the maximum capacity of the EV clusters. Fig. 2.2 shows the upper and lower bounds for dispatchability limits of PV generation when the SoC of EV clusters at the departure time is 100%. In this case, the lower bound for dispatchability limit on phase C, at hour 10 is reduced by 30 kW compared to that in Case 1 and reached 116.383 kW. At hour 10, 30 kW is injected by the EV clusters to reduce the lower bound for PV dispatchability limit. At hour 11, the lower bound for dispatchability limit in Case 1 was 107.946 kW and it increases to 137.946kW in this case as the batteries of EV clusters on phase C are being charged by 30kW. Fig. 2.3 also shows the impact of vehicle-to-grid (V2G). When EV clusters are unable to inject power back to the grid (no V2G), the lower bound for PV generation is higher or equal to the lower bound in Case 1.

Fig. 2.3 shows the lower bound for the dispatchability limit of PV generation on phase A and phase C for Case 2 with two hours shifting in arrival and departure times. The SoC of EVs at the departure time is 100 percent. As shown in Fig 2.3a, on phase A, the lower bound at hours 10 and 11, are increased from 2.917 kW and 10.592kW to 62.917 kW and 40.592 kW when the arrival and departure times are shifted by two hours. In phase C as it is shown in Fig. 2.3b, the lower bound at hour 8 is decreased from 50.291kW to 20.291kW when the arrival and departure times are shifted by two hours.

2.3.3 Uncertainty in maximum PV generation, demand, state of charge (SoC) of EVs at arrival and departure times, capacity and maximum real power dispatch of EVs

In this case, the forecast error for maximum PV generation, load, SoC of EVs at arrival and departure times, capacity and maximum real power dispatch of EV clusters are represented by a normal distribution function with a mean equal to those in Case 2. The standard deviation for maximum PV generation and demand is 0.0167 of the mean value and the standard deviation for the SoC of EV clusters at the departure and arrival times, capacity and maximum real power dispatch of EV clusters are 0.06 of the mean values. In this case, 200 scenarios are considered. The expected upper bound and lower bounds for dispatchability limits of PV generation units and those for Case 2 are shown for phases A and C in Fig. 2.4a and Fig. 2.4b respectively.

2.4 Conclusion

In this chapter, the dispatchability limit for PV generation in the unbalanced distribution networks is quantified. It is shown that EV clusters with no V2G will increase the lower bound of dispatchability of PV generation. While V2G can reduce the lower bound for dispatchability limits of PV generation, integrating EVs into the distribution network will increase the lower bound for the dispatchability limit of PV generation as the EVs are being charged for departure. Furthermore, the impact of arrival and departure times for EV clusters are shown in the case study.

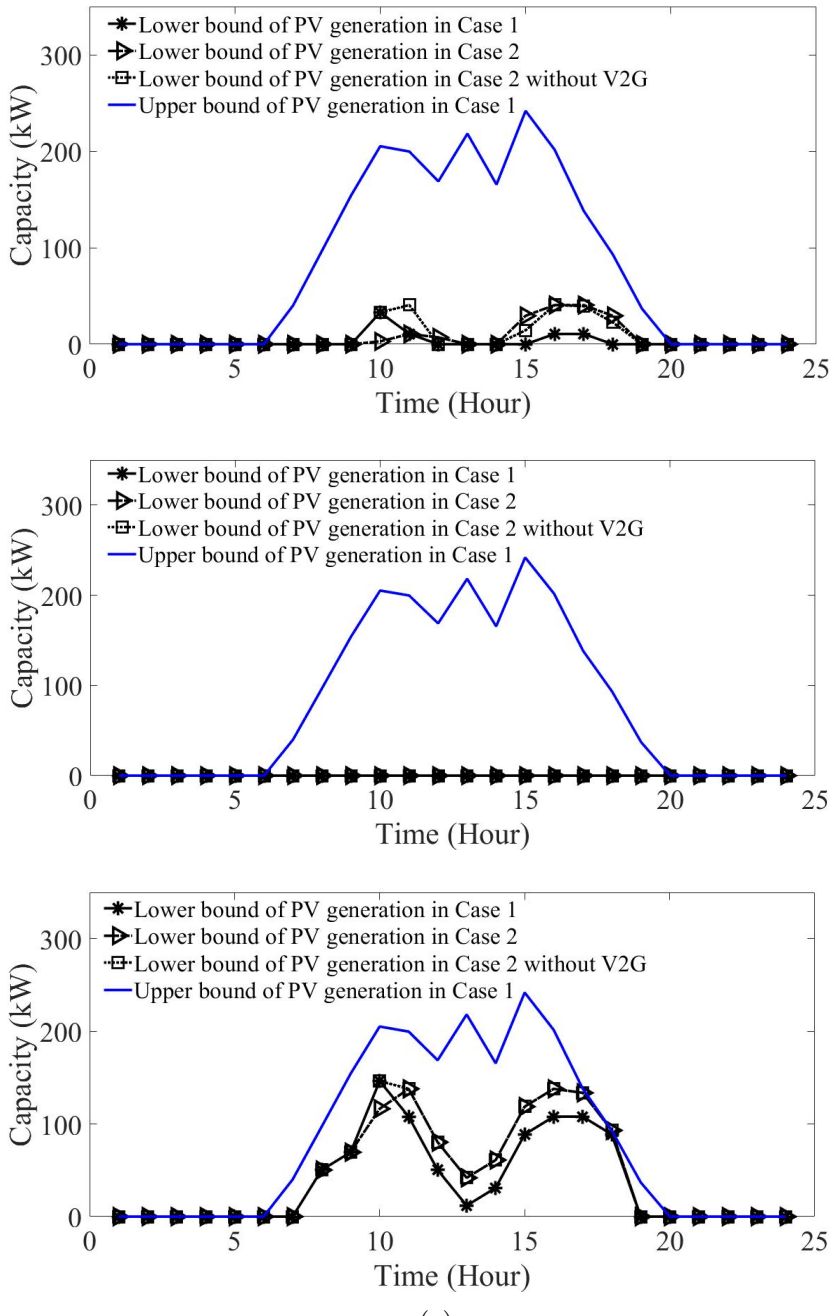

(c)

Figure 2.2: The total dispatchability limits for (a) phase A, (b) phase B and (c) phase C with deterministic demand and maximum PV generation with and without EV clusters

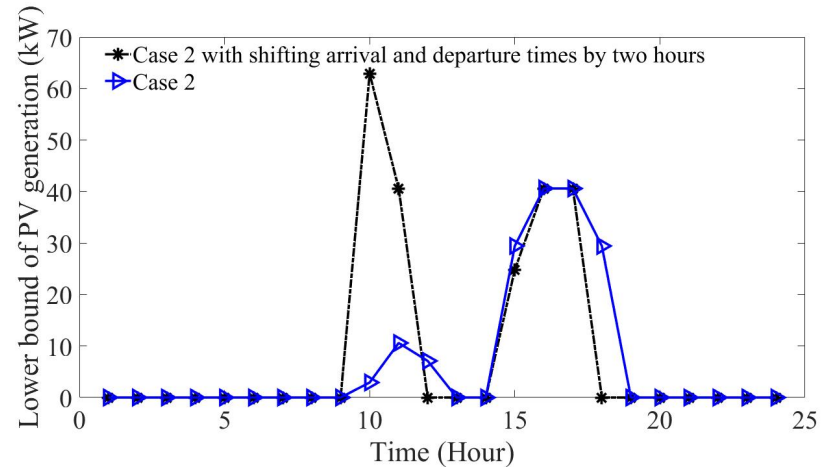

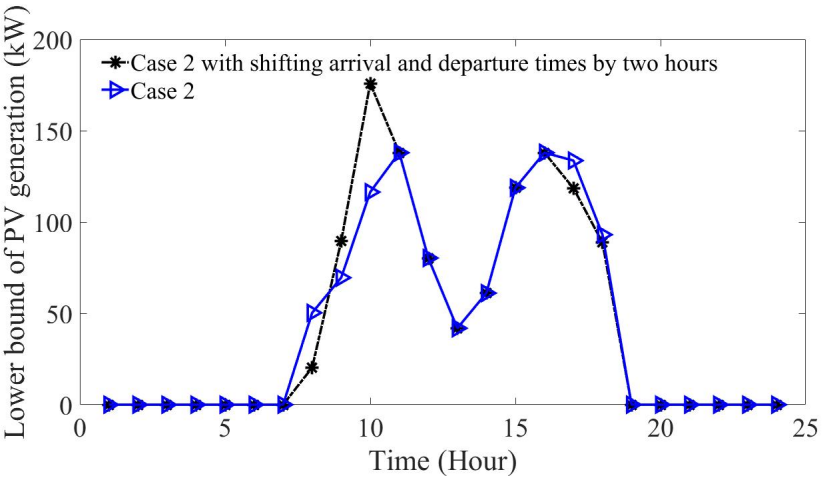

(b)

Figure 2.3: The effects of arrival and departure time on the total dispatchability limits for (a) phase A, (b) phase C

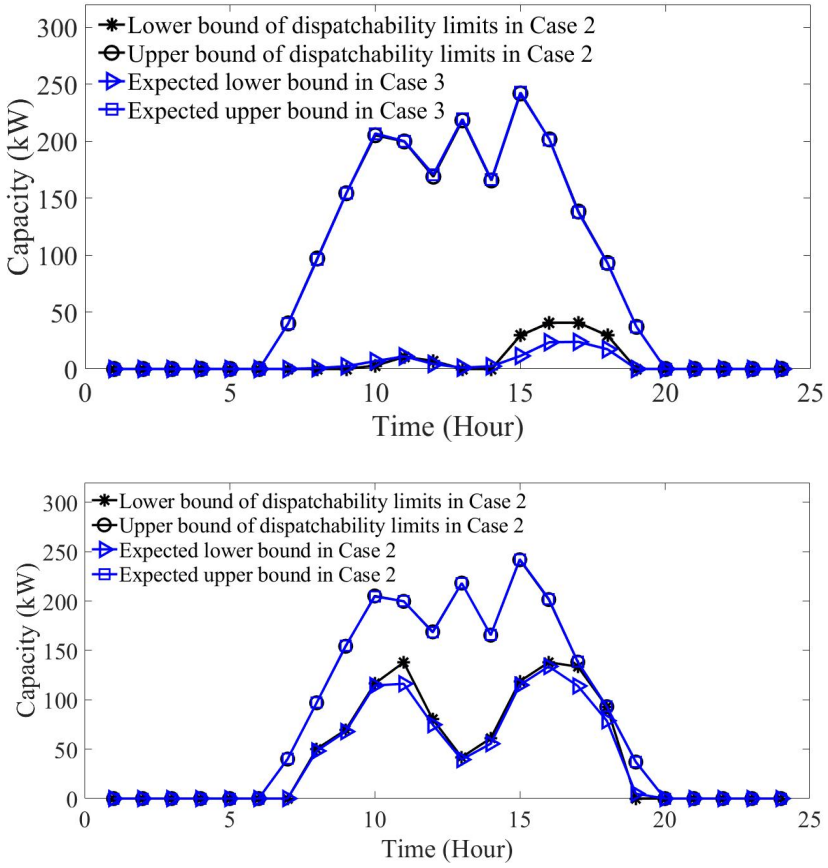

(b)

Figure 2.4: The expected dispatchability limits of PV generation considering the uncertainty in maximum PV generation, SoC of EV clusters at the arrival and departure times and demand, (a) phase A (b) phase C

Chapter 3

Feasible Dispatch Limits of PV Generation with Uncertain Interconnection of EVs in the Unbalanced Distribution Network

This chapter presents a framework to determine the feasible dispatch limits of solar photovoltaic (PV) generation in the unbalanced distribution networks considering the interconnection of electric vehicles (EVs) and associated uncertainties. The proposed framework determines the lower and upper dispatch limits of PV generation considering the worst-case realization of a) the minimum and maximum storage capacity in EVs, b) the minimum and maximum power dispatch of EVs, c) the lower and upper bounds for the arrival and departure times, and d) the available energy at arrival and departure times. The unbalanced operation of the distribution network as well as the uncertainty in the maximum PV generation and demand forecasts were considered. The problem formulation and solution approach are validated using the modified IEEE 34-bus and IEEE 123-bus distribution systems. The impacts of the budget of uncertainty and the vehicle-to-grid operation mode of EV clusters were addressed in the case studies. It is shown that integrating EVs with charging capability will increase the lower dispatch limit or increase the upper dispatch limit of the PV generation. Moreover, the increase in the budget of uncertainty will reduce the difference between the upper and lower dispatch limits by increasing the lower dispatch or decreasing the upper dispatch limit of the PV generation. Finally, it is shown that the vehicle-to-grid capability will reduce the total lower dispatch limit or increase the total upper dispatch limit of the PV generation in the operation horizon. In the previous chapter [98], the dispatch limits of PV generation in the distribution network considering the uncertainty in EV interconnection were addressed using scenarios. In this chapter, the research is extended by capturing the worst-case realization of the maximum and minimum power and energy capacity, the available energy at arrival and departure times, and the arrival and departure times of EV clusters. Furthermore, the formulated problem is extended to a large-scale network.The contributions of this chapter

are as follows:

- A mathematical formulation is proposed to quantify the dispatch limits of the PV generation on each phase considering the unbalanced operation of the distribution network.
- The proposed formulation addresses the worst-case realization of a) the arrival and departure times for EVs, b) the available energy at arrival and departure times, c) the maximum and minimum available energy and power for EVs, to quantify the dispatch limits of PV generation in the distribution network.
- The uncertainties associated with the maximum PV generation and demand are captured in the developed formulation using scenarios.

The rest of the chapter is organized as follows: section 3.1 presents the problem formulation, in which the detailed descriptions of the objective function and constraints are presented. The robust optimization solution methodology is presented in section 3.2. The numerical results are discussed in section 3.3. In this section, to evaluate the effectiveness of the proposed approach for small-scale and large-scale distribution networks, the modified IEEE 34-bus and IEEE 123-bus three-phase distribution systems are considered. Finally, the conclusion is presented in section 3.4.

Nomenclature

Sets and Indices:

- b Index of bus.
- d Index of demand.
- e Index of electric vehicle cluster.
- i Index of distributed generation.
- l Index of distribution branch.
- n Index of distribution feeder.
- v Index of PV generation unit.
- m Index of scenario.

Variables:

- $l_{v,t}^{\phi,m}$ Lower limit for PV generation v on phase ϕ at time t.
- $u_{v,t}^{\phi,m}$ Upper limit for PV generation v on phase ϕ at time t.
- $IA_{e,t}^{\phi,m}$ Binary variable indicating the arrival of EV cluster e on phase ϕ in scenario m.
- $IC_{e,t}^{\phi,m}$ Interconnection of EV cluster e on phase ϕ to the distribution network.
- $IC_{e,t}^{A,\phi,m}$ Auxiliary binary variable to determine the connectivity of EV clusters.
- $IC_{e,t}^{D,\phi,m}$ Auxiliary binary variable to determine the connectivity of EV clusters.
- $ID_{e,t}^{\phi,m}$ Binary variable indicating the departure of EV cluster e on phase ϕ in scenario m.
- $E_{e,t}^{\phi,m}$ Energy capacity of EV cluster e on phase ϕ at time t.
- $P_{(.),t}^{\phi,m}$ Real power of a unit on phase ϕ at time t.
- $P_{e,t}^{\phi,m,ch}$ Charging power of EV cluster e on phase ϕ at time t in scenario m.
- $P_{e,t}^{\phi,m,dc}$ Discharging power of EV cluster e on phase ϕ at time t in scenario m.
- $Q_{(.),t}^{\phi,m}$ Reactive power of a unit on phase ϕ at time t.
- $PL_{l,t}^{\phi,m}$ Real power flow of branch l on phase ϕ at time t.
- $QL_{l,t}^{\phi,m}$ Reactive power flow of branch l on phase ϕ at time t.
- $s_{b,t}^{(.),\phi,m}$ Positive slack variable.
- $SL_{l,t}^{\phi,m}$ Apparent power flow of branch l on phase ϕ at time t.
- $\boldsymbol{U}_t^m$ Squared voltage vector in scenario m at time t.
- $\delta_{e,t}^{\phi,m}$ Auxiliary binary variable representing the uncertainty in minimum energy storage capacity of EV cluster e connected to phase ϕ.

- $\gamma_{e,t}^{\phi,m}$ Auxiliary binary variable representing the uncertainty in maximum energy storage capacity of EV cluster e connected to phase ϕ.

- $\beta_{e,t}^{\phi,m,arv}$ Auxiliary binary variable representing the uncertainty in available energy storage of EV cluster e connected to phase ϕ at arrival time.

- $\beta_{e,t}^{\phi,m,dep}$ Auxiliary binary variable representing the uncertainty in available energy storage of EV cluster e connected to phase ϕ at departure time.

- $\mu_{e,t}^{\phi,m,ch}$ Auxiliary binary variable representing the uncertainty in charging power of EV cluster e connected to phase ϕ.

- $\tau_{e}^{\phi,m,arv}$ Auxiliary binary variable representing the uncertainty in the arrival time of EV cluster e connected to phase ϕ.

- $\tau_{e}^{\phi,m,dep}$ Auxiliary binary variable representing the uncertainty in the departure time of EV cluster e connected to phase ϕ.

- $\mu_{e,t}^{\phi,m,dc}$ Auxiliary binary variable representing the uncertainty in discharging power of EV cluster e connected to phase ϕ.

- $c_{t}^{\phi,m}$ Auxiliary variable representing the time sequence.

- $T_{e}^{\phi,m,arv}$ Arrival time for EV cluster e connected to phase ϕ.

- $T_{e}^{\phi,m,dep}$ Departure time for EV cluster e connected to phase ϕ.

Parameters

- A_{v}^{ϕ} Area covered by the solar PV cells v connected to phase ϕ.

- $AD_{d,b}$ Element of demand-bus incidence matrix.

- $AE_{e,b}$ Element of energy storage-bus incidence matrix.

- $AI_{i,b}$ Element of unit-bus incidence matrix.

- $AL_{l,b}$ Element of line-bus incidence matrix.

– $AV_{v,b}$ Element of PV-bus incidence matrix.

– $AN_{n,b}$ Element of feeder-bus incidence matrix.

– $\hat{E}_e^{\phi,min}$ The lower uncertainty bound for the minimum available energy for EV cluster e on phase ϕ.

– $\hat{E}_e^{\phi,max}$ The lower uncertainty bound for the maximum available energy for EV cluster e on phase ϕ.

– $\widetilde{E}_e^{\phi,min}$ The difference between the lower and upper uncertainty bounds for the minimum available energy for EV cluster e on phase ϕ.

– $\widetilde{E}_e^{\phi,max}$ The difference between the lower and upper uncertainty bounds for the maximum available energy for EV cluster e on phase ϕ.

– $\hat{l}_e^{\phi,arv}$ The lower uncertainty bound for the available energy at arrival time.

– $\hat{l}_e^{\phi,dep}$ The lower uncertainty bound for the available energy at departure time.

– $\widetilde{l}_e^{\phi,arv}$ The difference between the lower and upper uncertainty bounds for available energy at arrival time.

– $\widetilde{l}_e^{\phi,dep}$ The difference between the lower and upper uncertainty bounds for available energy at departure time.

– $\hat{P}_e^{\phi,ch,max}$ The lower uncertainty bound for the maximum charging power for EV cluster e on phase ϕ.

– $\hat{P}_e^{\phi,dc,max}$ The lower uncertainty bound for the maximum discharging power for EV cluster e on phase ϕ.

– $\widetilde{P}_e^{\phi,ch,max}$ The difference between the lower and upper uncertainty bounds for the maximum charging power of EV cluster e on phase ϕ.

– $\widetilde{P}_e^{\phi,dc,max}$ The difference between the lower and upper uncertainty bounds for the maximum discharging power of EV cluster e on phase ϕ.

– $IR^{m}_{v,t}$ Solar radiation for PV solar generation v at time t in scenario m.

– $\boldsymbol{p}_l$ Vector of available phases on the branch l in distribution network.

– $SL^{\phi,max}_{l}$ Apparent power capacity of branch l on phase ϕ.

– $P^{\phi,max}_{(.)}$ Maximum real power of a unit on phase ϕ.

– $Q^{\phi,max}_{(.)}$ Maximum reactive power of a unit on phase ϕ.

– $S^{\phi,max}_{(.)}$ Maximum apparent power of a unit on phase ϕ.

– PF_n Acceptable power factor at distribution feeder n.

– $\hat{T}^{\phi,arv}_{e}$ Forecasted arrival time for EV cluster e connected to phase ϕ.

– $\hat{T}^{\phi,dep}_{e}$ Forecasted departure time for EV cluster e connected to phase ϕ.

– $\widetilde{T}^{\phi,arv,min}_{e}$ The lower uncertainty bound for the arrival time of EV cluster e connected to phase ϕ.

– $\widetilde{T}^{\phi,arv,max}_{e}$ The upper uncertainty bound for the arrival time of EV cluster e connected to phase ϕ.

– $\widetilde{T}^{\phi,dep,min}_{e}$ The lower uncertainty bound for the departure time of EV cluster e connected to phase ϕ.

– $\widetilde{T}^{\phi,dep,max}_{e}$ The upper uncertainty bound for the departure time of EV cluster e connected to phase ϕ.

– $\Lambda^{\phi,arv}$ Budget of uncertainty for arrival time on phase ϕ.

– $\Lambda^{\phi,dep}$ Budget of uncertainty for departure time on phase ϕ.

– $\Gamma^{\phi,E_{min}}$ Budget of uncertainty for minimum energy capacity in EV clusters connected to phase ϕ.

– $\Gamma^{\phi,E_{max}}$ Budget of uncertainty for maximum energy capacity in EV clusters connected to phase ϕ.

– Γ^{ϕ}_{ch} Budget of uncertainty for charging power capacity of EV clusters connected to phase ϕ.

– Γ^{ϕ}_{dc} Budget of uncertainty for discharging power capacity of EV clusters connected to phase ϕ.

– $\Gamma^{\phi,arv}$ Budget of uncertainty for available energy in EV clusters connected to phase ϕ at arrival time.

– $\Gamma^{\phi,dep}$ Budget of uncertainty for available energy in EV clusters connected to phase ϕ at departure time.

– η^{e}_{ch} Charging efficiency of EV cluster e.

– η^{e}_{dc} Discharging efficiency of EV cluster e.

– NT Total simulation period.

3.1 Problem Formulation

The proposed problem formulation addresses the uncertainty in the arrival and departure times, the charging and discharging power capacity, the maximum and minimum storage capacity, and the available energy at arrival and departure times for the EVs. The uncertainties in the forecasted maximum solar PV generation and electricity demand are captured in scenarios.

The problem formulation is shown in (3.1)-(3.60). The objective of this problem is shown in (3.1). The first term in the objective function aims to maximize the difference between the lower and upper dispatch limits of the PV generation units while ensuring that the PV outputs are within these limits. As shown in the second term of the objective function, the feasibility of the dispatched PV generation is ensured by minimizing the mismatch in nodal power balance with the worst-case realization of the uncertain variables. Minimizing the binary variable $V^{\phi,m}_{v,t}$ maintains the PV generation within the lower and upper dispatch limits. The next term is the normalized difference between the upper and lower dispatch limits of PV generation. In the second part of the objective function, vector $\boldsymbol{\nu}^{\boldsymbol{\phi,m}}_{\boldsymbol{e,t}}$ is a vector composed

of the binary variables associated with the uncertainties in EVs (i.e. $\delta_{e,t}^{\phi,m} \in \boldsymbol{\nu_{e,t}^{\phi,m}}, \gamma_{e,t}^{\phi,m} \in \boldsymbol{\nu_{e,t}^{\phi,m}}, \beta_{e,t}^{\phi,m,arv} \in \boldsymbol{\nu_{e,t}^{\phi,m}}, \beta_{e,t}^{\phi,m,dep} \in \boldsymbol{\nu_{e,t}^{\phi,m}}, \mu_{e,t}^{\phi,m,dc} \in \boldsymbol{\nu_{e,t}^{\phi,m}}, \mu_{e,t}^{\phi,m,ch} \in \boldsymbol{\nu_{e,t}^{\phi,m}}, \tau_{e}^{\phi,m,arv} \in \boldsymbol{\nu_{e,t}^{\phi,m}}$ and $\tau_{e}^{\phi,m,dep} \in \boldsymbol{\nu_{e,t}^{\phi,m}}$).

The real and reactive power balances at each node of the distribution network are enforced by (3.2) and (3.3) respectively. The distribution branch power flow is formulated by (3.4), (5.5) as presented in [99]. Here, $PL_{l,t}^{\phi,m} \in \boldsymbol{PL}_t^m$, $QL_{l,t}^{\phi,m} \in \boldsymbol{QL}_t^m$, $U_{b,t}^{\phi,m} \in \boldsymbol{U}_{b,t}^m$ and $\widetilde{\boldsymbol{R}}_l$, $\widetilde{\boldsymbol{X}}_l$ are obtained using [99]. The big-M method is used in (3.4) and (3.5) to address the availability of phases on the distribution branch. The circular constraint representing the complex power flow limit in a distribution branch is linearized in (3.6)-(3.11) using the technique presented in [97]. The real and reactive power outputs of a DG unit are bounded by (3.12) and (3.13) respectively. Constraints (3.14)-(3.19) enforce the limits on the real and reactive power supply of the distribution feeder. The acceptable power factor would limit the exchanged reactive power at the main distribution feeder as shown in (3.18) and (3.19). Constraints (3.20)-(3.21) show the limits on the real and reactive power outputs of the PV unit. As shown in (3.20) and (3.22), the PV generation is limited by the nominal capacity of the unit and the collected solar energy. The reactive power output of the PV unit is within the upper and lower capacity limits as shown in (3.21). The relationship between the lower and upper dispatch limits of PV generation is shown in (3.23). The upper PV dispatch limit is constrained by the nominal capacity of the PV generation unit as shown in (3.24). As enforced by (3.25) and (3.26), if $V_{v,t}^{\phi,m}$ is 0, the PV generation is within the dispatch limits and otherwise, it is out of the dispatch limits. Here, the worst-case realization of the PV generation is characterized by the lower or upper dispatch limits as shown in (3.27).

In the proposed formulation, EVs with similar characteristics are considered as a cluster. The uncertainties associated with the arrival and departure times i.e. $T_e^{\phi,m,arv}$ and $T_e^{\phi,m,dep}$, during which an EV cluster is connected to the distribution network are addressed by (3.28)-(3.44). Here, the arrival time is between a lower and an upper limit as shown in (3.28)-(3.29). The lower and upper limits are formulated using the forecasted arrival time and a difference between the forecasted arrival time and the uncertain boundaries. Similarly, the departure time is between the lower and upper limits as shown in (3.30), (3.31). The relationship between the arrival time and the binary variable representing the arrival of the EV cluster

($IC_{e,t}^{A,\phi,m}$) is shown in (3.32), (3.33). As shown here, if $t \geq T_e^{\phi,m,arv}$ then ($IC_{e,t}^{A,\phi,m} = 1$) and otherwise ($IC_{e,t}^{A,\phi,m} = 0$). Similarly, the relationship between the departure time and the binary variable representing the departure of the EV cluster ($IC_{e,t}^{D,\phi,m}$) is shown in (3.34), (3.35). As shown here, if $t \geq T_e^{\phi,m,dep}$ then ($IC_{e,t}^{D,\phi,m} = 0$) and otherwise, ($IC_{e,t}^{D,\phi,m} = 1$). Here, $c_t^{\phi,m}$ is an auxiliary variable that accounts for the time index, and $T_e^{\phi,m,arv} \cdot IC_{e,t}^{A,\phi,m}$ is a nonlinear term that is further linearized using McCormick envelopes [100]. A similar technique is used to handle the nonlinear terms in (5.30)-(5.32). The interconnection state of an EV cluster is determined using (3.38)-(3.40). Here, $IC_{e,t}^{\phi,m} = 1$ if the vehicle cluster e arrives at the charging station ($IC_{e,t}^{A,\phi,m} = 1$), and does not leave the charging station i.e. ($IC_{e,t}^{D,\phi,m} = 1$). The arriving and departing states of an EV cluster are determined by (3.41) and (3.42). Here, if an EV cluster leaves the charging station then $ID_{e,t}^{\phi,m} = 1$, and when an EV cluster arrives at the charging station $IA_{e,t}^{\phi,m} = 1$. The budgets of uncertainty for arrival and departure times are enforced by (3.43) and (3.44) respectively.

$$\min_{u_{v,t}^{\phi,m}, l_{v,t}^{\phi,m}, V_{v,t}^{\phi,m}} \sum_m \sum_v \sum_\phi \sum_t (V_{v,t}^{\phi,m} - (u_{v,t}^{\phi,m} - l_{v,t}^{\phi,m})/P_v^{\phi,max}) + \max_{\sigma_{v,t}^{\phi,m}, \boldsymbol{\nu_{e,t}^{\phi,m}}} \min_{s_{(.)}^{(.)}} \sum_m \sum_b \sum_\phi \sum_t (s_{b,t}^{1,\phi,m} + s_{b,t}^{2,\phi,m} + s_{b,t}^{3,\phi,m} + s_{b,t}^{4,\phi,m}) \quad (3.1)$$

s.t.

$$\sum_l AL_{l,b} PL_{l,t}^{\phi,m} + \sum_i AI_{i,b} P_{i,t}^{\phi,m} + \sum_v AV_{v,b} P_{v,t}^{\phi,m} + \sum_e AE_{e,b} (P_{e,t}^{\phi,m,dc} - P_{e,t}^{\phi,m,ch}) + \sum_n AN_{n,b} P_{n,t}^{\phi,m} + s_{b,t}^{1,\phi,m} - s_{b,t}^{2,\phi,m} = \sum_d AD_{d,b} P_{d,t}^{\phi,m} \quad (3.2)$$

$$\sum_l AL_{l,b} QL_{l,t}^{\phi,m} + \sum_i AI_{i,b} Q_{i,t}^{\phi,m} + \sum_v AV_{v,b} Q_{v,t}^{\phi,m} + \sum_e AE_{e,b} Q_{e,t}^{\phi,m} + \sum_n AN_{n,b} Q_{n,t}^{\phi,m} + s_{b,t}^{3,\phi,m} - s_{b,t}^{4,\phi,m} = \sum_d AD_{d,b} Q_{d,t}^{\phi,m} \quad (3.3)$$

$$AL_{l,b} \cdot \boldsymbol{U}_{b,t}^m + 2(\widetilde{\boldsymbol{R}}_l \cdot \boldsymbol{PL}_{l,t}^m + \widetilde{\boldsymbol{X}}_l \cdot \boldsymbol{QL}_{l,t}^m) \leq M \cdot (1 - \boldsymbol{p}_l) \quad (3.4)$$

$$AL_{l,b} \cdot \boldsymbol{U}_{b,t}^m + 2(\widetilde{\boldsymbol{R}}_l \cdot \boldsymbol{PL}_{l,t}^m + \widetilde{\boldsymbol{X}}_l \cdot \boldsymbol{QL}_{l,t}^m) \geq -M \cdot (1 - \boldsymbol{p}_l) \quad (3.5)$$

$$-p_l^\phi \cdot SL_l^{\phi,max} \leq PL_{l,t}^{\phi,m} \leq p_l^\phi \cdot SL_l^{\phi,max} \quad (3.6)$$

$$-p_l^{\phi} \cdot SL_l^{\phi,max} \leq QL_{l,t}^{\phi,m} \leq p_l^{\phi} \cdot SL_l^{\phi,max} \tag{3.7}$$

$$-\sqrt{2} \cdot p_l^{\phi} \cdot SL_l^{\phi,max} \leq PL_{l,t}^{\phi,m} + QL_{l,t}^{\phi,m} \tag{3.8}$$

$$PL_{l,t}^{\phi,m} + QL_{l,t}^{\phi,m} \leq \sqrt{2} \cdot p_l^{\phi} \cdot SL_l^{\phi,max} \tag{3.9}$$

$$-\sqrt{2} \cdot p_l^{\phi} \cdot SL_l^{\phi,max} \leq PL_{l,t}^{\phi,m} - QL_{l,t}^{\phi,m} \tag{3.10}$$

$$PL_{l,t}^{\phi,m} - QL_{l,t}^{\phi,m} \leq \sqrt{2} \cdot p_l^{\phi} \cdot SL_l^{\phi,max} \tag{3.11}$$

$$0 \leq P_{i,t}^{\phi,m} \leq P_i^{\phi,max} \tag{3.12}$$

$$-Q_i^{\phi,max} \leq Q_{i,t}^{\phi,m} \leq Q_i^{\phi,max} \tag{3.13}$$

$$-S_n^{\phi,max} \leq P_{n,t}^{\phi,m} \leq S_n^{\phi,max} \tag{3.14}$$

$$-S_n^{\phi,max} \leq Q_{n,t}^{\phi,m} \leq S_n^{\phi,max} \tag{3.15}$$

$$-\sqrt{2} \cdot S_n^{\phi,max} \leq P_{n,t}^{\phi,m} + Q_{n,t}^{\phi,m} \leq \sqrt{2} \cdot S_n^{\phi,max} \tag{3.16}$$

$$-\sqrt{2} \cdot S_n^{\phi,max} \leq P_{n,t}^{\phi,m} - Q_{n,t}^{\phi,m} \leq \sqrt{2} \cdot S_n^{\phi,max} \tag{3.17}$$

$$Q_{n,t}^{\phi,m} \leq tan\left(\cos^{-1} PF_n\right) \cdot P_{n,t}^{\phi,m} \tag{3.18}$$

$$Q_{n,t}^{\phi,m} \geq -tan\left(\cos^{-1} PF_n\right) \cdot P_{n,t}^{\phi,m} \tag{3.19}$$

$$0 \leq P_{v,t}^{\phi,m} \leq P_v^{\phi,max} \tag{3.20}$$

$$-Q_v^{\phi,max} \leq Q_{v,t}^{\phi,m} \leq Q_v^{\phi,max} \tag{3.21}$$

$$P_{v,t}^{\phi,m} \leq A_v^{\phi}.IR_{v,t}^{m} \tag{3.22}$$

$$0 \leq l_{v,t}^{\phi,m} \leq u_{v,t}^{\phi,m} \tag{3.23}$$

$$u_{v,t}^{\phi,m} \leq P_v^{\phi,max} \tag{3.24}$$

$$\left(P_v^{\phi,max} - A_v^{\phi}.IR_{v,t}^{m}\right).V_{v,t}^{\phi,m} - l_{v,t}^{\phi,m} \geq -A_v^{\phi}.IR_{v,t}^{m} \tag{3.25}$$

$$A_v^{\phi}.IR_{v,t}^{m} \cdot V_{v,t}^{\phi,m} + u_{v,t}^{\phi,m} \leq A_v^{\phi} \cdot IR_{v,t}^{m} \tag{3.26}$$

$$P_{v,t}^{\phi,m} = l_{v,t}^{\phi,m} + \left(u_{v,t}^{\phi,m} - l_{v,t}^{\phi,m}\right).\sigma_{v,t}^{\phi,m} \tag{3.27}$$

$$T_e^{\phi,m,arv} \geq \hat{T}_e^{\phi,arv} - \ \tau_e^{\phi,m,arv} \cdot \widetilde{T}_e^{\phi,arv,min} \tag{3.28}$$

$$T_e^{\phi,m,arv} \leq \hat{T}_e^{\phi,arv} + \ \tau_e^{\phi,m,arv} \cdot \widetilde{T}_e^{\phi,arv,max} \tag{3.29}$$

$$T_e^{\phi,m,dep} \geq \hat{T}_e^{\phi,dep} - \tau_e^{\phi,m,dep} \cdot \widetilde{T}_e^{\phi,dep,min} \tag{3.30}$$

$$T_e^{\phi,m,dep} \leq \hat{T}_e^{\phi,dep} + \tau_e^{\phi,m,dep} \cdot \widetilde{T}_e^{\phi,dep,max} \tag{3.31}$$

$$c_t^{\phi,m} - T_e^{\phi,m,arv} \cdot IC_{e,t}^{A,\phi,m} \geq 0 \tag{3.32}$$

$$c_t^{\phi,m} - \left(NT - T_e^{\phi,m,arv}\right) \cdot IC_{e,t}^{A,\phi,m} \leq T_e^{\phi,m,arv} \tag{3.33}$$

$$c_t^{\phi,m} + \left(NT - T_e^{\phi,m,dep}\right) \cdot IC_{e,t}^{D,\phi,m} \leq NT \tag{3.34}$$

$$c_t^{\phi,m} + T_e^{\phi,m,dep} \cdot IC_{e,t}^{D,\phi,m} \geq T_e^{\phi,m,dep} \tag{3.35}$$

$$c_t^{\phi,m} \leq NT \tag{3.36}$$

$$c_t^{\phi,m} - c_{t-1}^{\phi,m} = 1 \tag{3.37}$$

$$IC_{e,t}^{\phi,m} \leq IC_{e,t}^{A,\phi,m} \tag{3.38}$$

$$IC_{e,t}^{\phi,m} \leq IC_{e,t}^{D,\phi,m} \tag{3.39}$$

$$IC_{e,t}^{\phi,m} \geq IC_{e,t}^{A,\phi,m} + IC_{e,t}^{D,\phi,m} - 1 \tag{3.40}$$

$$IC_{e,t-1}^{\phi,m} - \ IC_{e,t}^{\phi,m} = ID_{e,t-1}^{\phi,m} - IA_{e,t}^{\phi,m} \tag{3.41}$$

$$ID_{e,t-1}^{\phi,m} + IA_{e,t}^{\phi,m} \leq 1 \tag{3.42}$$

$$\sum_e \tau_e^{\phi,m,arv} \leq \Lambda_\phi^{arv} \tag{3.43}$$

$$\sum_e \tau_e^{\phi,m,dep} \leq \Lambda_\phi^{dep} \tag{3.44}$$

$$\hat{E}_e^{\phi,min} + \ \delta_{e,t}^{\phi,m} \cdot \widetilde{E}_e^{\phi,min} - M(1 - IC_{e,t}^{\phi,m}) \leq E_{e,t}^{\phi,m} \tag{3.45}$$

$$E_{e,t}^{\phi,m} \leq \hat{E}_e^{\phi,max} + \gamma_{e,t}^{\phi,m} \cdot \widetilde{E}_e^{\phi,max} + M(1 - IC_{e,t}^{\phi,m}) \tag{3.46}$$

$$E_{e,t}^{\phi,m} \leq \left(\hat{l}_e^{\phi,arv} + \beta_{e,t}^{\phi,m,arv} \cdot \tilde{l}_e^{\phi,arv}\right) \cdot \left(\hat{E}_e^{\phi,min} + \delta_{e,t}^{\phi,m} \cdot \tilde{E}_e^{\phi,min}\right) + M \cdot \left(1 - IA_{e,t}^{\phi,m}\right) \tag{3.47}$$

$$E_{e,t}^{\phi,m} \geq \left(\hat{l}_e^{\phi,arv} + \beta_{e,t}^{\phi,m,arv} \cdot \tilde{l}_e^{\phi,arv}\right) \cdot \left(\hat{E}_e^{\phi,min} + \delta_{e,t}^{\phi,m} \cdot \tilde{E}_e^{\phi,min}\right) - M \cdot \left(1 - IA_{e,t}^{\phi,m}\right) \tag{3.48}$$

$$E_{e,t}^{\phi,m} \leq \left(\hat{l}_e^{\phi,dep} + \beta_{e,t}^{\phi,m,dep} \cdot \tilde{l}_e^{\phi,dep}\right) \cdot \left(\hat{E}_e^{\phi,max} + \gamma_{e,t}^{\phi,m} \cdot \tilde{E}_e^{\phi,max}\right) + M \cdot \left(1 - ID_{e,t}^{\phi,m}\right) \tag{3.49}$$

$$E_{e,t}^{\phi,m} \geq \left(\hat{l}_e^{\phi,dep} + \beta_{e,t}^{\phi,m,dep} \cdot \tilde{l}_e^{\phi,dep}\right) \cdot \left(\hat{E}_e^{\phi,max} + \gamma_{e,t}^{\phi,m} \cdot \tilde{E}_e^{\phi,max}\right) - M \cdot \left(1 - ID_{e,t}^{\phi,m}\right) \tag{3.50}$$

$$0 \leq P_{e,t}^{\phi,m,ch} \leq IC_{e,t}^{\phi,m} . \left(\hat{P}_e^{\phi,ch,max} + \mu_{e,t}^{\phi,m,ch} . \tilde{P}_e^{\phi,ch,max}\right) \tag{3.51}$$

$$0 \leq P_{e,t}^{\phi,m,dc} \leq IC_{e,t}^{\phi,m} . \left(\hat{P}_e^{\phi,dc,max} + \mu_{e,t}^{\phi,m,dc} . \tilde{P}_e^{\phi,dc,max}\right) \tag{3.52}$$

$$E_{e,t}^{\phi,m} - E_{e,t-1}^{\phi,m} - \eta_{ch}^{e} P_{e,t}^{\phi,m,ch} + P_{e,t}^{\phi,m,dc} / \eta_{dc}^{e} \leq M \cdot \left(1 - IC_{e,t}^{\phi,m}\right) \tag{3.53}$$

$$E_{e,t}^{\phi,m} - E_{e,t-1}^{\phi,m} - \eta_{ch}^{e} P_{e,t}^{\phi,m,ch} + P_{e,t}^{\phi,m,dc} / \eta_{dc}^{e} \geq -M \cdot \left(1 - IC_{e,t}^{\phi,m}\right) \tag{3.54}$$

$$\sum_{e} \sum_{t} \delta_{e,t}^{\phi,m} \leq \Gamma_{\phi}^{E_{min}} \tag{3.55}$$

$$\sum_{e} \sum_{t} \gamma_{e,t}^{\phi,m} \leq \Gamma_{\phi}^{E_{max}} \tag{3.56}$$

$$\sum_{e} \sum_{t} \beta_{e,t}^{\phi,m,arv} \leq \Gamma_{arv}^{\phi} \tag{3.57}$$

$$\sum_{e} \sum_{t} \beta_{e,t}^{\phi,m,dep} \leq \Gamma_{dep}^{\phi} \tag{3.58}$$

$$\sum_{e} \sum_{t} \mu_{e,t}^{\phi,m,ch} \leq \Gamma_{ch}^{\phi} \tag{3.59}$$

$$\sum_{e} \sum_{t} \mu_{e,t}^{\phi,m,dc} \leq \Gamma_{dc}^{\phi} \tag{3.60}$$

Once, an EV cluster e is connected to the grid, constraints (3.45) and (3.46) enforce the limits for the available energy in its batteries. The available energy at arrival and departure times is enforced by (3.47)-(3.50) using the big-M method. The available energy at arrival and departure times is uncertain and defined as a portion of the maximum and minimum capacity of the EV cluster batteries. In (3.47), the first term on the right-hand side represents the uncertainty in the state of charge in terms of the minimum battery capacity of EVs and the second term represents the uncertainty in the minimum capacity of EV

batteries connected to the distribution network. Similarly, in (3.49), the first term on the right-hand side represents the uncertainty in the state of charge in terms of the maximum battery capacity of EVs while the second term represents the uncertainty in the maximum capacity of EV batteries connected to the distribution network. The power dispatch for an EV cluster is limited by (3.51), (3.52). The charging and discharging power of an EV cluster before the arrival time and after the departure time is zero. The hourly stored energy in an EV cluster is determined by its charging and discharging power dispatch as shown by (3.53) and (3.54). The budget of uncertainty for the minimum and maximum battery capacity of EV clusters, the available energy at arrival and departure times, and the maximum charging and discharging power of EV clusters are enforced by (3.55)-(3.60) respectively.

3.2 Solution Methodology

The proposed solution methodology is based on the column and constraint generation (C&CG) technique. The steps taken to solve this problem are as follows:

1) Step 1 - Initialization: Initialize the upper and lower bounds and the iteration counter k as follows: $LB = -\infty$, $UB = \infty$, $k = 0$

2) Step 2 - Solve the master problem: Solve the problem (3.61)-(3.67) and update the lower bound.

$$\min_{\boldsymbol{x}} \ \boldsymbol{c}^{\top}\boldsymbol{x} + \eta \tag{3.61}$$

s.t.

$$\boldsymbol{A}\boldsymbol{x} \leq \boldsymbol{d} \tag{3.62}$$

$$\eta \geq \boldsymbol{b}^{\top}\boldsymbol{s}^{\omega} \tag{3.63}$$

$$\boldsymbol{D}\boldsymbol{y}^{\omega} \leq \boldsymbol{g}; \forall \omega \leq k \tag{3.64}$$

$$\boldsymbol{H}\boldsymbol{y}^{\omega} + \boldsymbol{s}^{\omega} = \boldsymbol{f}; \forall \omega \leq k \tag{3.65}$$

$$(\boldsymbol{E} + \boldsymbol{M}\boldsymbol{\sigma}_{\omega}^{*})\boldsymbol{x} + \boldsymbol{G}\boldsymbol{y}^{\omega} = \boldsymbol{h}; \forall \omega \leq k \tag{3.66}$$

$$\boldsymbol{N}\boldsymbol{\nu}_{\omega}^{*} + \boldsymbol{F}\boldsymbol{y}^{\omega} \leq \boldsymbol{q}; \forall \omega \leq k \tag{3.67}$$

Here, $\boldsymbol{x}$ represents the vector of first-stage decision variables i.e. $\left[l_{v,t}^{\phi,m}, u_{v,t}^{\phi,m}, V_{v,t}^{\phi,m}\right]$, and $\boldsymbol{y}$ represents the second-stage recourse decision variables i.e. $P_{v,t}^{\phi,m}$, $P_{e,t}^{\phi,m,ch}$, $P_{e,t}^{\phi,m,dc}$, $P_{n,t}^{\phi,m}$,

$P_{i,t}^{\phi,m}$, $Q_{v,t}^{\phi,m}$, $Q_{n,t}^{\phi,m}$, $Q_{i,t}^{\phi,m}$, and the state variables $PL_{l,t}^{\phi,m}$, $QL_{l,t}^{\phi,m}$ and $\boldsymbol{U}_{b,t}^{m}$. The constraint (3.62) represents (3.23)-(3.26); constraint (3.64) represents the set of constraints (3.4)-(3.22). The constraint (3.65) represents (3.2) and (3.3). Constraint (3.66) represents (3.27) and constraint (3.67) represents (3.45)-(3.60). The lower bound is determined using (3.68).

$$LB = \sum_{m}\sum_{v}\sum_{\phi}\sum_{t}\left[\hat{V}_{v,t}^{\phi,m} - (\hat{u}_{v,t}^{\phi,m} - \hat{l}_{v,t}^{\phi,m})/P_{v}^{\phi,max}\right] + \hat{\eta}_{k+1} \tag{3.68}$$

3) Step 3 - Solve subproblem: Solve the subproblem (3.69)-(3.75) and update the upper bound using (3.82). Here, (3.74) represents (3.28)-(3.40) and (3.42)-(3.44). The constraint (3.75) represents (3.41). To solve the subproblem, the problem (3.69)-(3.75) is transformed into (3.76)-(3.81) using the duality theory. The nonlinear terms $\boldsymbol{\sigma}^{\top}\boldsymbol{\pi}_3$ and $\boldsymbol{\nu}^{\top}\boldsymbol{\pi}_4$ are linearized using McCormick envelopes [100].

$$\max_{\boldsymbol{\sigma}_{v,t}^{\phi,m},\boldsymbol{\nu}_{e,t}^{\phi,m}} \min_{\boldsymbol{s}} \boldsymbol{b}^{\top}\boldsymbol{s} \tag{3.69}$$

s.t.

$$\boldsymbol{D}\boldsymbol{y} \leq \boldsymbol{g} \qquad : \boldsymbol{\pi}_1 \tag{3.70}$$

$$\boldsymbol{H}\boldsymbol{y} + \boldsymbol{s} = \boldsymbol{f} \qquad : \boldsymbol{\pi}_2 \tag{3.71}$$

$$\boldsymbol{G}\boldsymbol{y} = \boldsymbol{h} - (\boldsymbol{E} + \boldsymbol{M}\boldsymbol{\sigma})\boldsymbol{x}^{*} \qquad : \boldsymbol{\pi}_3 \tag{3.72}$$

$$\boldsymbol{F}\boldsymbol{y} \leq \boldsymbol{q} - \boldsymbol{N}\boldsymbol{\nu} \qquad : \boldsymbol{\pi}_4 \tag{3.73}$$

$$\boldsymbol{W}\boldsymbol{z} \leq \boldsymbol{R} \tag{3.74}$$

$$\boldsymbol{Q}\boldsymbol{z} = \boldsymbol{J} \tag{3.75}$$

$$\Theta = \max_{\boldsymbol{\sigma}_{v,t}^{\phi,m},\boldsymbol{\nu}_{e,t}^{\phi,m},\boldsymbol{s}} \boldsymbol{g}^{\top}\boldsymbol{\pi}_1 + \boldsymbol{f}^{\top}\boldsymbol{\pi}_2 + \left[\boldsymbol{h} - (\boldsymbol{E} + \boldsymbol{M}\boldsymbol{\sigma})\boldsymbol{x}^{*}\right]^{\top}\boldsymbol{\pi}_3 + (\boldsymbol{q} - \boldsymbol{N}\boldsymbol{\nu})^{\top}\boldsymbol{\pi}_4 \tag{3.76}$$

$$\boldsymbol{D}^{\top}\boldsymbol{\pi}_1 + \boldsymbol{H}^{\top}\boldsymbol{\pi}_2 + \boldsymbol{G}^{\top}\boldsymbol{\pi}_3 + \boldsymbol{F}^{\top}\boldsymbol{\pi}_4 \leq 0 \tag{3.77}$$

$$\boldsymbol{\pi}_2 \leq \boldsymbol{b}, \qquad \boldsymbol{\pi}_3 \quad free \tag{3.78}$$

$$\boldsymbol{\pi}_1,\ \boldsymbol{\pi}_4\ \leq 0 \tag{3.79}$$

$$\boldsymbol{W}\boldsymbol{z} \leq \boldsymbol{R} \tag{3.80}$$

$$\boldsymbol{Q}\boldsymbol{z} = \boldsymbol{J} \tag{3.81}$$

$$UB = min\{UB, \sum_{m}\sum_{v}\sum_{\phi}\sum_{t}(\hat{V}_{v,t}^{\phi,m} - \frac{\hat{u}_{v,t}^{\phi,m} - \hat{l}_{v,t}^{\phi,m}}{p_v^{\phi,max}}) + \Theta^{*(k+1)}\} \tag{3.82}$$

4) Step 4 - Checking the convergence criterion: If $UB - LB \leq \varepsilon$, then terminate the algorithm, otherwise go to *Step 5*.

5) Step 5 - Generate columns and constraints: Add constraints (3.63)-(3.67) to the master problem and go to *Step 2*. Algorithm 1 is the proposed algorithm to determine the PV dispatch limits in which K represents the maximum number of iterations.

Algorithm 1 The proposed algorithm to quantify the PV dispatch limits

Initialization: $k = 0$, $\varepsilon \leq 10^{-3}$, $LB = -\infty$ and $UB = \infty$
Repeat for $m \in \mathcal{M}$
while $k \leq K$ **do**
  Solve the master problem (3.61)-(3.67).
  Update the LB as given in (3.68).
  Solve the subproblem (3.76)-(3.81).
  Update the UB as given in (3.82).
  Check the convergence criteria:
  if $(UB - LB \leq \varepsilon)$ **then**
    Stop
  else
    Generate column and constraints (3.63)-(3.67) and set $k = k + 1$.
  end if
end while

3.3 Numerical Results

Two test cases are considered in this section. The first test case uses the modified IEEE 34-bus system and the second test case presents the modified IEEE 123-bus system. The simulations are performed on a server with dual 14 Core Intel Xeon 2.6 GHz and 380 GB of memory. CPLEX 12.8 is used as the solver.

3.3.1 Modified IEEE 34-bus system

The modified IEEE 34-bus distribution system is considered as a test case. The hourly peak demand and hourly PV outputs are shown in Fig. 3.1. One three-phase and three single-phase dispatchable DG units are installed as shown in Table 3.1. Here, DG1 is a three-phase DG unit and DG2-DG4 are single-phase DG units connected to phases A, B, and C respectively. Three single-phase PV units, i.e. PV1, PV2, and PV3 are connected to phases A, B, and C respectively. The characteristics of the PV generation units are shown in Table 3.2. Table 3.3 shows the characteristics of the EV clusters. Here, the interconnection of EV cluster 1 is three-phase; however, the EV clusters 2-4 are connected to phases A, B, and C respectively. The maximum charging power for each EV is 7.4 kW. The peak demand on phase A is 593.88 kW, 349.86 $kVar$, the peak demand on phase B is 572.32 kW and 337.12 $kVar$, and the peak demand on phase C is 567.42 kW and 336.14 $kVar$. Considering the driving range of 27.9 miles per day for each EV [101], and 30 kWh battery capacity, the forecasted stored energy at arrival time is 60% of the maximum capacity and the EV. The charging and discharging efficiency for the EV clusters are 90%. The following cases are considered:

Case 1 – PV dispatch limits with forecasted PV generation and demand.

Case 2 – PV dispatch limits with forecasted PV generation and demand, and the uncertainty in the EV interconnection.

Case 3 – PV dispatch limits with stochastic forecasted PV generation and demand, and the uncertainty in the EV interconnection.

3.3.1.1 Case 1 – PV dispatch limits with forecasted PV generation and demand

In this case, the PV dispatch limits are procured without considering any EV interconnection to the distribution network. The forecasted values of the maximum PV generation and

Table 3.1: Dispatchable DG Units' Characteristics

DG	Bus	P^{min} (kW)	P^{max} (kW)	Q^{min} (kVAR)	Q^{max} (kVAR)
1	4	0	60	-30	30
2	6	0	50	-25	25
3	24	0	20	-15	15
4	16	0	20	-15	15

Table 3.2: PV Generation Units' Characteristics

PV	Bus	P^{min} (kW)	P^{max} (kW)	Q^{min} (kVAR)	Q^{max} (kVAR)
1	17	0	150	-75	75
2	22	0	150	-75	75
3	30	0	150	-75	75

Table 3.3: Characteristics of EV Units

EV cluster	Number of vehicles	Bus	P^{max} (kW)	E^{min} (kWh)	E^{max} (kWh)
1	24	4	177.6	72	720
2	3	6	22.2	9	90
3	4	24	29.6	12	120
4	3	16	22.2	9	90

demand are used in this case. The PV dispatch limits on each phase are demonstrated in Fig. 3.2. At hours in which the lower limit of PV generation is greater than zero, the distribution feeder and DGs are incapable of supplying the demand, and therefore; the rest of the demand is supplied by the PV generation units. For example, on phase B at hour 11, the lower limit of the PV generation is 27.927 kW. At this hour, the total real power demand is 566.480 kW, and the dispatch of the main distribution feeder, DG1, and DG3, are 498.553 kW, 20 kW, and 20 kW respectively. Here, DGs and the distribution feeder reached their maximum capacity on this phase, and consequently, the rest of the load (i.e. 27.927 kW) is supplied by the PV generation units.

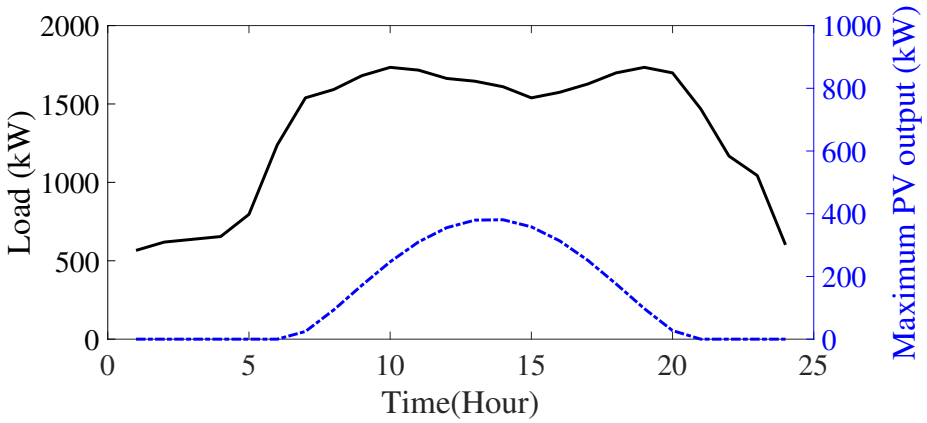

Figure 3.1: Demand and maximum PV generation profiles

Table 3.4: Total Lower PV Dispatch Limits with the Budget of Uncertainty

	Budget of Uncertainty [%]						Total lower dispatch limits on each phase (kWh)			Covergence
Scenario	$\Gamma_{\phi}^{E_{min}}$	$\Gamma_{\phi}^{E_{max}}$	$\Gamma_{arv}^{\phi,m}$	$\Gamma_{dep}^{\phi,m}$	Γ_{ch}^{ϕ}	Γ_{dc}^{ϕ}	Phase A	Phase B	Phase C	Iterations
1 (Case 2)	100	100	100	100	100	100	245.630	345.487	268.537	7
2	0	0	100	100	100	100	210.630	293.460	230.770	6
3	0	0	0	0	100	100	179.130	257.460	197.770	4
4	0	0	0	0	0	0	179.130	257.460	197.770	4
-			Case 1				80.493	111.88	82.873	2

3.3.1.2 Case 2 – PV dispatch limits with forecasted PV generation and demand, and the uncertainty in the EV interconnection

In Case 2, the EV interconnection and the worst-case realization of the uncertain parameters in the EV clusters including the maximum and minimum EV battery capacities, the maximum charging and discharging power for EVs, the available energy at arrival and departure times, as well as the arrival and departure times are considered.

The uncertainty sets for maximum available energy are $[684, 720]$ kWh, $[81, 90]$ kWh, $[108, 120]$ kWh, and $[81, 90]$ kWh for the first to fourth EV clusters, respectively. The uncertainty sets for the minimum available energy are $[72, 144]$ kWh, $[9, 18]$ kWh, $[12, 24]$ kWh, and $[9, 18]$ kWh for the first to fourth EV clusters, respectively. The uncertainty sets for available energy at arrival time are $[396, 468]$ kWh, $[49.5, 58.5]$ kWh, $[66, 78]$ kWh, and $[49.5, 58.5]$

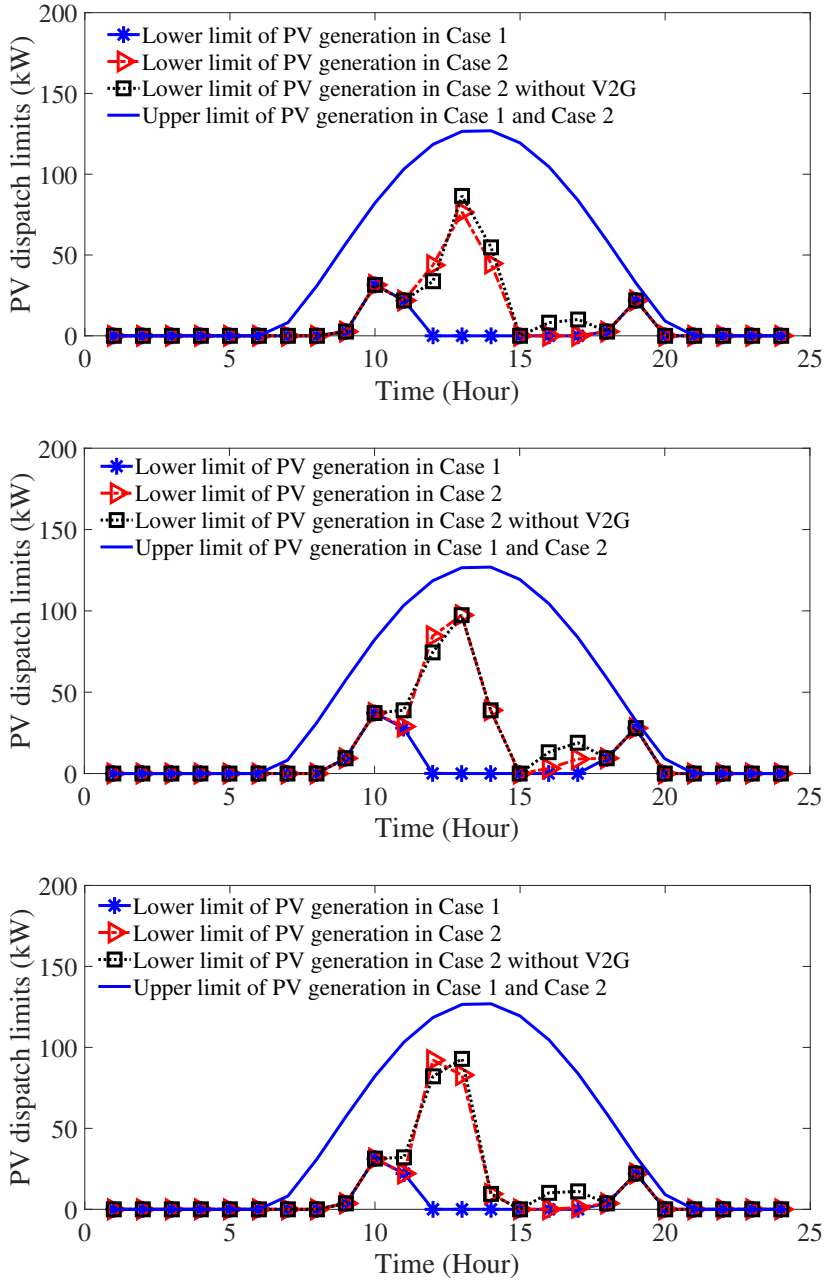

(c)

Figure 3.2: The total PV dispatch limits for (a) phase A, (b) phase B and (c) phase C in Case 1 and Case 2 with and without V2G.

kWh for first to fourth EV clusters, respectively. The uncertainty sets for the available energy at departure time are $[583.2, 720]$ kWh, $[72.9, 90]$ kWh, $[97.2, 120]$ kWh, and $[72.9, 90]$ kWh for first to fourth EV clusters, respectively. The uncertainty sets for the maximum

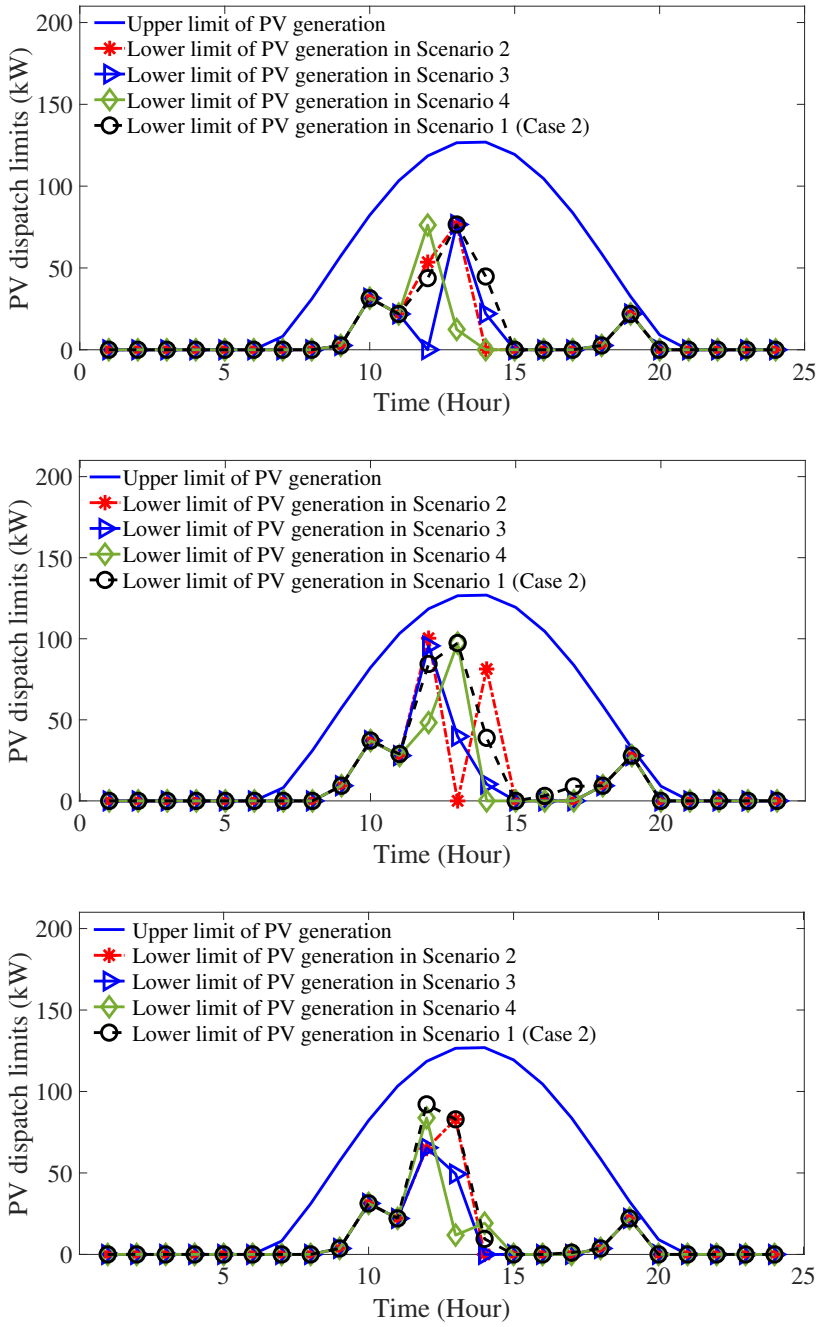

(c)

Figure 3.3: The total PV dispatch limits for (a) phase A, (b) phase B and (c) phase C in Case 2 with the budget of uncertainty.

charging/discharging power dispatch are $[177.6, 213.2]$ kW, $[22.2, 26.64]$ kW, $[29.6, 35.52]$ kW, and $[22.2, 26.64]$ kW for the first to fourth EV clusters, respectively. Finally, the

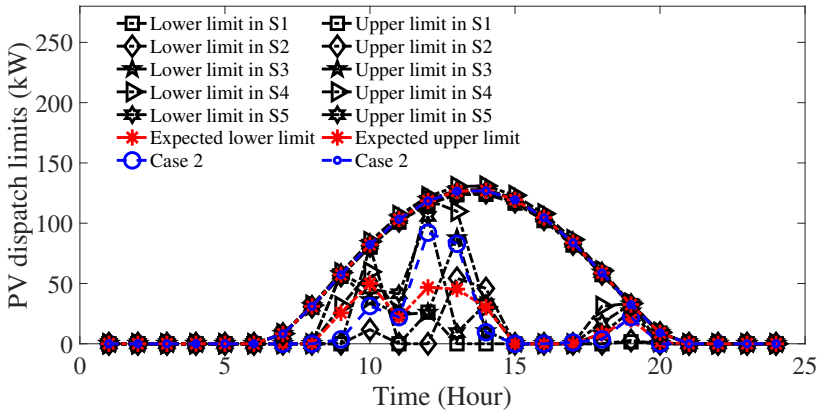

Figure 3.4: The PV dispatch limits for stochastic PV generation and demand in 5 scenarios and the expected value for 100 scenarios on phase C.

Table 3.5: Worst-Case Realization of Arrival and Departure Times for the IEEE 34-bus System

	Arrival and departure times for EV clusters on buses 6, 24 and 16 [hour]											
Scenario	$T_1^{a,arv}$	$T_1^{a,dep}$	$T_1^{b,arv}$	$T_1^{b,dep}$	$T_1^{c,arv}$	$T_1^{c,dep}$	$T_2^{a,arv}$	$T_2^{a,dep}$	$T_3^{b,arv}$	$T_3^{b,arv}$	$T_4^{c,arv}$	$T_4^{c,dep}$
1 (Case 2)	10	17	10	17	10	17	10	17	10	15	8	15
2	8	15	8	17	8	17	10	15	10	15	10	17
3	10	17	10	17	10	17	10	15	8	17	8	15
4	10	17	10	17	10	17	10	17	10	15	8	15

uncertainty sets for arrival and departure times are $T_e^{\Phi,arv} \in [8, 10]$ and $T_e^{\Phi,dep} \in [15, 17]$, respectively.

Fig. 3.2 demonstrates the dispatch limits for the PV generation units in this case. As shown in this figure, the lower PV dispatch limits on all phases at all hours are either equal or greater than those in Case 1. The solution algorithm converges after 7 iterations in this case. Considering the interconnection of EVs to the distribution network, the following observations were made:

a) The impact of V2G on the dispatch limits of PV generation

To investigate the impacts of V2G on the PV dispatch limits, it is assumed that the EV clusters are unable to discharge and inject power back to the grid (non-V2G mode). Fig. 3.2 shows the dispatch limits for PV generation with and without V2G mode. Here, the lower

Table 3.6: Total Lower Dispatch Limits of the PV Generation

	Budget of Uncertainty (%)						Total lower dispatch limits on each phase (kWh)		
Scenario	Λ^a_{arv}	Λ^a_{dep}	Λ^b_{arv}	Λ^b_{dep}	Λ^c_{arv}	Λ^c_{dep}	Phase A	Phase B	Phase C
5 (Case 2)	100	100	100	100	100	100	245.630	345.487	268.537
6	50	50	50	50	50	50	223.430	301.033	240.797
7	0	0	100	100	100	100	186.183	345.487	268.537
8	0	0	0	0	100	100	186.183	287.967	268.537
9	0	0	0	0	0	0	186.183	287.967	214.500

dispatch limits for PV generation at all hours are either higher than or equal to the lower dispatch limits in Case 1, because the EVs are incapable of injecting power to the grid. As shown in Fig. 3.2c, on phase C at hours 12, 13, and 14, the lower PV dispatch limits are increased from 0 kW in Case 1 to 33.773 kW, 86.597 kW and 54.767 kW respectively.

b) The impact of the budget of uncertainty

The budget of uncertainty is defined as the maximum number of changes allowed for the uncertain parameters within the defined uncertainty sets. Such changes are represented by the changes in the binary variables $\delta^{\phi,m}_{e,t}$, $\gamma^{\phi,m}_{e,t}$, $\beta^{\phi,m,arv}_{e,t}$, $\beta^{\phi,m,dep}_{e,t}$, $\mu^{\phi,m,ch}_{e,t}$, $\mu^{\phi,m,dc}_{e,t}$, $\tau^{\phi,m,arv}_{e}$, $\tau^{\phi,m,dep}_{e}$, during the operation horizon. For instance, for maximum EV clusters' energy capacity, $\Gamma^{E_{max}}_{\phi} = 0$ means that the budget of uncertainty is 0%, while for the EV clusters on each phase in 24 hours, $\Gamma^{E_{max}}_{\phi} = 48$ indicates that the budget of uncertainty is 100%. To evaluate the impact of the budget of uncertainty on the PV dispatch limits, multiple scenarios shown in Table 3.4, are considered. This table shows the total lower dispatch limits for the PV generation in the distribution network by limiting the budget of uncertainty for 1) the minimum and maximum EV energy capacity, 2) minimum and maximum charging and discharging power, and 3) available energy at arrival and departure times. In these scenarios, the budgets of uncertainty for the arrival and departure times are 100%. Table 3.5 shows the worst-case realization of the arrival and departure times for the EV clusters on phases A, B, and C in the scenarios presented in Table 3.4. Fig. 3.3 demonstrates the PV dispatch limits on phases A, B, and C in these scenarios.

The impacts of the budgets of uncertainty (Λ^{ϕ}_{arv} and Λ^{ϕ}_{dep}) on the total lower PV dispatch

limits are shown using the scenarios in Table 3.6. Here, the budgets of uncertainty for the maximum and minimum energy and power capacities of EVs as well as the energy at arrival and departure times are 100%. As shown in this table, when the budgets of uncertainty for arrival and departure times decrease from 100% to 50%, the total lower dispatch limits on phases A, B, and C decrease by 9.04%, 12.87%, and 10.33% respectively. It is worth noting that 100% budget of uncertainty for the arrival and departure times means, $\Lambda^{\phi}_{arv} = 2$ and $\Lambda^{\phi}_{dep} = 2$ and 0% budget of uncertainty means $\Lambda^{\phi}_{arv} = 0$ and $\Lambda^{\phi}_{dep} = 0$.

As it is shown in Fig. 3.3 and Table 3.4, once the budget of uncertainty is 100% for all the uncertain variables (Case 2), the total lower PV dispatch limit reaches its maximum value. In Table 3.4, the highest total lower PV dispatch limits are 245.630 kWh, 345.487 kWh, and 268.537 kWh on phases A, B, and C respectively. Moreover, once the budgets of uncertainty for the EVs' energy and power capacity, and the available energies at arrival and departure times, are zero the total lower PV dispatch limits for the PV generation on phases A, B, and C reach the lowest values of 179.130 kWh, 257.460 kWh, and 197.770 kWh respectively. Table 3.4 shows the number of iterations in which the proposed solution algorithm converged.

Table 3.7: Lower PV Dispatch Limits Considering the Uncertainty in the Forecasted PV Generation and Demand

Scenario	Phase A	Phase B	Phase C
S1	122.714	196.331	108.155
S2	127.682	201.118	114.754
S3	257.925	337.235	277.360
S4	319.060	394.124	343.449
S5	415.159	482.840	450.023
Expected Value	238.142	311.915	249.399
Case 2	245.630	345.487	268.537

3.3.1.3 Case 3 – PV dispatch limits with stochastic forecasted PV generation and demand, and the uncertainty in the EV interconnection

In this case, the forecast errors in demand and maximum PV generation are captured by generating 100 scenarios. The Gaussian probability distribution is used to represent the forecast error of the maximum PV generation. The mean value of the probability distribution is the forecasted PV generation in Cases 1 and 2, and the standard deviation is 0.0166 of the mean value. The hourly total upper and lower dispatch limits of PV generation on phase C in 5 scenarios (S1-S5) and the expected upper and lower limits for 100 scenarios are shown in Fig. 3.4. Furthermore, Table 3.7 shows the day-ahead total lower dispatch limits for 5 scenarios and the expected value for 100 scenarios for all phases. The expected upper and lower dispatch limits of PV generation for 100 scenarios are compared to those presented in Case 2. As shown in Table 3.7, the expected total lower PV dispatch limits are smaller than those in Case 2.

3.3.2 Modified IEEE 123-Bus System

Here, the real and reactive peak demands on phase A are 1420 kW and 775 $kVar$; on phase B are 915 kW, 515 $kVar$; and on phase C are 1155 kW and 635 $kVar$, respectively. As shown in Table 3.8, 12 solar PV generation units are installed and the characteristics of the DG units are shown in Table 3.9. Here, DG4 and DG5 are single-phase DGs connected to phase A, and other DG units are three-phase resources. The characteristics of 6 EV clusters are shown in Table 3.10 where EV clusters 1 and 4 are on phase A, EV clusters 2 and 5 are on phase B, and EV clusters 3 and 6 are on phase C. The upper and lower limits of PV generation are evaluated in the following cases:

Case 1 – PV dispatch limits with forecasted PV generation and demand

Case 2 – PV dispatch limits with forecasted PV generation and demand, and the uncertainty in the EV interconnection

3.3.2.1 Case 1 – PV dispatch limits with forecasted PV generation and demand

In this case, the feasible dispatch limits for PV generation are determined while ignoring the EV interconnections to the network. The lower and upper limits for PV generation on phases A, B, and C are shown in Fig. 3.5a, Fig. 3.5b, and Fig. 3.5c respectively. As shown

Table 3.8: Characteristics of PV Generation Units in the IEEE 123-Bus System

PV	Bus	P^{min}	P^{max}	Q^{min}	Q^{max}
1	1	0	400	-200	200
2	13	0	400	-200	200
3	18	0	400	-200	200
4	25	0	400	-200	200
5	40	0	200	-100	100
6	48	0	200	-100	100
7	60	0	200	-100	100
8	70	0	400	-200	200
9	81	0	200	-100	100
10	87	0	400	-200	200
11	101	0	400	-200	200
12	115	0	400	-200	200

Table 3.9: Characteristics of DG Units in the IEEE 123-Bus System

DG	Bus	P^{min}	P^{max}	Q^{min}	Q^{max}
1	29	0	100	-60	60
2	8	0	100	-60	60
3	44	0	100	-60	60
4	111	0	150	-75	75
5	122	0	50	-25	25

Table 3.10: Characteristics of EV Clusters in the IEEE 123-Bus System

EV cluster	Number of vehicles	Bus	P^{max}	E^{min}	E^{max}
1	20	13	148	60	600
2	12	51	88.8	36	360
3	10	65	74	30	300
4	6	18	44.4	18	180
5	20	40	148	60	600
6	10	88	74	30	300

in these figures, once the PV generation is more than demand the excess PV generation is curtailed. At hour 13, the total real demand on phase A is 1405.80 kW; the PV generation units serve the load in this hour and the main distribution feeder and DGs serve 0 kW. The available PV generation at this hour is 1776.768 kW and the PV generation curtailment is 370.968 kW. The lower PV dispatch limits on phases A, B, and C are zero at all hours, which shows that the main distribution feeder and DGs can supply the demand on these phases.

3.3.2.2 Case 2 – PV dispatch limits with forecasted PV generation and demand, and the uncertainty in the EV interconnection

In this case, the maximum battery capacity of each EV is 30 kWh and the minimum capacity is 10% of maximum capacity. EVs can leave at the departure time with a fully charged battery and the forecasted available energy at arrival time is 25% of the maximum EV's battery capacity. The uncertainty sets for the maximum available energy in EV clusters 1-6 are $[540, 600]$ kWh, $[324, 360]$ kWh, $[270, 300]$ kWh, $[162, 180]$ kWh, $[540, 600]$ kWh, and $[270, 300]$ kWh respectively. The uncertainty sets for the minimum available energy for EV clusters 1-6 are $[60, 72]$ kWh, $[36, 43.2]$ kWh, $[30, 36]$ kWh, $[18, 21.6]$ kWh, $[60, 72]$ kWh, and $[30, 36]$ kWh respectively. The uncertainty sets for the available energy at arrival time for EV clusters 1-6 are $[120, 172.8]$ kWh, $[72, 103.68]$ kWh, $[60, 86.4]$ kWh, $[36, 51.84]$ kWh, $[120, 172.8]$ kWh, and $[60, 86.4]$ kWh respectively. The uncertainty sets for the available energy at departure time for EV clusters 1-6 are $[480, 600]$ kWh, $[288, 360]$ kWh, $[240, 300]$ kWh, $[144, 180]$ kWh, $[480, 600]$ kWh, and $[240, 300]$ kWh respectively. The uncertainty sets for the maximum charging/discharging power dispatch for EV clusters 1-6 are $[148, 207.2]$ kW, $[88.8, 124.32]$ kW, $[74, 103.6]$ kW, $[44.4, 62.16]$ kW, $[148, 207.2]$ kW, and $[74, 103.6]$ kW respectively. The uncertainty sets for arrival and departure times are similar to the previous case study. The impacts of V2G operation mode and the budget of uncertainty on the PV dispatch limits are investigated.

a) The impact of V2G operating mode on PV dispatch limits

Fig. 3.5 demonstrates the upper PV dispatch limits with and without V2G capability of the EV clusters. As shown in this figure, once the EVs are connected to the distribution network the upper dispatch limits on all phases are increased compared to Case 1. Table

Table 3.11: Total Upper PV Dispatch Limits in Case 1 and Case 2 with and without V2G

Case	Phase A (kWh)	Phase B (kWh)	Phase C (kWh)
Case 1	12746.876	9358.380	11124.780
Case 2 (with V2G)	13377.627	10022.187	11422.419
Case 2 without V2G	13252.216	9813.846	11357.312

Table 3.12: Total Upper PV Dispatch Limits Considering the Budget of Uncertainty

	Total upper limits on each phase (kWh)		
Scenarios	Phase A	Phase B	Phase C
1 (Case 2)	13377.627	10022.187	11422.419
2	13411.323	10063.659	11435.379
3	13445.019	10105.131	11431.467
4	13445.019	10105.131	11448.339
Case 1	12746.876	9358.380	11124.780

3.11 shows the total upper PV dispatch limit on each phase. As shown in this table, the total upper dispatch limits are increased with V2G capability compared to the case in which EVs do not have V2G capability. Similar to Case 1, the total lower PV dispatch limits on all phases are zero which shows that the main distribution feeder and DGs are capable of supplying the demand. The solution is procured in 6 iterations once the V2G capability of EV clusters is considered.

b) The impact of the budget of uncertainty

Here, similar scenarios shown in Table 3.4 are considered. For all scenarios, the minimum and maximum arrival and departure times are similar to the previous test case. Table 3.12 shows the total upper dispatch limits of PV generation on phases A, B, and C. As shown in this table, the increase in the budget of uncertainty from 0% to 100% will decrease the total upper dispatch limits by 67.392 kW, 82.944 kW and 25.920 kW on phases A, B, and C respectively. Fig. 3.6a, Fig. 3.6b, and Fig. 3.6c demonstrate the effect of the budget

Table 3.13: Total Upper PV Dispatch Limits with Budget of Uncertainty for Arrival/Departure Times

	Total upper limits on each phase (kWh)			Convergence
Scenarios	Phase A	Phase B	Phase C	Iteration
5	13377.627	9968.197	11422.419	6
6	13411.371	10042.433	11422.419	4
7	13421.494	10022.187	11448.747	3
8	13421.494	10076.177	11458.467	3
9	13421.494	10076.177	11469.291	2

Table 3.14: Worst-Case Realization of Arrival and Departure Times in the IEEE 123-bus system

	Arrival and departure times for EV clusters [hour]											
Scenario	$T_1^{a,arv}$	$T_1^{a,dep}$	$T_2^{b,arv}$	$T_2^{b,dep}$	$T_3^{c,arv}$	$T_3^{c,dep}$	$T_4^{a,arv}$	$T_4^{a,dep}$	$T_5^{b,arv}$	$T_5^{b,arv}$	$T_6^{c,arv}$	$T_6^{c,dep}$
1 (Case 2)	10	15	8	17	8	15	8	17	10	15	8	15
2	8	17	8	15	8	15	10	17	8	15	8	15
3	10	17	10	15	10	17	10	15	10	17	10	15
4	10	17	10	15	10	17	10	15	10	17	10	15

of uncertainty on the hourly upper and lower PV dispatch limits on phases A, B, and C, respectively. Here, as the budget of uncertainty decreases the total upper dispatch limits will increase which means less total PV curtailment in the operation horizon. Furthermore, the lower dispatch limits are not affected by the budget of uncertainty. The worst-case realization of the arrival and departure times for the EV clusters are shown in Table 3.14.

Similar to Table 3.6, the impacts of the budget of uncertainty for the arrival and departure

Table 3.15: Simulation time of scenarios in Tables XIV and IV for the IEEE 123-bus system

Scenario	Simulation time (hr: min)	Iteration
1 (Case 2)	3:55	6
2	3:13	5
3	2:38	4
4	3:06	5
Case 1	0:33	2

times, i.e. Λ^{ϕ}_{arv} and Λ^{ϕ}_{dep}, on the total upper PV dispatch limits are shown in Table 3.13. Here, when the budget of uncertainty decreases from 100% to 0%, the total upper dispatch limits on phases A, B, and C increase by 43.867 kW, 107.98 kW, and 46.872 kW respectively. Table 3.13, also shows the number of iterations in which the proposed algorithm converged. It is worth noting that as the number of uncertain variables (i.e. the available energy at arrival and departure times, the maximum and minimum energy and power capacity of the EV clusters, and the arrival and departure times of the EV clusters) increases, the number of constraints formed by using the McCormick envelopes increases. This will increase the number of iterations and the solution time. Table 3.15 shows the simulation times and the number of iterations for scenarios shown in Table 3.12 for the IEEE 123-bus system.

3.4 Conclusion

This chapter presents a framework to quantify the dispatch limits for the PV generation in the unbalanced distribution networks with EV interconnection. The presented framework captures the uncertainties associated with the interconnection of EVs, the available energy at arrival and departure times, as well as the uncertainty in power and energy capacity of the EV clusters. It is shown that integrating the EVs with no V2G will increase the lower or upper dispatch limit of the PV generation as the distribution feeder and DG capacities are limited, and the energy requirement for charging the EVs will increase the lower and upper PV dispatch limits. Moreover, the impact of the budget of uncertainty and the operating mode of EVs (V2G and non-V2G) on the dispatch limits of the PV generation, are investigated. It is shown that increasing the budget of uncertainty for EVs will increase the total lower dispatch limits or decrease the total upper dispatch limits of PV generation in the day-ahead operation. Moreover, V2G reduces the total lower dispatch limits or increases the total upper dispatch limits of PV generation. To capture the uncertainty associated with maximum forecasted PV generation and demand, a scenario-based approach is used to determine the upper and lower dispatch limits of the PV generation. The worst-case realization of the EV interconnection parameters is considered in each scenario and the expected lower and upper PV dispatch limits are calculated.

Future research in this domain could focus on data-driven approaches based on a limited

number of observed samples to quantify the uncertainty associated with the EV interconnection and determine the upper and lower dispatch limits of PV generation. Such approaches could capture distribution network loss to quantify the locational PV dispatch limits in the distribution network.

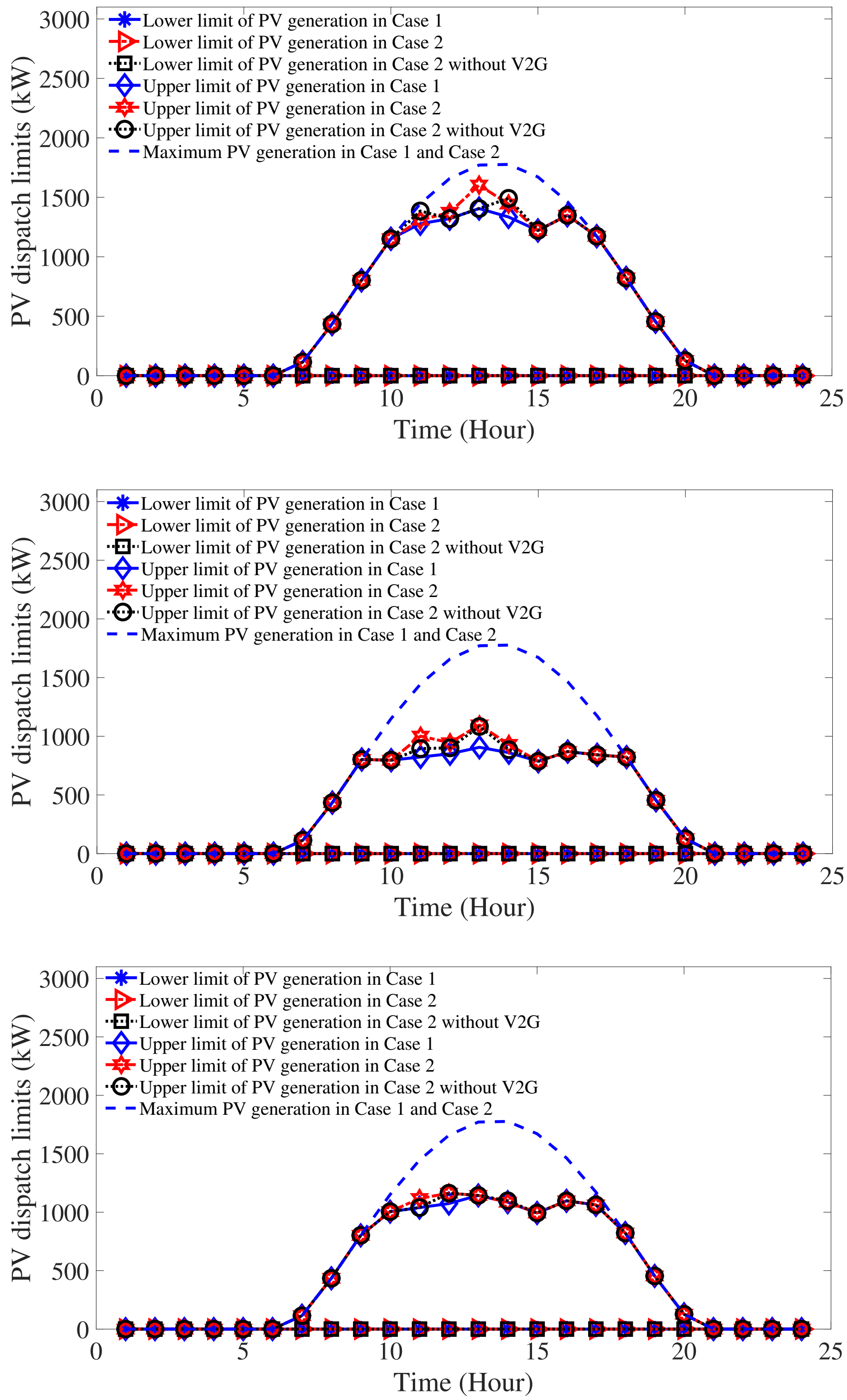

(c)

Figure 3.5: The total PV's dispatch limits for (a) phase A, (b) phase B and (c) phase C in Case 1, and Case 2 with and without V2G.

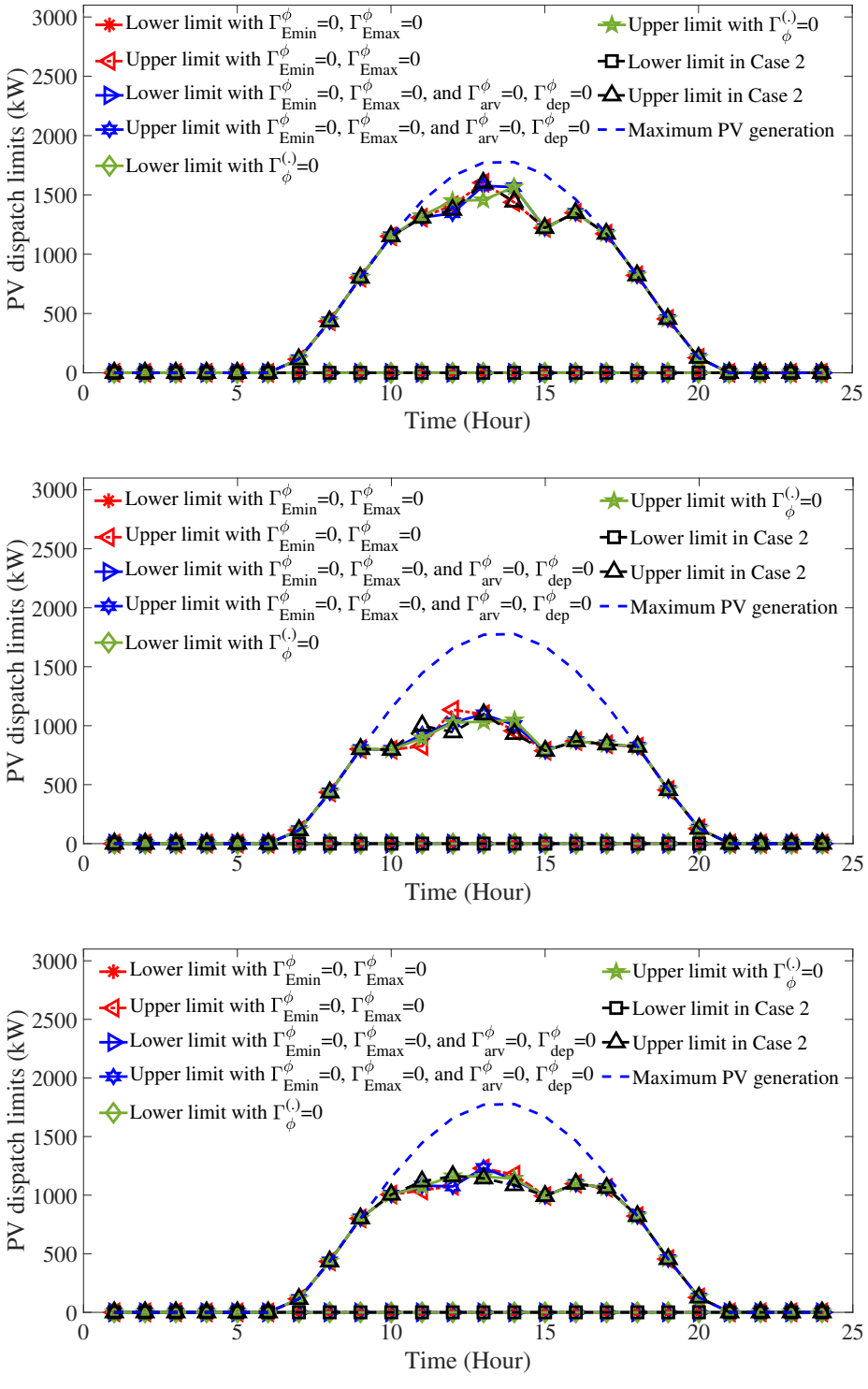

(c)

Figure 3.6: The impact of budget of uncertainty on the PV dispatch limits on (a) phase A, (b) phase B and (c) phase C.

Chapter 4

Solar Photovoltaic Dispatch Margins with Stochastic Unbalanced Demand in Distribution Networks

The increase in the generation capacity of the variable photovoltaic units introduces new challenges to the operation of the unbalanced three-phase distribution networks. In this chapter, a two-stage optimization problem is formulated to identify the feasible dispatch margins of photovoltaic generation considering the distribution network operation constraints. The proposed problem is solved using the column-and-constraint generation approach. The distribution network constraints are formulated as second-order cone constraints. The uncertainty in the forecasted demand and maximum photovoltaic generation as well as the unbalanced operation of the distribution network is considered in the proposed approach. The dispatch margins of photovoltaic generation are quantified considering the worst-case realization of demand in the distribution network. The impacts of energy storage and the ramping limits of the dispatchable generation resources on the dispatch margins of photovoltaic generation are addressed in this network. The dispatch margins of photovoltaic generation are quantified in the modified IEEE 13-bus system. It is shown that enforcing the ramping rates for the dispatchable units will increase the lower dispatch margins of photovoltaic generation, and leveraging energy storage increases the difference between the lower and upper photovoltaic dispatch margins. While earlier research addressed the dispatch limits for renewable resources, the challenges corresponding to the integration of such variable resources in distribution networks including the unbalanced operation of the networks, the uncertainty in demand, and the risk associated with exceeding these limits require further investigation. In the chapter 2, the dispatchability limits of PV generation in the unbalanced distribution network are quantified using a linear approximation of the power flow in the distribution network considering the uncertainties associated with the interconnection of electric vehicles. Furthermore, the impacts of ramp rates and energy storage on the PV

dispatch margins in a distribution network with limited utility grid resources were not investigated. The contributions of this chapter are as follows:

- A framework to determine the dispatch margins for PV resources in the unbalanced distribution network is proposed by formulating a mixed-integer second-order cone programming (MISOCP) problem which is solved as a two-stage problem using the column-and-constraint generation technique.
- The uncertainty in the forecasted maximum PV solar generation is captured by introducing scenarios and the uncertainty in demand is characterized by uncertainty sets.
- The impact of energy storage facilities, as well as the ramping limits of dispatchable generation resources on the PV dispatch margins in the distribution network are investigated.

The rest of the chapter is organized as follows, Section 5.1 presents the formulated problem to determine the PV dispatch margins in the unbalanced distribution networks; Section 5.2 proposes the solution methodology; Section 5.3 presents the numerical analysis to show the effectiveness of the proposed formulation and solution approach, and Section 5.4 presents the conclusion.

Nomenclature

Sets and Indices:

- b Index of bus
- d Index of demand
- e Index of energy storage
- i Index of distributed generation
- l Index of distribution branch
- n Index of distribution feeder
- v Index of PV generation

– m Index of scenario

– $\mathcal{S}$ Set of scenarios

– $\mathcal{B}$ Set of buses

Variables:

– $l_{v,t}^{\varphi,m}$ Lower margin of PV dispatch in scenario m

– $u_{v,t}^{\varphi,m}$ Upper margin of PV dispatch in scenario m

– $\tilde{l}_{v,t}^{\varphi}$ Risk-based lower margin of PV dispatch

– $\tilde{u}_{v,t}^{\varphi}$ Risk-base upper margin of PV dispatch

– $C_{e,t}^{\varphi,m}$ Available energy in the energy storage unit

– $P_{(.),t}^{\varphi,m}$ Real power output of a unit

– $Q_{(.),t}^{\varphi,m}$ The reactive power output of a unit

– $PL_{l,t}^{\varphi,m}$ Real power flow in a distribution branch

– $QL_{l,t}^{\varphi,m}$ Reactive power flow in a distribution branch

– $SL_{l,t}^{\varphi,m}$ Apparent power flow in a distribution branch

– $\mathbf{U}_{b,t}^{m}$ Vector of square of voltage magnitudes

– $\mathbf{I}_{l,t}^{m}$ Vector of square of current magnitudes

– $s_{b,t}^{(.),\varphi,m}$ Slack variables

– $\sigma_{v,t}^{\varphi,m}$ Auxiliary binary variables representing the worst-case realization of PV generation

– $\rho_{d,t}^{(.),\varphi,m}$ Auxiliary binary variable representing the worst-case realization of demand

– μ Dual variable

Parameters:

- **AD** Bus-demand incidence matrix
- **AE** Bus-energy storage incidence matrix
- **AG** Bus-distributed generation incidence matrix
- **AL** Bus-branch incidence matrix
- **AV** Bus-photovoltaic incidence matrix
- **AN** Bus-feeder incidence matrix
- **LN** Feeder-branch incidence matrix
- **BN** Feeder-bus incidence matrix
- **BF** Bus-branch incidence matrix for buses at the sending end of the branches
- **AI** Bus-branch incidence matrix for buses at the receiving end of the branches
- $\underline{\mathbf{V}}_b, \overline{\mathbf{V}}_b$ Vector of square of voltage magnitude's lower and upper limits
- $\bar{\mathbf{I}}_l$ Vector of square of current magnitude's upper limits
- $C_e^{0,\varphi}$ The initial energy of an energy storage unit
- $P_{v,t}^{\varphi,f,m}$ Forecasted maximum PV generation
- $P_v^{\varphi,max}$ Capacity of a PV generation unit
- $\boldsymbol{r}_l$ Resistance matrix of a distribution branch
- $\boldsymbol{x}_l$ Inductive reactance matrix of a distribution branch
- $\boldsymbol{p}_l$ Vector of binary parameters representing the availability of phases in a distribution branch
- $SL_l^{\varphi,max}$ Apparent power capacity of a distribution branch

- $P_{(.)}^{\varphi,max}$ Real power capacity of a unit
- $Q_{(.)}^{\varphi,max}$ Reactive power capacity of a unit
- $\underline{P}_{d,t}^{\varphi}, \overline{P}_{d,t}^{\varphi}$ Lower and upper bounds of uncertain real power demand
- $P_{d,t}^{\varphi,f}$ Forecasted real power demand
- $\underline{Q}_{d,t}^{\varphi}, \overline{Q}_{d,t}^{\varphi}$ Lower and upper bounds of uncertain reactive power demand
- $Q_{d,t}^{\varphi,f}$ Forecasted reactive power demand
- $S_{(.)}^{\varphi,max}$ Maximum apparent power of a unit
- PF_n Power factor at distribution feeder
- Γ_t^{φ} The budget of uncertainty for real and reactive power

4.1 Problem Formulation

Determining the PV dispatch margins could be considered as finding the largest uncertainty set for which a robust optimization problem could be solved to determine the feasible operation decisions in the distribution network. This problem is formulated as an optimization problem in which the objective is to maximize the PV generation range such that the distribution feeder and other dispatchable generation resources could accommodate the PV generation without violating the network constraints. Here, such limits are determined considering the unbalanced generation and demand in the distribution network and the unbalanced distribution network topology. The problem formulation is shown in (4.1)-(4.32). The objective function is shown in (4.1) where the objective is to expand the feasibility region for PV dispatch by maximizing the distance between the lower and upper margins while ensuring the existence of PV dispatch within these margins. Here, once $V_{v,t}^{\varphi,m} = 0$, the PV dispatch is within the upper and lower margins, and otherwise, the PV output will be outside of the dispatch margins. Therefore, minimizing $V_{v,t}^{\varphi,m}$ would accommodate the PV output between the upper and lower margins. The second term in the minimization problem is the normalized difference between the upper and lower dispatch margins of PV. The worst-case

realizations of PV generation and demand are determined using the formulated max-min problem in which the slack variables that represent the mismatches in real and reactive power are minimized in (4.1).

The distribution network constraints are given in (4.2)-(4.9). The nodal real and reactive power balances are enforced in (4.2) and (4.3), respectively. Here, $PL_{l,t}^{\varphi,m} \in \boldsymbol{PL}_{l,t}^{m}$, $P_{i,t}^{\varphi,m} \in \boldsymbol{PG}_{i,t}^{m}$, $P_{v,t}^{\varphi,m} \in \boldsymbol{PV}_{v,t}^{m}$, $P_{e,t}^{\varphi,m} \in \boldsymbol{PE}_{e,t}^{m}$, $P_{n,t}^{\varphi,m} \in \boldsymbol{PN}_{n,t}^{m}$, and $P_{d,t}^{\varphi,m} \in \boldsymbol{PD}_{d,t}^{m}$. Similar variables are defined for the reactive power generation and demand in the network i.e. $QL_{l,t}^{\varphi,m} \in \boldsymbol{QL}_{l,t}^{m}$, $Q_{i,t}^{\varphi,m} \in \boldsymbol{QG}_{i,t}^{m}$, $Q_{v,t}^{\varphi,m} \in \boldsymbol{QV}_{v,t}^{m}$, $Q_{e,t}^{\varphi,m} \in \boldsymbol{QE}_{e,t}^{m}$, $Q_{n,t}^{\varphi,m} \in \boldsymbol{QN}_{n,t}^{m}$, and $Q_{d,t}^{\varphi,m} \in \boldsymbol{QD}_{d,t}^{m}$. The power flow in distribution branch is formulated by (4.4), (4.5). Here, $\widetilde{\boldsymbol{R}}_l$ and $\widetilde{\boldsymbol{X}}_l$ are the resistance and inductive reactance matrices of the unbalanced branch l that are determined using the formulation presented in [99]. The big-M method is used to relax the power flow constraint once the certain phases on a distribution branch do not exist and $p_l^{\varphi} \in \mathbf{p}_l$. The relationship between the real and reactive power at the sending end of each branch is presented as (4.6) using a quadratic constraint which is further reformulated as a second-order cone constraint [102,103]. Similar constraint is presented in (4.7) to enforce the real and reactive power capacity of the distribution feeder. The branch currents and nodal voltages are limited by (4.8) and (4.9) respectively.

The operation constraints of feeder, DG, PV generation, and energy storage system (ESS), are given in (4.10)-(4.20). The real power from the feeder is restricted by (4.10) and the reactive power supplied by the distribution feeder is constrained by (4.11)-(4.12) considering the acceptable power factor at the feeder. The dispatched real power of a DG unit is limited by the minimum and maximum real power capacity of the unit as enforced by (4.13). A similar constraint is considered for the reactive power dispatch of the unit. The power ramp for dispatchable DG units is enforced by (4.14). Moreover, the PV output is limited by the forecasted generation as shown in (4.15). The reactive power output of a PV unit is within the upper and lower acceptable limits as shown in (4.16). Similar constraints are considered for the real and reactive power dispatch of the ESS. The available energy in the ESS is calculated using (4.17) where the stored energy is within the minimum and maximum limits as enforced by (4.18) [104]. The available energy in the ESS at the beginning and end of the simulation period is enforced to be the same as shown in (4.19) and (4.20).

The rest of the constraints are given in (4.21)-(4.32). The lower dispatch margin is lower than the upper margin as shown in (4.21) and the upper margin is limited by the maximum PV capacity as shown in (4.22). As enforced by (4.23)-(4.24), if $V_{v,t}^{\varphi,m} = 1$, the lower and upper dispatch margins are zero. The worst-case realization of the uncertain PV generation within the polyhedral uncertainty set is determined by (4.25) [105]. The slack variables are positive as enforced by (4.26). Considering the worst-case realization of the demand would impose new constraints (4.27)-(4.32) to the problem. Here, the uncertainty in demand is captured by a polyhedral set and therefore, the real and reactive demand is represented by (4.27) and (4.28) respectively. The auxiliary binary variables used to enforce the uncertain real and reactive demands are mutually exclusive as shown in (4.29) and (4.30). The conservativeness of the solution is determined by the budget of uncertainty. Here, the budget of uncertainty is considered for the real and reactive demands using (4.31) and (4.32) respectively. As Γ_t^{φ} increases in (4.31), and (4.32) the budget of uncertainty will increase and the solution will be more conservative.

$$\min_{u_{v,t}^{\varphi,m}, l_{v,t}^{\varphi,m}, V_{v,t}^{\varphi,m}} \sum_{v,\varphi,m,t} \left[V_{v,t}^{\varphi,m} - (u_{v,t}^{\varphi,m} - l_{v,t}^{\varphi,m}) / P_v^{\varphi,max} \right] + \max_{\sigma_{v,t}^{\varphi,m}, \rho_{d,t}^{(.),\varphi,m}} \min_{s_{(.)}^{(.)}} \sum_{b,\varphi,m,t} \left(s_{b,t}^{1,\varphi,m} + s_{b,t}^{2,\varphi,m} + s_{b,t}^{3,\varphi,m} + s_{b,t}^{4,\varphi,m} \right) \quad (4.1)$$

s.t.

$$\mathbf{AL} \cdot \mathbf{PL}_{l,t}^{m} - \mathbf{AI} \cdot \mathbf{I}_{l,t}^{m} \cdot \widetilde{\mathbf{R}}_l + \mathbf{AG} \cdot \mathbf{PG}_{i,t}^{m} + \mathbf{AV} \cdot \mathbf{PV}_{v,t}^{m} + \mathbf{AE} \cdot \mathbf{PE}_{e,t}^{m} + \mathbf{AN} \cdot \mathbf{PN}_{n,t}^{m} + s_{b,t}^{1,\varphi,m} - s_{b,t}^{2,\varphi,m} = \mathbf{AD} \cdot \mathbf{PD}_{d,t}^{m} \quad (4.2)$$

$$\mathbf{AL} \cdot \mathbf{QL}_{l,t}^{m} - \mathbf{AI} \cdot \mathbf{I}_{l,t}^{m} \cdot \widetilde{\mathbf{X}}_l + \mathbf{AG} \cdot \mathbf{QG}_{i,t}^{m} + \mathbf{AV} \cdot \mathbf{QV}_{v,t}^{m} + \mathbf{AE} \cdot \mathbf{QE}_{e,t}^{m} + \mathbf{AN} \cdot \mathbf{QN}_{n,t}^{m} + s_{b,t}^{3,\varphi,m} - s_{b,t}^{4,\varphi,m} = \mathbf{AD} \cdot \mathbf{QD}_{d,t}^{m} \quad (4.3)$$

$$\mathbf{AL}^{\top} \cdot \mathbf{U}_{b,t}^{m} + 2(\widetilde{\mathbf{R}}_l \cdot \mathbf{PL}_{l,t}^{m} + \widetilde{\mathbf{X}}_l \cdot \mathbf{QL}_{l,t}^{m}) + (\widetilde{\mathbf{R}}_l^2 + \widetilde{\mathbf{X}}_l^2) \cdot \mathbf{I}_{l,t}^{m} \leq M \cdot (1 - \mathbf{p}_l) \quad (4.4)$$

$$\mathbf{AL}^{\top} \cdot \mathbf{U}_{b,t}^{m} + 2(\widetilde{\mathbf{R}}_l \cdot \mathbf{PL}_{l,t}^{m} + \widetilde{\mathbf{X}}_l \cdot \mathbf{QL}_{l,t}^{m}) + (\widetilde{\mathbf{R}}_l^2 + \widetilde{\mathbf{X}}_l^2) \cdot \mathbf{I}_{l,t}^{m} \geq -M \cdot (1 - \mathbf{p}_l) \quad (4.5)$$

$$(\mathbf{PL}_{l,t}^{m})^2 + (\mathbf{QL}_{l,t}^{m})^2 \leq (\mathbf{BF} \cdot \mathbf{U}_{b,t}^{m}) \cdot \mathbf{I}_{l,t}^{m} \tag{4.6}$$

$$(\mathbf{PN}_{n,t}^{m})^2 + (\mathbf{QN}_{n,t}^{m})^2 \leq (\mathbf{BN} \cdot \mathbf{U}_{b,t}^{m}) \cdot (\mathbf{LN} \cdot \mathbf{I}_{l,t}^{m}) \tag{4.7}$$

$$\mathbf{I}_{l,t}^{m} \leq \bar{\mathbf{I}}_{l} \tag{4.8}$$

$$\underline{\mathbf{V}}_{b} \leq \mathbf{U}_{b,t}^{m} \leq \overline{\mathbf{V}}_{b} \tag{4.9}$$

$$P_{n}^{\varphi,min} \leq P_{n,t}^{\varphi,m} \leq P_{n}^{\varphi,max} \tag{4.10}$$

$$Q_{n,t}^{\varphi,m} \leq tan\left(\cos^{-1} PF_{n}\right) \cdot P_{n,t}^{\varphi,m} \tag{4.11}$$

$$Q_{n,t}^{\varphi,m} \geq -tan\left(\cos^{-1} PF_{n}\right) \cdot P_{n,t}^{\varphi,m} \tag{4.12}$$

$$P_{i}^{\varphi,min} \leq P_{i,t}^{\varphi,m} \leq P_{i}^{\varphi,max} \tag{4.13}$$

$$-R_{i} \leq P_{i,t}^{\varphi,m} - P_{i,t-1}^{\varphi,m} \leq R_{i} \tag{4.14}$$

$$0 \leq P_{v,t}^{\varphi,m} \leq P_{v,t}^{\varphi,f,m} \tag{4.15}$$

$$-Q_{v}^{\varphi,max} \leq Q_{v,t}^{\varphi,m} \leq Q_{v}^{\varphi,max} \tag{4.16}$$

$$C_{e,t}^{\varphi,m} = C_{e,t-1}^{\varphi,m} - P_{e,t}^{\varphi,m} \tag{4.17}$$

$$C_{e}^{\varphi,min} \leq C_{e,t}^{\varphi,m} \leq C_{e}^{\varphi,max} \tag{4.18}$$

$$C_{e,0}^{\varphi,m} = C_{e,24}^{\varphi,m} \tag{4.19}$$

$$C_{e,0}^{\varphi,m} = C_{e}^{0,\varphi,m} \tag{4.20}$$

$$0 \leq l_{v,t}^{\varphi,m} \leq u_{v,t}^{\varphi,m} \tag{4.21}$$

$$u_{v,t}^{\varphi,m} \leq P_{v}^{\varphi,max} \tag{4.22}$$

$$\left(P_{v}^{\varphi,max} - P_{v,t}^{\varphi,f,m}\right).V_{v,t}^{\varphi,m} - l_{v,t}^{\varphi,m} \geq -P_{v,t}^{\varphi,f,m} \tag{4.23}$$

$$P_{v,t}^{\varphi,f,m} \cdot V_{v,t}^{\varphi,m} + u_{v,t}^{\varphi,m} \leq P_{v,t}^{\varphi,f,m} \tag{4.24}$$

$$P_{v,t}^{\varphi,m} = l_{v,t}^{\varphi,m} + \left(u_{v,t}^{\varphi,m} - l_{v,t}^{\varphi,m}\right).\sigma_{v,t}^{\varphi,m} \tag{4.25}$$

$$s_{b,t}^{1,\varphi,m}, s_{b,t}^{2,\varphi,m}, s_{b,t}^{3,\varphi,m}, s_{b,t}^{4,\varphi,m} \geq 0 \tag{4.26}$$

$$P_{d,t}^{\varphi,m} = \underline{P}_{d,t}^{\varphi} \cdot \rho_{d,t}^{1p,\varphi,m} + P_{d,t}^{\varphi,f} \cdot \rho_{d,t}^{2p,\varphi,m} + \overline{P}_{d,t}^{\varphi} \cdot \rho_{d,t}^{3p,\varphi,m} \tag{4.27}$$

$$Q_{d,t}^{\varphi,m} = \underline{Q}_{d,t}^{\varphi} \cdot \rho_{d,t}^{1q,\varphi,m} + Q_{d,t}^{\varphi,f} \cdot \rho_{d,t}^{2q,\varphi,m} + \overline{Q}_{d,t}^{\varphi} \cdot \rho_{d,t}^{3q,\varphi,m} \tag{4.28}$$

$$\rho_{d,t}^{1p,\varphi,m} + \rho_{d,t}^{2p,\varphi,m} + \rho_{d,t}^{3p,\varphi,m} = 1 \tag{4.29}$$

$$\rho_{d,t}^{1q,\varphi,m} + \rho_{d,t}^{2q,\varphi,m} + \rho_{d,t}^{3q,\varphi,m} = 1 \tag{4.30}$$

$$\sum_{d} (\rho_{d,t}^{1p,\varphi,m} + \rho_{d,t}^{3p,\varphi,m}) \leq \Gamma_t^{\varphi} \tag{4.31}$$

$$\sum_{d} (\rho_{d,t}^{1q,\varphi,m} + \rho_{d,t}^{3q,\varphi,m}) \leq \Gamma_t^{\varphi} \tag{4.32}$$

4.2 Solution Methodology

The compact form of the problem formulation is presented in (4.33)-(4.38) as follows:

$$\min_{\boldsymbol{x}} \ \boldsymbol{c}^{\top}\boldsymbol{x} + \max_{\boldsymbol{\xi}} \ \min_{\boldsymbol{y}} \ \boldsymbol{b}^{\top}\boldsymbol{y} \tag{4.33}$$

s.t.

$$\boldsymbol{A}\boldsymbol{x} \leq \boldsymbol{d} \tag{4.34}$$

$$\boldsymbol{F}\boldsymbol{x} + \boldsymbol{Q}\boldsymbol{y} + (\boldsymbol{D} \cdot \boldsymbol{x})^{\top}\boldsymbol{\xi} + \boldsymbol{M}\boldsymbol{\xi} = \boldsymbol{h} \tag{4.35}$$

$$\boldsymbol{E}\boldsymbol{y} \leq \boldsymbol{g} \tag{4.36}$$

$$\|\boldsymbol{G}\boldsymbol{y}\|_2 \leq \boldsymbol{m}^{\top}\boldsymbol{y} \tag{4.37}$$

$$\boldsymbol{L}\boldsymbol{\xi} \leq \boldsymbol{w} \tag{4.38}$$

The problem is reformulated as a two-stage robust optimization problem, where $\boldsymbol{x}$ is the vector of first-stage decision variables i.e. $\left[l_{v,t}^{\varphi,m}, u_{v,t}^{\varphi,m}, V_{v,t}^{\varphi,m}\right]$ and $\boldsymbol{y}$ is the vector of second-stage recourse decision variables i.e. $P_{v,t}^{\varphi,m}$, $P_{e,t}^{\varphi,m}$, $P_{n,t}^{\varphi,m}$, $P_{i,t}^{\varphi,m}$, $Q_{v,t}^{\varphi,m}$, $Q_{n,t}^{\varphi,m}$, $Q_{i,t}^{\varphi,m}$, $PL_{l,t}^{\varphi,m}$, $QL_{l,t}^{\varphi,m}$ and $s_{b,t}^{(.),\varphi,m}$ as well as the voltage magnitude on the buses ($\boldsymbol{U}_{b,t}^{m}$). Here, $\boldsymbol{\xi}$ is a vector representing the uncertain variables where $\rho_{d,t}^{(.),\varphi,m} \in \boldsymbol{\xi}$ and $\sigma_{v,t}^{\varphi,m} \in \boldsymbol{\xi}$. The constraint (4.34) represents (4.21)-(4.24); constraint (4.35) represents the set of constraints (4.2)-(4.3), (4.25),

(4.27) and (4.28). Constraint (4.37) represents constraints (4.6)-(4.7). Constraints (4.38), represents constraints (4.29)-(4.32). The rest of the constraints are represented by constraint (4.36).

The proposed solution approach is based on the column-and-constraint generation algorithm presented in [86]. The flowchart of the proposed solution methodology is shown in Fig. 4.1. As shown in this figure, in the master problem (first stage), the upper and lower margins of PV generation are determined by maximizing the difference between the upper and lower margins, using the normalized term $(u_{v,t}^{\varphi,m} - l_{v,t}^{\varphi,m})/P_v^{\varphi,max}$ in the objective function. By solving the subproblem at the second stage, the operation decisions considering the worst-case realization of the uncertain variables are determined. The solution procedure is presented in the following steps.

1) Step 1 – Initialize the iteration count at $k = 0$ and the convergence threshold at $\varepsilon_1 \leq 10^{-3}$. Set the $LB = -\infty$ and $UB = \infty$.

2) Step 2 – Solve the master problem with the objective function shown in (4.39) and the constraints (4.40)-(4.44). Determine the solution for $l_{v,t}^{\varphi,m}, u_{v,t}^{\varphi,m}, V_{v,t}^{\varphi,m}$ by fixing the solution obtained from the subproblem (e.g. ξ^*). The upper and lower margins of the PV generation determined in the master problem ($\boldsymbol{x}^*$) are passed to the subproblem.

$$\min_{\boldsymbol{x}} \quad \boldsymbol{c}^\top \boldsymbol{x} + \eta \tag{4.39}$$

s.t.

$$\boldsymbol{A}\boldsymbol{x} \leq \boldsymbol{d} \tag{4.40}$$

$$\eta \geq \boldsymbol{b}^\top \boldsymbol{y}^l; \forall l \leq k \tag{4.41}$$

$$\boldsymbol{F}\boldsymbol{x} + \boldsymbol{Q}\boldsymbol{y}^l + (\boldsymbol{D} \cdot \boldsymbol{x})^\top \boldsymbol{\xi}^* + \boldsymbol{M}\boldsymbol{\xi}^* = \boldsymbol{h}; \forall l \leq k \tag{4.42}$$

$$\boldsymbol{E}\boldsymbol{y}^l \leq \boldsymbol{g}; \forall l \leq k \tag{4.43}$$

$$\left\| \boldsymbol{G}\boldsymbol{y}^l \right\|_2 \leq \boldsymbol{m}^\top \boldsymbol{y}^l; \forall l \leq k \tag{4.44}$$

Update the LB using (4.45):

$$LB = \boldsymbol{c}^\top \boldsymbol{x}^* + \hat{\eta}_{k+1} \tag{4.45}$$

3) Step 3 –Solve the subproblem with the objective function in (4.46) and constraints (4.47)-(4.50).

$$\max_{\boldsymbol{\xi}} \quad \min_{\boldsymbol{y}} \quad \boldsymbol{b}^{\top}\boldsymbol{y} \tag{4.46}$$

s.t.
$$\boldsymbol{Q}\boldsymbol{y} = \boldsymbol{h} - (\boldsymbol{D}\cdot\boldsymbol{x}^{*})^{\top}\boldsymbol{\xi} - \boldsymbol{M}\boldsymbol{\xi} - \boldsymbol{F}\boldsymbol{x}^{*} \quad : \boldsymbol{\mu}_1 \tag{4.47}$$

$$\boldsymbol{E}\boldsymbol{y} \leq \boldsymbol{g} \qquad : \boldsymbol{\mu}_2 \tag{4.48}$$

$$\|\boldsymbol{G}\boldsymbol{y}\|_2 \leq \boldsymbol{m}^{\top}\boldsymbol{y} \qquad : \boldsymbol{\mu}_3, \boldsymbol{\mu}_4 \tag{4.49}$$

$$\boldsymbol{L}\boldsymbol{\xi} \leq \boldsymbol{w} \tag{4.50}$$

Here, the subproblem (4.46)-(4.50) is reformulated as (4.51)-(4.55) using the duality theory.

$$\psi(\boldsymbol{y}) = \max_{\boldsymbol{\xi}} \left[\boldsymbol{h} - (\boldsymbol{D}\cdot\boldsymbol{x}^{*})^{\top}\boldsymbol{\xi} - \boldsymbol{M}\boldsymbol{\xi} - \boldsymbol{F}\boldsymbol{x}^{*}\right]^{\top}\boldsymbol{\mu}_1 + \boldsymbol{g}^{\top}\boldsymbol{\mu}_2 \tag{4.51}$$

s.t.
$$\boldsymbol{Q}^{\top}\boldsymbol{\mu}_1 + \boldsymbol{E}^{\top}\boldsymbol{\mu}_2 \leq \boldsymbol{b} \tag{4.52}$$

$$\|\boldsymbol{\mu}_3\|_2 \leq \boldsymbol{\mu}_4 \tag{4.53}$$

$$\boldsymbol{L}\boldsymbol{\xi} \leq \boldsymbol{w} \tag{4.54}$$

$$\boldsymbol{\mu}_2 \leq 0, \quad \boldsymbol{\mu}_1 \quad free \tag{4.55}$$

The nonlinear term $\boldsymbol{\mu}_1\boldsymbol{\xi}$ in (4.51) is linearized using McCormick envelopes. Considering $\boldsymbol{\upsilon} = \boldsymbol{\mu}_1\boldsymbol{\xi}$, the nonlinear term $\boldsymbol{\upsilon}$ is linearized by (4.56)-(4.59) [106].

$$\boldsymbol{\upsilon} \geq \underline{\boldsymbol{\mu}}_1\boldsymbol{\xi} + \boldsymbol{\mu}_1\underline{\boldsymbol{\xi}} - \underline{\boldsymbol{\mu}}_1\underline{\boldsymbol{\xi}} \tag{4.56}$$

$$\boldsymbol{\upsilon} \geq \overline{\boldsymbol{\mu}}_1\boldsymbol{\xi} + \boldsymbol{\mu}_1\overline{\boldsymbol{\xi}} - \overline{\boldsymbol{\mu}}_1\overline{\boldsymbol{\xi}} \tag{4.57}$$

$$\boldsymbol{\upsilon} \leq \overline{\boldsymbol{\mu}}_1\boldsymbol{\xi} + \boldsymbol{\mu}_1\underline{\boldsymbol{\xi}} - \overline{\boldsymbol{\mu}}_1\underline{\boldsymbol{\xi}} \tag{4.58}$$

$$\boldsymbol{\upsilon} \leq \boldsymbol{\mu}_1 \overline{\boldsymbol{\xi}} + \underline{\boldsymbol{\mu}}_1 \boldsymbol{\xi} - \underline{\boldsymbol{\mu}}_1 \overline{\boldsymbol{\xi}} \tag{4.59}$$

Update the upper bound of the solution using (4.60) and go to *Step 4*.

$$UB = min\{UB, \boldsymbol{c}^\top \boldsymbol{x}^{*(k+1)} + \psi(\boldsymbol{y}^{*(k+1)})\} \tag{4.60}$$

4) Step 4 – Check if $UB - LB \leq \varepsilon_1$. If this condition is satisfied, terminate the procedure; otherwise, go to *Step 5*.

5) Step 5 – Generate the columns and constraints by creating additional decision variables and adding constraint (4.41)-(4.44). Set $k = k + 1$ and go to *Step 2*.

4.3 Numerical Results

In this section, the modified IEEE-13 bus system is considered as a test case. The simulations are performed on a PC with Intel 3.4 GHz Core i5 processor and 8 GB memory, using MOSEK solver. The diagram of the modified IEEE 13-bus system is shown in Fig. 4.2 and the characteristics of dispatchable DG and PV units are shown in Tables 4.1 and 4.2 respectively. All DG units except DG4 are three-phase units. DG4 is a single-phase unit installed on phase C. The total peak real power demand on phases A, B, and C are 1175 kW, 1039 kW, and 1252 kW respectively. The total peak reactive power demand on phases A, B, and C are 616 kVAr, 665 kVAr, and 771 kVAr respectively. Fig. 4.3 shows the demand profile and the total PV generation in the operation horizon. The forecasted PV generation is determined based on the solar radiation for location ID 883549 on 8/9/2017 from [107]. The approximated feeder capacity is 2800 kW with the least acceptable power factor of 0.82. The dispatch margins of PV generation in the three-phase unbalanced system are evaluated in Cases 1-3 and the impacts of ramping limits of DG units and ESS on the dispatch margins of PV generation are evaluated in Case 4.

Case 1 – PV dispatch margins with forecasted maximum PV generation and demand.

Case 2 – PV dispatch margins with forecasted maximum PV generation and worst-case realization of demand.

Case 3 – PV dispatch margins with uncertain maximum PV generation and uncertain demand.

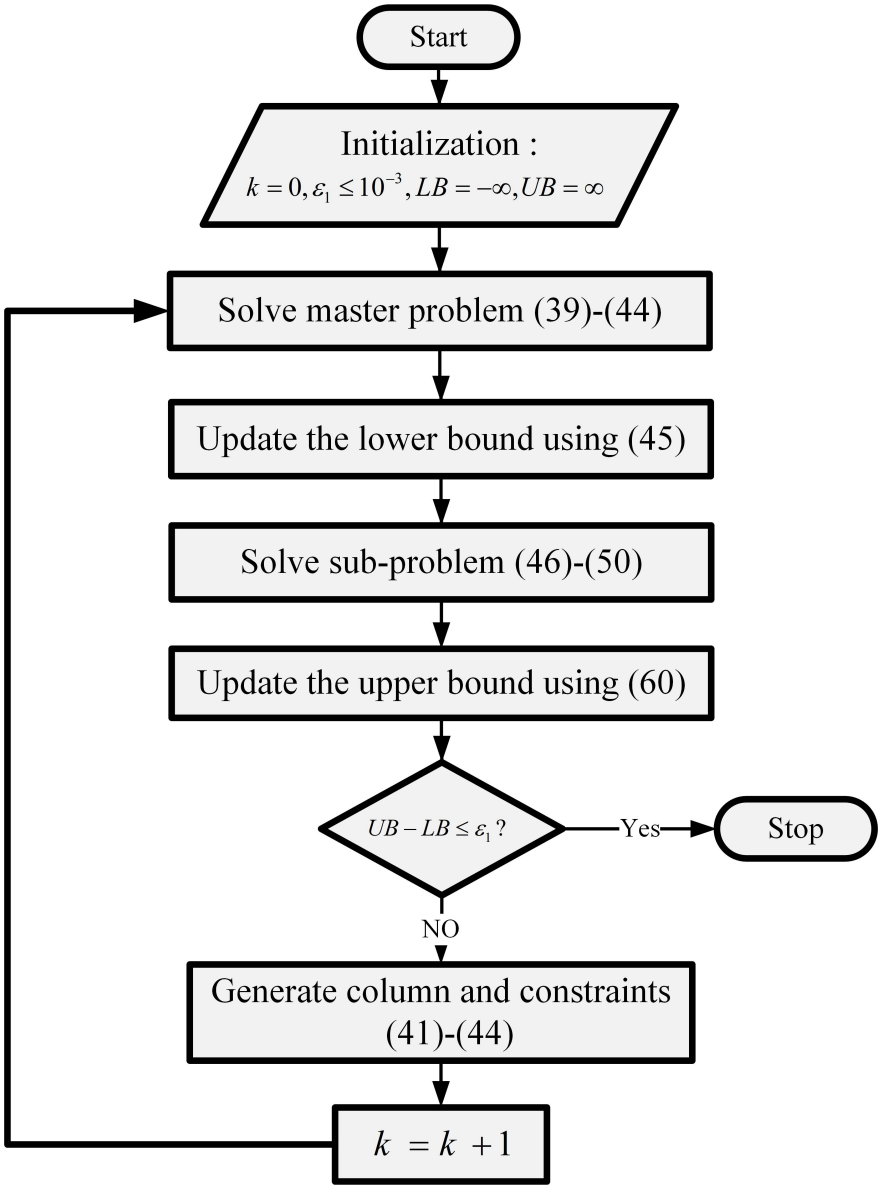

Figure 4.1: The proposed solution algorithm

Case 4 - Operation in island mode with the loss of the main feeder

4.3.1 Case1 – PV dispatch margins with forecasted maximum PV generation and demand

In this case, the demand and maximum PV generation follow the respective forecasted profiles. The dispatch margins of PV generation on phase C are shown in Fig. 4.4. Here, the lower dispatch margin of PV generation on phase C is increased from 11.018 kW at hour 8, to 23.585 kW and 73.917 kW at hours 9 and 10 respectively. Similarly, the lower dispatch

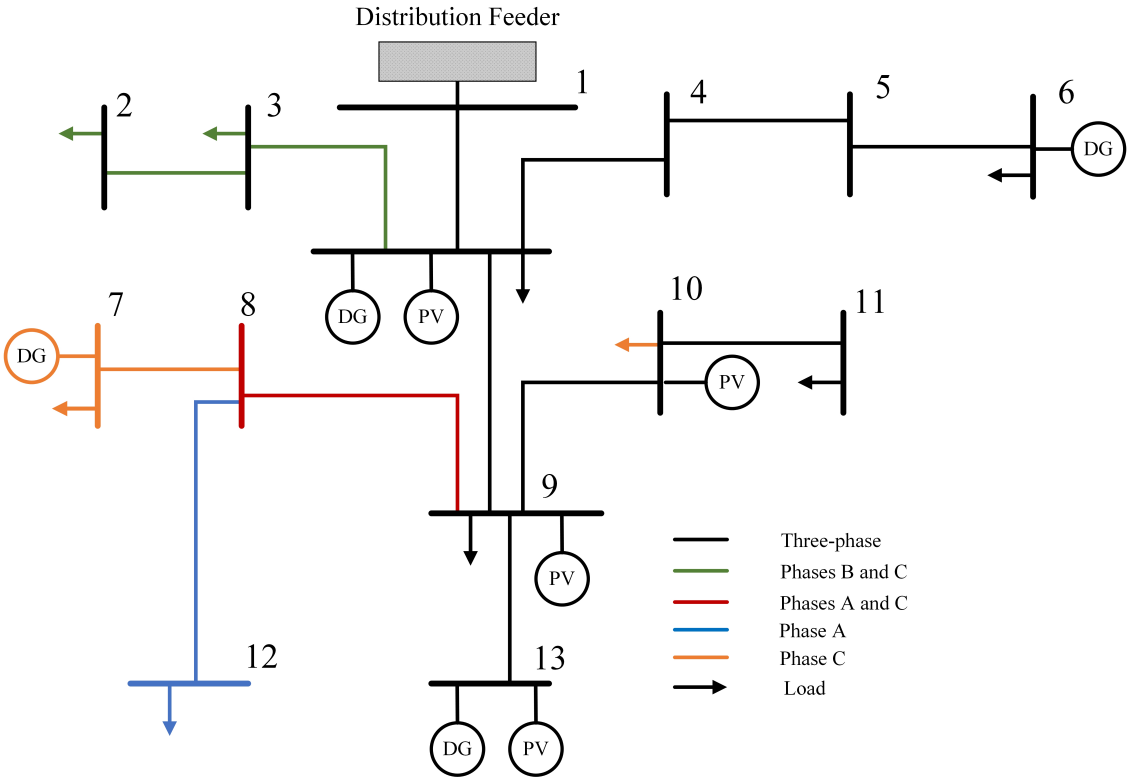

Figure 4.2: The modified IEEE 13-bus distribution network.

Table 4.1: Dispatchable DG Units' Characteristics

DG	Bus	P^{min} (kW)	P^{max} (kW)	Q^{min} (kVAR)	Q^{max} (kVAR)
1	4	0	200	-100	100
2	6	0	200	-100	100
3	13	0	250	-120	120
4	7	0	40	-20	20

margin of PV generation is increased from 36.182 kW at hour 15, to 48.752 kW at hours 16 and 17. At hour 10, the demand on phase C is 1252 kW, and the total output of the feeder and DG units is 1229.094 kW. The power loss at this hour is 51.094 kW and therefore, the total power loss and demand at this hour is 1303.094 kW. Decreasing the dispatch of PV generation will result in the increase in the dispatch of DG units and the main feeder; however, the total dispatch of DG units and the main feeder cannot exceed 1229.094 kW

Table 4.2: PV Generation Units' Characteristics

PV	Bus	P^{min}	P^{max}	Q^{min}	Q^{max}
1	13	0	200	-100	100
2	10	0	200	-100	100
3	9	0	200	-100	100
4	4	0	100	-50	50

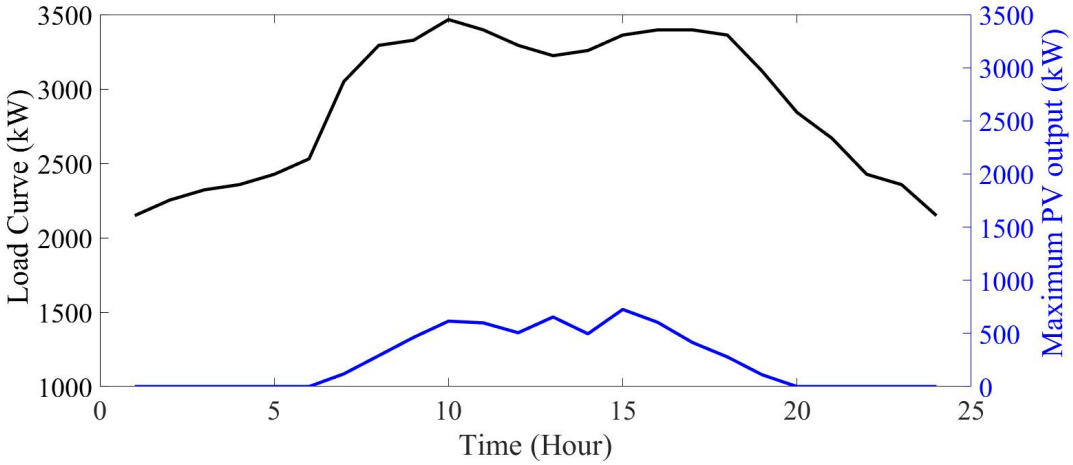

Figure 4.3: Daily profile of demand and maximum PV generation.

as they reach their maximum power capacities. Therefore, the lower PV dispatch margin at hour 10 on phase C is 73.917 kW. Similarly, at hour 11, the demand on phase C is 1226.9 kW and the total output power of the feeder and DG units is 1230.848 kW. At this hour the power loss is 52.640 kW and therefore, the total power loss and demand reaches 1279.6 kW. The lower dispatch margin of PV generation on phase C at this hour is 48.752 kW. In this case, the lower dispatch margins on phase B are zero at all hours.

4.3.2 Case 2 – PV dispatch margins with forecasted maximum PV generation and worst-case realization of demand

In this case, the uncertainty set for demand is within 0.95 and 1.05 of the forecasted values. The upper and lower margins for PV generations were determined considering the worst-case realization of demand within the uncertainty set. The budget of uncertainty is defined as the portion of demand entities that have the flexibility to variate within the

uncertainty set. If the budget of uncertainty is 0%, the demand equals the forecasted value. When the budget of uncertainty is increased to 100%, the demand on all phases at all buses could vary between the possible minimum and maximum values represented by the uncertainty set. The PV dispatch margins on phase C considering the forecasted demand as well as the worst-case realization of the demand are shown in Fig. 4.4. In Fig. 4.4, it is shown that when the budget of uncertainty is 100%, the lower PV dispatch margin increases. In Fig. 4.4, with 100% budget of uncertainty, at hour 10, the demand in the distribution network is 1306.10 kW, the power loss is 12.173 kW and the outputs of the feeder and DG are at their maximum and their total output reaches 1189.99 kW. Therefore, at this hour, the rest of the demand is supplied by the PV units, and the lower margin of PV dispatch increases to 128.282 kW.

The upper margins for PV generation in Case 1 and Case 2 are the same. In Case 2, the lower margins at hours 17 and 18 are 101.907 kW and 89.008 kW respectively. At hour 18, the difference between the lower and upper margins reaches 4.043 kW as the PV generation decreases and the demand reaches 1266.917 kW.

In this case, the maximum PV generation is the same for all phases; however, the demand on phase C is larger than that on the other two phases; therefore, the lower PV dispatch margin on phase C is higher than that on the other phases. Here, the PV generation on phase C is dispatched to serve the demand if the power capacities of the feeder and distributed generation are not adequate to serve the demand on this phase. The dispatch margins for PV generation units on phase C are shown in Fig. 4.5. As shown in this figure, at hour 10, both the minimum and maximum dispatch margin for PV2 and PV3 are 58.538 kW, which indicates that at this hour, the generation unit of PV3 has to be fully dispatched to serve the demand.

The uncertainty in demand will increase the lower PV dispatch margin. Fig. 4.6 shows the difference between the upper and lower margins of the total PV generation as the budget of uncertainty varies from 0% to 100%. As shown in Fig. 4.6, as the budget of uncertainty increases, the difference between the upper and lower dispatch margins will decrease. With a 100% budget of uncertainty, at hour 13, the total real demand of 3376.645 kW and the total loss of 120.484 kW are supplied by the main distribution feeder, DG units and PV

generation units. The main distribution feeder and DG units supply 3300.989 kW and the PV generation units serve 196.14 kW.

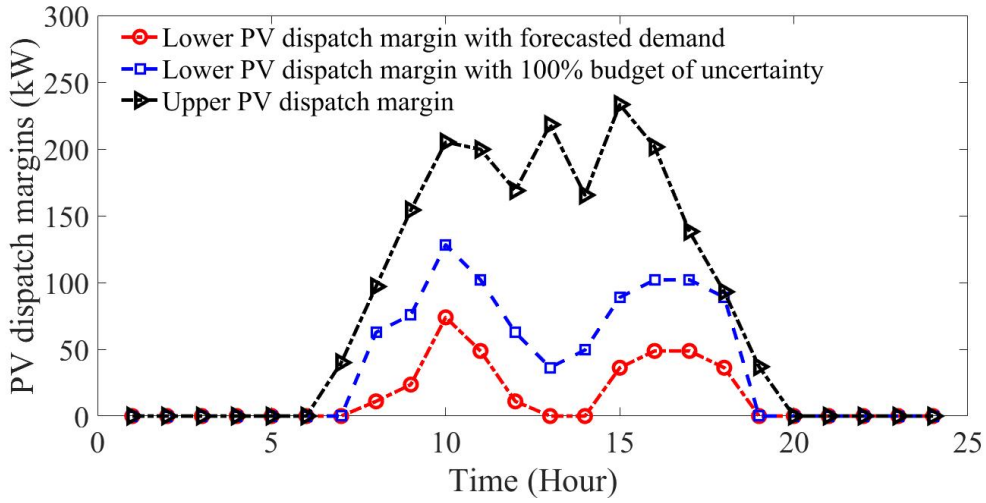

Figure 4.4: The total dispatch margins on phase C with forecasted demand (Case 1) and the worst-case realization of demand with 100% budget uncertainty (Case 2).

4.3.3 Case 3 – PV dispatch margins with uncertain maximum PV generation and demand

Here, the Gaussian probability distribution function is used to represent the forecast errors in the maximum PV generation and demand, and Monte-Carlo simulation is used to generate 100 scenarios. The mean of the probability distribution function is the forecasted values in Cases 1 and 2, and the standard deviation is 0.025 of the mean values. The total upper and lower PV dispatch margins on phase C in 5 scenarios and the expected upper and lower dispatch margins are shown in Fig. 4.7. In Fig. 4.8, the expected upper and lower PV dispatch margins are compared with those procured in Case 1. As shown in this figure, the lower PV dispatch margin, in this case, is higher than that in Case 1.

Here, the lower and upper dispatch margins (i.e., $\tilde{u}^{\varphi}_{v,t}$ and $\tilde{l}^{\varphi}_{v,t}$), are determined in a way that the risk of violating these margins are constrained as shown in (4.61) and (4.62). Fig. 4.7

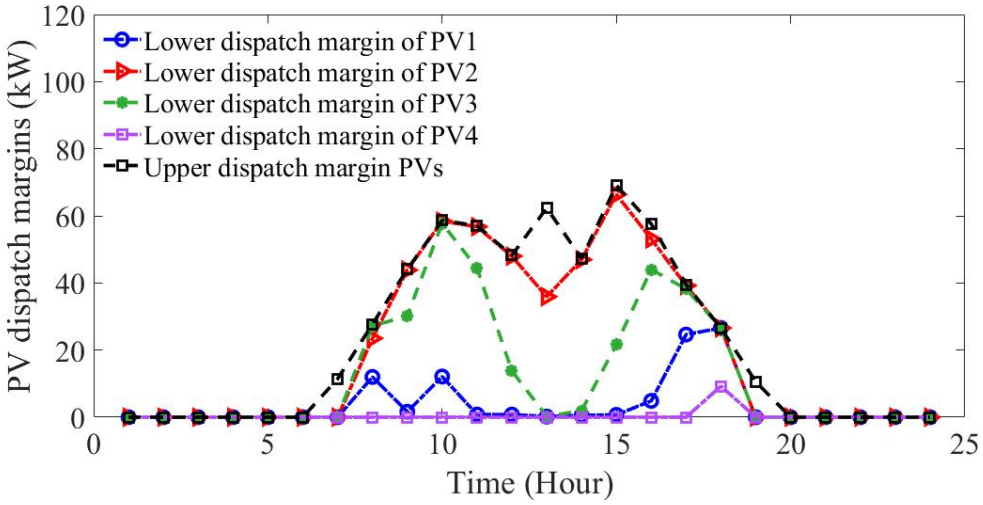

Figure 4.5: The dispatch margins of PV generation units on phase C (Case 2)

shows the upper and lower margins for which the probability of exceeding these margins does not exceed 10%. Here, the upper and lower dispatch margins are determined so that such limits do not violate in more than 10% of scenarios. Fig. 4.8 shows the procured risk-based upper and lower dispatch margins (i.e. $\tilde{u}^{\varphi}_{v,t}$ and $\tilde{l}^{\varphi}_{v,t}$) compared to those procured in Case 1, and the expected lower and upper dispatch margins for 100 scenarios in this case. Table 4.3, shows the total lower and upper dispatch limits of PV generation once the probability of exceeding such limits is increased from 5% to 50%. As shown in this table, as the probability of violating the upper and lower bounds increases, the risk-based upper margin decreases while the risk-based lower margin increases.

Once the uncertainty in demand is represented by polyhedral sets with 100% budget of uncertainty, the expected upper and lower dispatch margins for phases A, B, and C are shown in Fig. 4.10. Here, the total expected upper dispatch margins on all phases are 1956.4 kWh which is equal to the expected upper dispatch margin of PV generation with scenario-based demand. Furthermore, similar to the case with scenario-based demand, the total expected lower dispatch margin on phase B is zero, as the demand on phase B can be supplied by the feeder and DGs. The total expected lower dispatch margins on phases A and C are 558.59 kWh and 891.77 kWh, respectively. These margins are higher than the total expected lower dispatch margins with scenario-based demand on these phases, i.e.

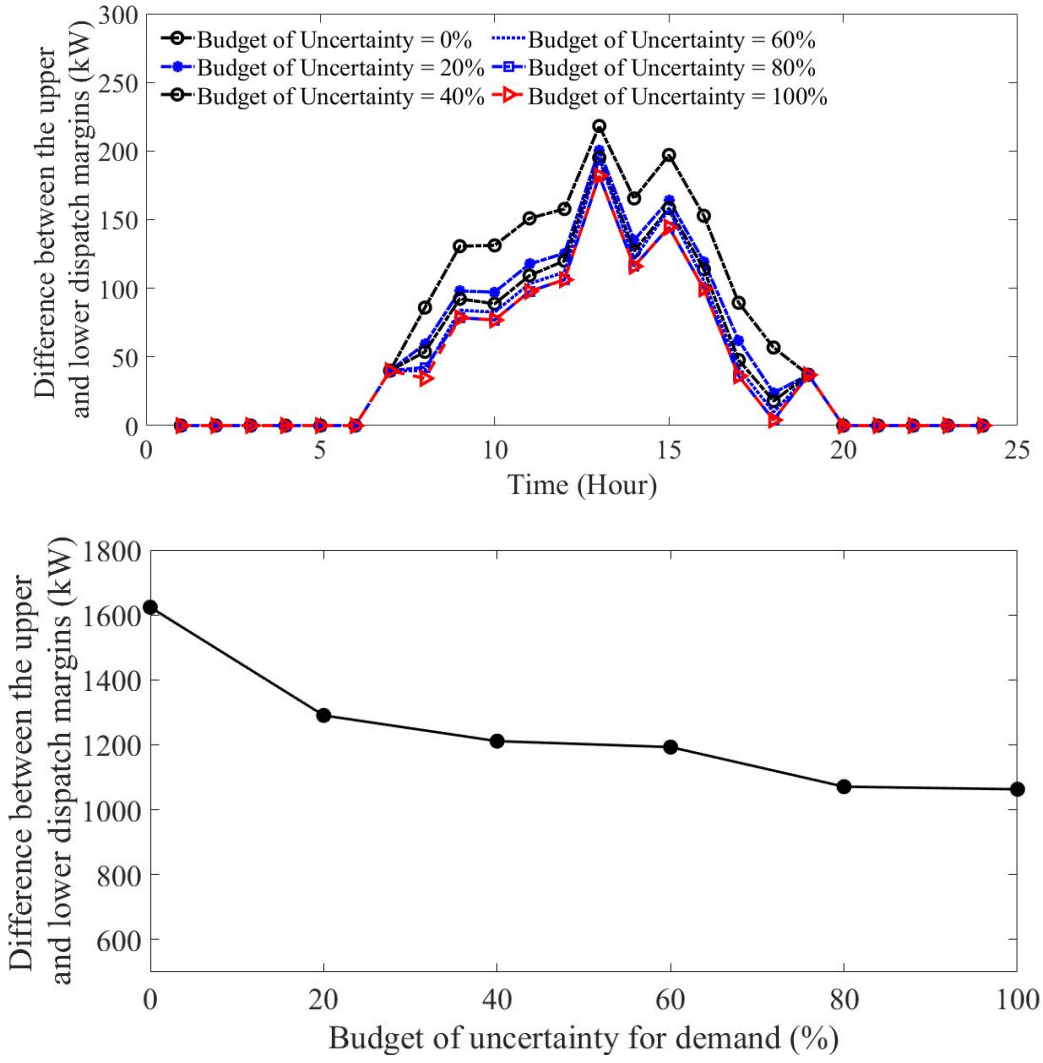

(b)

Figure 4.6: The difference between the upper and lower PV dispatch margins for different budgets of uncertainty in demand (a) total hourly difference (b) total day-ahead difference.

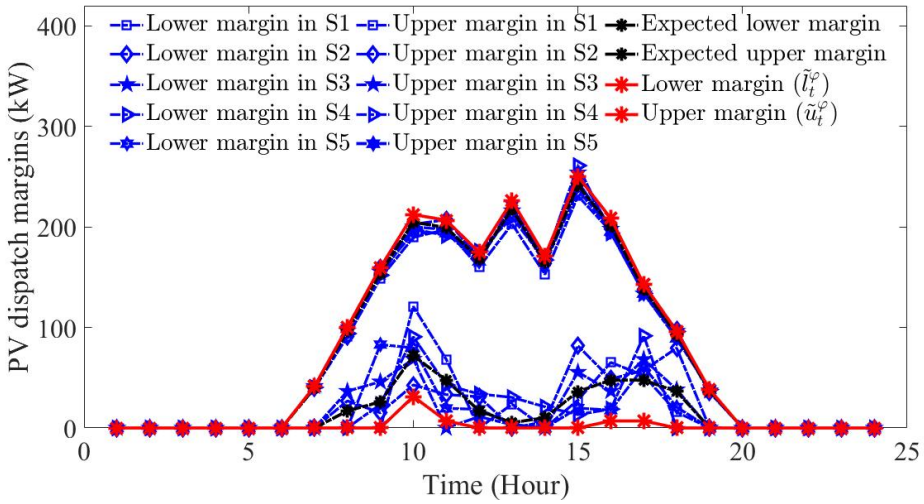

Figure 4.7: The total PV dispatch margins on phase C in five scenarios S1-S5, the expected PV dispatch margins, and the risk-based upper and lower dispatch margins for $\varepsilon = 0.1$ in Case 3

Table 4.3: The total risk-based lower and upper dispatch margins of PV generation units on phase C in 24 hours

ε	Total Lower Dispatch Margin (kWh)	Total Upper Dispatch Margin (kWh)
0.05	17.47	2034.65
0.1	52.42	2028.16
0.2	113.22	2001.94
0.3	200.52	1987.62
0.4	237.54	1972.41
0.5	307.19	1956.04

125.85 kWh for phase A, and 362.17 kWh for phase C.

$$\mathbb{P}\left[\hat{u}_{v,t}^{\varphi,m} \leq \tilde{u}_{v,t}^{\varphi}\right] \geq 1-\varepsilon \tag{4.61}$$

$$\mathbb{P}\left[\hat{l}_{v,t}^{\varphi,m} \geq \tilde{l}_{v,t}^{\varphi}\right] \geq 1-\varepsilon \tag{4.62}$$

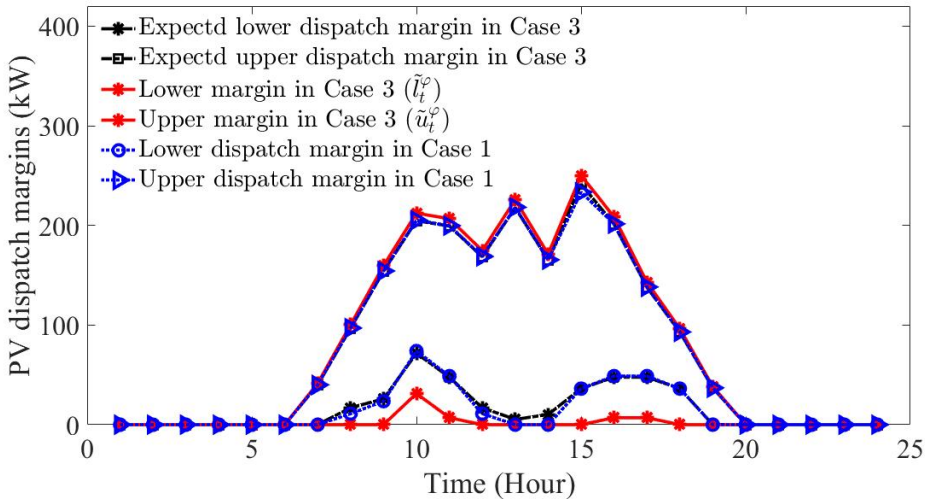

Figure 4.8: The expected upper and lower PV dispatch margins in Case 1 and Case 3 and the risk-based upper and lower dispatch margins with $\varepsilon = 0.1$

Table 4.4: Characteristics of dispatchable DG units in the islanded mode operation of the IEEE-13 bus system.

DG	Bus	Ramp Rate kW/hr	P^{max}	Q^{min}	Q^{max}
1	4	225	1010	-505	505
2	6	225	1010	-505	505
3	13	240	1260	-700	700
4	7	15	60	-30	30

Table 4.5: Characteristics of ESS in the island mode operation of the IEEE-13 bus system

ESS	Bus	Pmax	Qmax	Emin	Emax
1	4	200	120	0	200
2	10	200	120	0	200

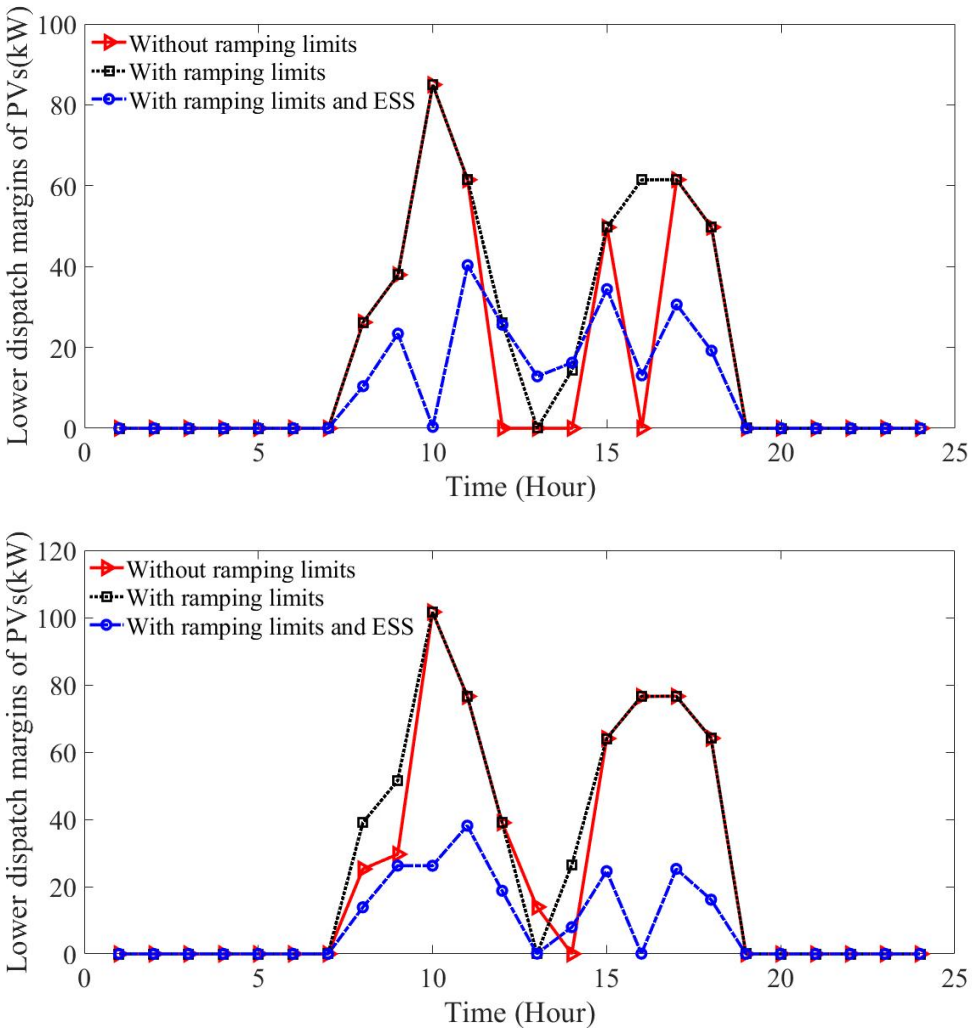

Figure 4.9: The lower PV dispatch margin on (a) phase A and (b) phase C for isolated distribution network considering the ramp rate for DG units and energy storage.

4.3.4 Case 4 – Operation in island mode with the loss of the main feeder

In this case, the main feeder is disconnected and the distribution network is supplied by the DG and PV generation units. The characteristics of the DG units are shown in Table 4.4. As shown in Fig. 4.9a, at hour 10, the peak demand on phase A is 1175 kW and the power loss is 47.551 kW. The total generation of DG units is 1137.562 kW.Therefore, the rest of the demand is served by the PV generation and the lower PV dispatch margin is $1175 + 47.551 - 1137.562 = 84.989$ kW. Similarly, in Fig. 4.9b, on phase C, the total demand is 1252 kW and the power loss is 44.025 kW and the total generation of DG units is 1195.02 kW,

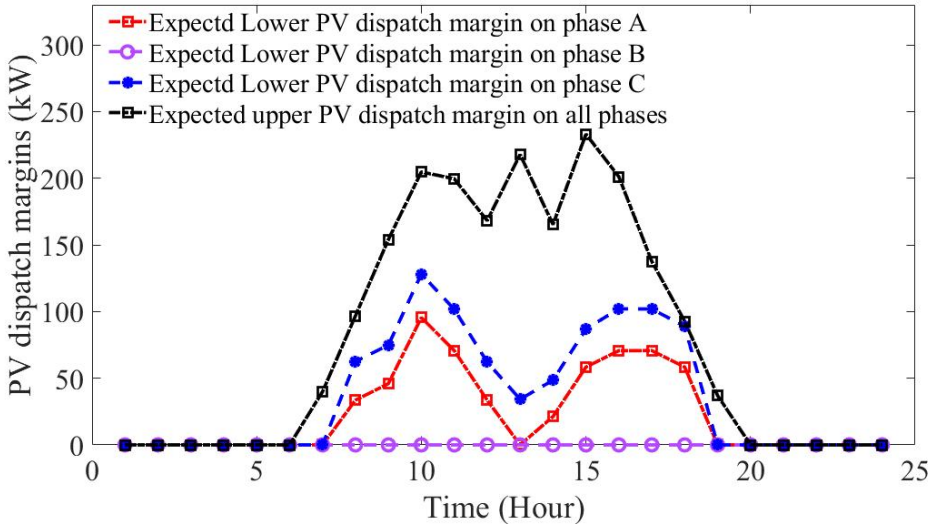

Figure 4.10: The expected dispatch margins of PV generation units on phases A, B and C with uncertain PV generation and worst-case realization of demand

therefore the rest of the demand i.e. $1252 + 44.025 - 1195.02 = 101.658\ kW$ is supplied by the PV generation and the lower PV dispatch margin is $101.658\ kW$. Furthermore, Fig. 4.9 demonstrates the effect of ramp rates on the PV dispatch margins. As shown in Fig. 4.9a, when ramp rates are not considered, the lower PV dispatch margins on phase A at hours 12, 16, are 0 kW. By considering the ramp rates for DG units as shown in Table 4.4, the lower PV dispatch margins at hours 12, and 16 are increased to 26.199 kW, and 61.481 kW respectively. Furthermore, the impact of ESSs on the PV dispatch margins are shown in Fig. 4.9. The characteristics of ESSs considered, in this case, are shown in Table 4.5. As shown in Fig. 4.9a, the lower PV dispatch margin on phase A is dramatically reduced after installing the ESSs. Here, the lower PV dispatch margins are decreased from 84.989 kW, and 101.658 kW at hour 10, to 0.340 kW and 26.221 kW on phases A, and C respectively. Considering the ramp rates for DG units will decrease the difference between the lower and upper PV dispatch margins. In the day-ahead operation horizon, the total difference between the upper and lower PV dispatch margins in the island operation mode of the distribution network ignoring the ramp rates of DG units are 1580.35 kWh, 1951.877 kWh, and 1580.35 kWh on phases A, B, and C, respectively. Once ramp rates are considered,

such values are reduced to 1478.23 kWh, 1951.877 kWh, and 1336.185 kWh for phases A, B, and C, respectively. Furthermore, utilizing the ESSs will increase the difference between the upper and lower PV dispatch margins. Here, integrating ESS with ramp rates of DG units will increase the total difference between the upper and lower dispatch margins in the day-ahead operation horizon to 1725.421 kWh, 1951.887 kWh and 1754.519 kWh on phases A, B, and C, respectively.

4.4 Conclusion

In this chapter, the upper and lower PV dispatch margins in unbalanced three-phase distribution systems are determined to ensure the security of the distribution network. A two-stage optimization problem is formulated and a solution approach is proposed to solve this problem. The modified IEEE 13-bus system is used to evaluate the effectiveness of the proposed formulation and solution methodology. It is shown that the worst-case realization of demand will increase the lower PV dispatch margins and decreases the difference between the lower and upper PV dispatch margins. Furthermore, increasing the budget of uncertainty for demand will decrease the difference between the lower and upper PV dispatch margins. The uncertainty in maximum PV generation and demand is considered using scenarios. Compared to the scenario-based models that address the uncertainty in demand, it is shown that the lower PV dispatch margins are higher once the worst-case realization of demand is considered. Furthermore, the risk associated with violating the upper and lower dispatch margins is considered. The impacts of the ramp rates of DG units and the installation of ESSs on the PV dispatch margins are investigated. It is shown that imposing the ramp rates for the DG units will increase the lower PV dispatch margins and leveraging ESSs increases the difference between the lower and upper PV dispatch margins and decreases the lower PV dispatch margins.

Chapter 5

Data-Driven Distributionally Robust Unbalanced Operation of Distribution Networks with High Penetration of Photovoltaic Generation and Electric Vehicles

The uncertainties associated with the large-scale integration of electric vehicles (EV) and renewable energy resources introduce new challenges to operating the unbalanced three-phase distribution networks. In this chapter, a data-driven distributionally robust optimization framework is proposed for the operation of the distribution network considering the uncertainties associated with the interconnected EV fleets and solar photovoltaic (PV) generation. The proposed framework leverages the column-and-constraint generation (C&CG) approach to minimize the operation cost considering the worst-case probability distributions of PV generation, the available energy in EV fleets, the arrival and departure times of EV fleets as well as their minimum and maximum energy capacities. The proposed approach is applied to the modified three-phase unbalanced IEEE 34-bus and IEEE 123-bus networks. To evaluate the performance of the proposed distributionally robust optimization framework, the results are compared to those procured by solving scenario-based stochastic programming and robust optimization problems. Furthermore, the impact of vehicle-to-grid capability on the operation of the distribution network is investigated and the in-sample and out-of-sample performances of the proposed framework are evaluated. In this chapter, a Wasserstein metric-based DRO problem is formulated and solved for the unbalanced distribution network operation considering the uncertainties associated with EVs and PV generation. The formulated problem is a two-stage optimization problem where the topology of the radial distribution network is determined in the first stage problem, and the distribution network operation cost is minimized considering the worst-case probability distribution of the uncertainties in the second stage problem. The contributions of this chapter are summarized as follows:

– A data-driven DRO problem is proposed for the unbalanced operation of the distribution

networks considering the network switching, and the performance of the procured solution is compared with the solutions to the SP and RO counterparts.

- The uncertainties associated with forecasted PV generation as well as the EVs i.e. the available energy at arrival and departure times, and the maximum and minimum available energy and power for EVs were considered.

- The V2G capability of EVs is addressed and the in-sample and out-of-sample performance of DRO and SP problems are compared.

The rest of the chapter is organized as follows. In section 5.1, a two-stage data-driven DRO problem is formulated using the constructed ambiguity set. The ambiguity set is formed using the empirical data and the Wasserstein metric is used as a distance measure. In section 5.2, the solution framework for the proposed problem is presented. C&CG technique is used to solve this problem. The numerical results and conclusion are presented in sections 5.3 and 5.4 respectively.

Nomenclature

Sets and Indices:

- b Index of bus.
- d Index of demand.
- e Index of electric vehicle cluster.
- i Index of distributed generation.
- k Index of phase.
- l Index of distribution branch.
- s Index of spanning tree.
- m, n Index of sample.
- f Index of distribution feeder.

– v Index of PV generation unit.

– $\mathbb{O}_s$ Set of the open switches in spanning tree s.

– $\mathbb{C}_s$ Set of the closed switches in spanning tree s.

– $\mathbb{S}$ Set of all spanning trees.

Variables:

– $\mathbf{U^m_{b,t}}$ Squared voltage vector on bus b.

– $E^m_{e,k,t}$ Energy capacity of EV cluster.

– $p^m_{(.),k,t}$ Real power of a unit.

– $p^{ch,m}_{e,k,t}$ Real charging power for electric vehicle cluster e.

– $p^{dc,m}_{e,k,t}$ Real discharging power for electric vehicle cluster e.

– $ps^m_{i,k,g,t}$ Power in segment g of the cost curve for a distributed generation.

– $q^m_{(.),k,t}$ Reactive power of a unit.

– $S^m_{(.),k,t}$ Apparent power on phase k.

– $y_{l,t}$ Binary variable representing the status of the distribution branch, 1 if connected, and 0 otherwise.

Parameters:

– $AD_{d,b}$ Element of demand-bus incidence matrix.

– $AE_{e,b}$ Element of energy storage-bus incidence matrix.

– $AI_{i,b}$ Element of unit-bus incidence matrix.

– $AL_{l,b}$ Element of line-bus incidence matrix.

– $AV_{v,b}$ Element of PV-bus incidence matrix.

- $AN_{f,b}$ Element of feeder-bus incidence matrix.
- $\hat{E}^{min}_{e,k,t}$ Forecasted minimum available energy for EV cluster.
- $\hat{E}^{max}_{e,k,t}$ Forecasted maximum available energy for EV cluster.
- $\hat{E}^{arv}_{e,k,t}$ Forecasted available energy at arrival time.
- $\hat{E}^{dep}_{e,k,t}$ Forecasted available energy at departure time.
- PF_f Power factor at distribution feeder f.
- $\overline{p}_{i,k,g}$ Maximum power at segment g of the generation cost curve.
- $\bar{p}_{(.),k,t}$ Maximum real power.
- $\bar{q}_{(.),k,t}$ Maximum reactive power.
- $\hat{p}^{ch,max,m}_{e,k,t}$ Maximum charging power for EV cluster e.
- $\hat{p}^{dc,max,m}_{e,k,t}$ Maximum discharging power for EV cluster e.
- $\bar{S}_{l,k}$ Maximum complex power of branch l on phase k.
- $I_{e,k,t}$ Binary parameter for interconnection of EV cluster.
- $I^{arv}_{e,k,t}$ Binary parameter for interconnection of EV cluster.
- $I^{dep}_{e,k,t}$ Binary parameter for interconnection of EV cluster.
- $w_{i,g}$ Marginal cost of the unit i in segment g.
- cc]Cost of load curtailment.
- $\rho_{f,t}$ Price of electricity of feeder.
- η^{ch}_e, η^{dc}_e Battery charging and discharging efficiency.
- $\phi_{l,k}$ Availability of phase k on branch l.
- $\underline{V}, \overline{V}$ Squared lower and upper limits of nodal voltage.

5.1 Problem Formulation

In this section, first, the formed ambiguity set for the probability distribution of uncertain variables is presented and later, the data-driven DRO problem is formulated using the procured ambiguity set.

5.1.1 Forming the ambiguity set

The probability distributions of the forecasted PV generation, the maximum and minimum capacity of EV clusters, the maximum power of EV clusters, and the available energy at arrival and departure times are considered to be uncertain. The historical data of PV generation and EV clusters' characteristics are used to construct an empirical probability distribution. Using the empirical data on the maximum and minimum available energy ($\hat{E}^{max}_{e,k,t}$, $\hat{E}^{min}_{e,k,t}$), maximum power consumption ($\hat{p}^{max}_{e,k,t}$), and the available energy at arrival and departure times ($\hat{E}^{arv}_{e,k,t}$, $\hat{E}^{dep}_{e,k,t}$) and the forecasted PV generation ($\hat{p}_{v,k,t}$), the empirical probability distribution for each variable is formed. For a set of empirical data of size N, the probability distribution of empirical data is $\hat{\Lambda} = (\hat{\theta}_1, ..., \hat{\theta}_n)$ where $\hat{\theta}_n = 1/N$. Based on the empirical probability distributions the unknown probability distributions of uncertain variables associated with PVs and EV clusters are procured with the confidence level β. Here, the Wasserstein metric shown in (5.1), is used to quantify the distance $\mathcal{D}_\nu(\Lambda, \hat{\Lambda})$ between the unknown probability distribution and the empirical probability distribution.

$$\mathcal{D}_\nu(\Lambda, \hat{\Lambda}) := \inf_{\pi} \sum_{|\nu|} \sum_{|\hat{\nu}|} \pi^{\nu,\hat{\nu}} \cdot \|\nu - \hat{\nu}\|_1 \tag{5.1}$$

Here, ν and $\hat{\nu}$ are the vectors of the uncertain variables with unknown and empirical probability distributions, respectively. Furthermore, $|\nu|$ and $|\hat{\nu}|$ are the sizes of vectors ν and $\hat{\nu}$ respectively. Furthermore, $\pi^{\nu,\hat{\nu}}$ represents the joint probability distribution of random variables ν and $\hat{\nu}$. The ambiguity set is defined as $\mathbb{D} = \left\{\mathcal{D}_\nu(\Lambda, \hat{\Lambda}) \leq \alpha\right\}$ where α is the maximum distance between the two probability distributions defined as $\alpha = D\sqrt{\frac{2}{N} \ln \frac{1}{(1-\beta)}}$ [65]. The ambiguity set is formed by (5.2)-(5.5) where $m = 1, ..., N$ and $n = 1, ..., N$ are the indices of the samples from unknown and empirical probability distributions, and $\pi^{m,n}$ is the joint probability of θ^m (unknown marginal probability of sample m) and $\hat{\theta}^n$ (marginal

probability of empirical data sample n). Here, the constraints (5.3) and (5.4) are enforcing the relationship between the joint probability distribution $\pi^{n,m}$ and the marginal probability distributions of unknown and empirical data samples. Constraint (5.5) shows the property of the unknown probability distribution.

$$\sum_{n}\sum_{m}\pi^{m,n}\left|\nu^{m}-\nu^{n}\right|\leq\alpha \tag{5.2}$$

$$\sum_{n}\pi^{m,n}=\theta^{m}, \qquad \forall m \tag{5.3}$$

$$\sum_{m}\pi^{m,n}=\hat{\theta}^{n}, \qquad \forall n \tag{5.4}$$

$$\sum_{m}\theta^{m}=1 \tag{5.5}$$

5.1.2 Formulation of Data-driven DRO Problem

In this section, a two-stage data-driven optimization problem is formulated for the unbalanced operation of the distribution network. In the first stage, the topology of the distribution network is determined by procuring the state of the switches in the network. In the second-stage problem, the worst-case realization of the probability distribution of the uncertain variables is determined within a bounded Wasserstein distance from the empirical probability distribution. The rest of the decision variables include the real and reactive power dispatch of DERs and the distribution feeder.

The states of the switches in the first-stage problem maintain the radial topology of the distribution network. Here, the radial distribution system is represented as a graph $\mathbf{G}=(\mathbf{V},\mathbf{E})$, where $\mathbf{V}$ denotes the set of vertices (buses) with K vertices and $\mathbf{E}$ denotes the set of edges (lines) with M edges where $K-1=M$. The spanning trees of the distribution network include all possible radial topologies. The following algorithm is developed to find the switching state of the distribution lines that ensures the radial operation of the distribution network:

Step 1: In a distribution network graph G with K vertices and M edges, find all combinations of edges with $K-1$ number of edges.

Step 2: Check if all K vertices are present in the selected combinations in Step 1. If so,

return these combinations as spanning trees, otherwise, discard it.

Step 3: The spanning trees form a set S in which in each spanning tree $s \in S$, the state of a switchable line that is open i.e., $l \in \mathbb{O}_s$ is 0, i.e., $y_{l,t} = 0$. Similarly, the state of the switchable line that is closed i.e., $l \in \mathbb{C}_s$ is 1, i.e., $y_{l,t} = 1$. As one of the spanning trees should be selected, constraint (5.8) is enforced. The selected spanning tree is formed by a certain combination of closed and open switches as shown in (5.8).

$$\min_{y_{l,t}} \mathbf{0} + \max_{\Lambda \in \mathbb{D}} \min_{\mathbf{p},\mathbf{q},\mathbf{U}} E_\theta \Bigg(\sum_f \sum_k \sum_t \rho_{f,t} \cdot p^m_{f,k,t} + \sum_b \sum_k \sum_t \sum_g \sum_i AI_{i,b} \cdot w_{i,g} \cdot ps^m_{i,k,g,t} + \sum_b \sum_k \sum_t cc \cdot AD_{d,b} \cdot \left(\overline{p}_{d,k,t} - p^m_{d,k,t} \right) \Bigg) \tag{5.6}$$

Subject to: (5.2)-(5.5),

$$\sum_{l=1}^{K-1} y_{l,t} = K - 1 \tag{5.7}$$

$$\sum_{s \in \mathbb{S}} \left(\prod_{l \in \mathbb{C}_s} y_{l,t} \cdot \prod_{l \in \mathbb{O}_s} \left(1 - y_{l,t} \right) \right) = 1 \tag{5.8}$$

$$\sum_l AL_{l,b} \cdot p^m_{l,k,t} + \sum_i AI_{i,b} \cdot p^m_{i,k,t} + \sum_v AV_{v,b} \cdot \hat{p}^m_{v,k,t} + \sum_f AN_{f,b} \cdot p^m_{f,k,t} + \sum_e AE_{e,b} \cdot (p^{dc,m}_{e,k,t} - p^{ch,m}_{e,k,t}) = \sum_d AD_{d,b} \cdot p^m_{d,k,t} \tag{5.9}$$

$$\sum_l AL_{l,b} \cdot q^m_{l,k,t} + \sum_i AI_{i,b} \cdot q^m_{i,k,t} + \sum_f AN_{f,b} \cdot q^m_{f,k,t} = \sum_d AD_{d,b} \cdot q^m_{d,k,t} \tag{5.10}$$

$$ps^m_{i,k,g,t} \leq \overline{p}_{i,k,g} \tag{5.11}$$

$$p^m_{i,k,t} = \sum_g ps^m_{i,k,g,t} \tag{5.12}$$

$$AL_{l,b} \cdot \mathbf{U}^m_{b,t} + 2(\widetilde{\mathbf{R}}_l \cdot \mathbf{p}^m_{l,t} + \widetilde{\mathbf{X}}_l \cdot \mathbf{q}^m_{l,t}) \leq M \cdot (1 - \boldsymbol{\phi}_l) \tag{5.13}$$

$$AL_{l,b} \cdot \mathbf{U}^m_{b,t} + 2(\widetilde{\mathbf{R}}_l \cdot \mathbf{p}^m_{l,t} + \widetilde{\mathbf{X}}_l \cdot \mathbf{q}^m_{l,t}) \geq -M \cdot (1 - \boldsymbol{\phi}_l) \tag{5.14}$$

$$\underline{V} \leq U^m_{b,k,t} \leq \overline{V} \tag{5.15}$$

$$p^m_{l,k,t} \geq -\phi_{l,k} \cdot y_{l,t} \cdot \bar{S}_{l,k} \cdot \cos(\frac{\pi}{8}) \tag{5.16}$$

$$p^m_{l,k,t} \leq \phi_{l,k} \cdot y_{l,t} \cdot \bar{S}_{l,k} \cdot \cos(\frac{\pi}{8}) \tag{5.17}$$

$$q^m_{l,k,t} \geq -\phi_{l,k} \cdot y_{l,t} \cdot \bar{S}_{l,k} \cdot \cos(\frac{\pi}{8}) \tag{5.18}$$

$$q^m_{l,k,t} \leq \phi_{l,k} \cdot y_{l,t} \cdot \bar{S}_{l,k} \cdot \cos(\frac{\pi}{8}) \tag{5.19}$$

$$p^m_{l,k,t} + q^m_{l,k,t} \geq -\phi_{l,k} \cdot y_{l,t} \cdot \bar{S}_{l,k} \cdot (\sin(\frac{\pi}{8}) + \cos(\frac{\pi}{8})) \tag{5.20}$$

$$p^m_{l,k,t} + q^m_{l,k,t} \leq \phi_{l,k} \cdot y_{l,t} \cdot \bar{S}_{l,k} \cdot (\sin(\frac{\pi}{8}) + \cos(\frac{\pi}{8})) \tag{5.21}$$

$$p^m_{l,k,t} - q^m_{l,k,t} \geq -\phi_{l,k} \cdot y_{l,t} \cdot \bar{S}_{l,k} \cdot (\sin(\frac{\pi}{8}) + \cos(\frac{\pi}{8})) \tag{5.22}$$

$$p^m_{l,k,t} - q^m_{l,k,t} \leq \phi_{l,k} \cdot y_{l,t} \cdot \bar{S}_{l,k} \cdot (\sin(\frac{\pi}{8}) + \cos(\frac{\pi}{8})) \tag{5.23}$$

$$0 \leq p^m_{i,k,t} \leq \bar{p}_{i,k} \tag{5.24}$$

$$-\bar{q}_{i,k} \leq q^m_{i,k,t} \leq \bar{q}_{i,k} \tag{5.25}$$

$$p^m_{d,k,t} \leq \bar{p}_{d,k,t} \tag{5.26}$$

$$q^m_{f,k,t} \leq tan\ (\cos^{-1} PF_f) \cdot p^m_{f,k,t} \tag{5.27}$$

$$q^m_{f,k,t} \geq -tan\ (\cos^{-1} PF_f) \cdot p^m_{f,k,t} \tag{5.28}$$

$$\hat{E}^{min,m}_{e,k,t} - M \cdot (1 - I_{e,k,t}) \leq E^m_{e,k,t} \tag{5.29}$$

$$E^m_{e,k,t} \leq \hat{E}^{max,m}_{e,k,t} + M \cdot (1 - I_{e,k,t}) \tag{5.30}$$

$$E^m_{e,k,t} \leq \hat{E}^{arv,m}_{e,k} + M \cdot \left(1 - I^{arv}_{e,k,t}\right) \tag{5.31}$$

$$E^m_{e,k,t} \geq \hat{E}^{arv,m}_{e,k} - M \cdot \left(1 - I^{arv}_{e,k,t}\right) \tag{5.32}$$

$$E^m_{e,k,t} \leq \hat{E}^{dep,m}_{e,k} + M \cdot \left(1 - I^{dep}_{e,k,t}\right) \tag{5.33}$$

$$E^m_{e,k,t} \geq \hat{E}^{dep,m}_{e,k} - M \cdot \left(1 - I^{dep}_{e,k,t}\right) \tag{5.34}$$

$$E^m_{e,k,t} - E^m_{e,k,t-1} - \eta^{ch}_e p^{ch,m}_{e,k,t} + p^{dc,m}_{e,k,t}/\eta^{dc}_e \leq M \cdot \left(1 - I_{e,k,t}\right) \tag{5.35}$$

$$E^{m}_{e,k,t} - E^{m}_{e,k,t-1} - \eta^{ch}_{e} p^{ch,m}_{e,k,t} + p^{dc,m}_{e,k,t}/\eta^{dc}_{e} \geq -M \cdot \left(1 - I_{e,k,t}\right) \tag{5.36}$$

$$0 \leq p^{ch,m}_{e,k,t} \leq I_{e,k,t} \cdot \hat{p}^{ch,max,m}_{e,k,t} \tag{5.37}$$

$$0 \leq p^{dc,m}_{e,k,t} \leq I_{e,k,t} \cdot \hat{p}^{dc,max,m}_{e,k,t} \tag{5.38}$$

$$Y_t \leq (y_{l,t})_{l \in \mathbb{O}_s} \tag{5.39}$$

$$Y_t \leq (y_{l,t})_{l \in \mathbb{C}_s} \tag{5.40}$$

$$Y_t \geq (y_{l,t})_{l \in \mathbb{C}_s} + (y_{l,t})_{l \in \mathbb{O}_s} - 1 \tag{5.41}$$

The objective function presented in (5.6), is the operation cost of DERs, the cost of supplying electricity from the distribution feeder and the penalty associated with the curtailed demand. To maintain the radial topology, (5.7) enforces the number of branches (edges) to be equal to $K-1$ and (5.8) would lead to selecting one set of switchable lines that form a spanning tree in the set $\mathbb{S}$. The nonlinear terms appear in (5.8) are linearized using (5.39)-(5.41). Here, Y_t is binary variable, (5.39) and (5.40) ensure that Y_t is zero if $(y_{l,t})_{l \in \mathbb{O}_s}$ or $(y_{l,t})_{l \in \mathbb{C}_s}$ is zero. The last constraint (5.40) ensures that Y_t is 1 if both $(y_{l,t})_{l \in \mathbb{O}_s}$ and $(y_{l,t})_{l \in \mathbb{O}_s}$ are 1.

Here, (5.9) and (5.10) show the nodal real and reactive power balance in the distribution network. The operation cost of the distributed generation (DG) unit is formulated as a quadratic function of the output power which is further linearized using a piece-wise linearization technique in (5.6), (5.11) and (5.12). Constraints (5.13) and (5.14), present the real and reactive power flow in distribution branch l, where, $\phi_{l,k} \in \phi_{\mathbf{l}}$, $U^{m}_{b,k,t} \in \mathbf{U^{m}_{b,t}}$. The nodal voltage is limited by lower and upper bounds as shown in (5.15). The voltage unbalance between the phases is small and the loss in the distribution branches is neglected. The real and reactive power flows satisfy a circular constraint where the squared real power flow and the squared reactive power flow on each branch are limited by the squared apparent power capacity of the branch. The circular constraint is further linearized by a convex polygon (5.16)-(5.23) using the methods proposed in [97, 108]. As the number of sides increases, the approximated polygon is a tighter representation of the circular constraint. Here, an octagon is used where the radius of the approximated enclosing circle of the octagon is $\bar{S}_{l,k} = S^{max}_{l,k} \cdot \sqrt{(2\pi/8)/(\sin(2\pi/8))}$. Similar constraints could be written for the distribution

feeder given the apparent power capacity of the feeder. Constraints (5.24) and (5.25) are limiting the real and reactive power for a DG unit by its capacity. The served demand is less than the total demand as enforced by (5.26). For distribution feeder f, the reactive power on each phase is limited by the acceptable power factor of the feeder as shown in (5.27)-(5.28). The limits on the available energy in an EV cluster e are shown in (5.29) and (5.30). As shown in these constraints, the limits on the available energy are enforced once the vehicle clusters are connected to the network, i.e. $I_{e,k,t} = 1$. The available energy at arrival time is limited by (5.31) and (5.32), where these constraints are enforced once the vehicle clusters are connected to the network at the arrival time, i.e. $I^{arv}_{e,k,t} = 1$. Similarly, the available energy at departure time is limited by (5.33) and (5.34), where (5.33) and (5.34) are enforced once the vehicle clusters are connected to the network at the departure time, i.e. $I^{dep}_{e,k,t} = 1$. Here, $I_{e,k,t} = 1$ for all hours between the arrival and departure times. The relationship between the available energy and the power dispatch of each EV cluster is enforced by (5.35) and (5.36). Constraint (5.37) and (5.38) enforce the limitation of charging and discharging power for each EV cluster.

The data-driven DRO problem is formulated as (5.6)-(5.38), (5.2)-(5.5) where the object function is reformulated as (5.42).

$$\max_{\Lambda\in\mathbb{D}} \min_{\mathbf{p},\mathbf{q},\mathbf{U}} \sum_m \theta^m \cdot \Bigg(\sum_f \sum_k \sum_t \rho_{f,t} \cdot p^m_{f,k,t} + \sum_b \sum_k \sum_t \sum_g \sum_i AI_{i,b} \cdot w_{i,g} \cdot ps^m_{i,g,k,t} + \sum_b \sum_k \sum_t cc \cdot AD_{d,b} \cdot \left(\overline{p}_{d,k,t} - p^m_{d,k,t}\right) \Bigg) \tag{5.42}$$

5.2 Solution Methodology

To solve the problem presented in (5.6)-(5.38), (5.2)-(5.5), the following solution algorithm based on C&CG technique is presented. Here, the abstract form of the problem is formulated as (5.43)-(5.47).

$$\min_{\boldsymbol{y}} \ \mathbf{0} + \max_{\Lambda\in\mathbb{D}} \min_{\boldsymbol{x}} \ \boldsymbol{b}^\top \boldsymbol{x} \tag{5.43}$$

subject to:

$$\boldsymbol{A}\boldsymbol{y} \leq \boldsymbol{d} \tag{5.44}$$

$$\boldsymbol{F}\boldsymbol{x} - \boldsymbol{E}\boldsymbol{y} \leq \boldsymbol{k} \tag{5.45}$$

$$\boldsymbol{G}\boldsymbol{x} - \boldsymbol{K}\boldsymbol{y} = \boldsymbol{g} \tag{5.46}$$

$$\boldsymbol{J}\boldsymbol{x} = \boldsymbol{h} \tag{5.47}$$

The proposed algorithm is presented in the following steps:

Step 1) Initialization: Initialize the upper bound $UB = \infty$, lower bound $LB = -\infty$, $\epsilon \leq 10^{-3}$ and the iteration counter $w = 0$.

Step 2) Solve the master problem: Solve the master problem for each iteration as follows:

$$\min_{\boldsymbol{y}} \quad \mathbf{0} + \eta \tag{5.48}$$

subject to:

$$\boldsymbol{A}\boldsymbol{y} \leq \boldsymbol{d} \tag{5.49}$$

$$\boldsymbol{\eta} \geq \boldsymbol{\theta}^{*}\mathbf{b}^{\top}\boldsymbol{x}^{(l)}, \quad \forall l \leq w \tag{5.50}$$

$$\boldsymbol{F}\boldsymbol{x}^{(l)} - \boldsymbol{E}\boldsymbol{y} \leq \boldsymbol{k}, \quad \forall l \leq w \tag{5.51}$$

$$\boldsymbol{G}\boldsymbol{x}^{(l)} - \boldsymbol{K}\boldsymbol{y} = \boldsymbol{g}, \quad \forall l \leq w \tag{5.52}$$

$$\boldsymbol{J}\boldsymbol{x}^{(l)} = \boldsymbol{h}, \quad \forall l \leq w \tag{5.53}$$

Update the LB as the following equation (5.54):

$$LB = \hat{\eta}_{w+1} \tag{5.54}$$

Step 3) Solve the subproblem: The objective function of the subproblem and it's constraints are given as follows;

$$\max_{\Lambda \in \mathbb{D}} \min_{\boldsymbol{x}} \quad \boldsymbol{b}^{\top}\boldsymbol{x} \tag{5.55}$$

subject to:

$$\boldsymbol{F}\boldsymbol{x} \leq \boldsymbol{k} + \boldsymbol{E}\boldsymbol{y}^{*} \tag{5.56}$$

$$\boldsymbol{G}\boldsymbol{x} = \boldsymbol{g} + \boldsymbol{K}\boldsymbol{y}^{*} \tag{5.57}$$

$$\boldsymbol{J}\boldsymbol{x} = \boldsymbol{h} \tag{5.58}$$

constraints (5.2)-(5.5)

Then, the subproblem presented in (5.55)-(5.58) is reformulated using it's dual form in (5.59)-(5.60):

$$\boldsymbol{Q}(\boldsymbol{y}) = \max_{\Lambda \in \mathbb{D}, \gamma, \lambda, \mu} (\boldsymbol{k} + \boldsymbol{E}\boldsymbol{y}^{*})^{\top}\boldsymbol{\gamma} + (\boldsymbol{g} + \boldsymbol{K}\boldsymbol{y}^{*})^{\top}\boldsymbol{\lambda} + \boldsymbol{h}^{\top}\boldsymbol{\mu} \tag{5.59}$$

subject to:

$$\boldsymbol{F}^{\top}\boldsymbol{\gamma} + \boldsymbol{G}^{\top}\boldsymbol{\lambda} + \boldsymbol{J}^{\top}\boldsymbol{\mu} \leq \boldsymbol{b} \tag{5.60}$$

constraints (5.2)-(5.5)

Where, γ, λ and μ are the dual variables for constraints (5.56), (5.57) and (5.58) respectively. Then update the UB using (5.61) and go to *Step 4*.

$$UB = min\{UB, \boldsymbol{Q}(\boldsymbol{y}^{*(w+1)})\} \tag{5.61}$$

Step 4) Check the convergence criterion: If $UB - LB \leq \epsilon$ end the process, otherwise proceed to step 5.

step 5) Generate columns and constraints: Add (5.50)-(5.53) to the master problem, set $w = w + 1$ and go back to step 2.

5.3 Numerical Results

In this section, the modified IEEE 34-bus and IEEE 123-bus distribution systems are considered. The simulations are carried out on a server with dual 14 Core Intel Xeon 2.6 GHz and 380 GB of memory and CPLEX 12.8 is used as a solver. Historical sample data are considered for PV generation and EV cluster interconnections. The EV cluster data include minimum and maximum energy capacity of EVs, the available energy at arrival and departure times, and the maximum power of EV clusters. The arrival and departure times are considered as parameters. Using a Gaussian probability distribution, sample data for PV generation are generated with the mean value equal to the forecasted PV generation and the standard deviation of 0.1 of the mean value. For EVs clusters, the sample data of available energy at the arrival and departure times, the maximum power output of EV clusters as well as the maximum and minimum available energy of EV clusters are generated using a Gaussian probability distribution with a mean equal to the forecasted values and the standard deviation equal to 0.1 of the mean value. The maximum charging/discharging power for single-phase and three-phase EVs are 7.4 kW and 22.2 kW, respectively. The charging and discharging efficiencies for an EV cluster are 90%. The load curtailment cost is 20 $/kWh. The available energy at the arrival time is 20% of the maximum energy capacity and the available energy at the departure time is 95% of the maximum energy capacity of the EV clusters. For the sake of simplicity, the arrival and departure times for all EV clusters are 9:00 and 18:00 respectively.

5.3.1 IEEE 34-bus system

The IEEE 34-bus distribution network supplies three-phase and single-phase loads where the peak real demands on phase A, phase B, and phase C are 606 kW, 584 kW, and 579 kW respectively. Similarly, the peak reactive demands on these phases are 357, 344, and 343 kVar respectively. Three 3-phase PV generation units are connected to the distribution network, where each has the maximum forecasted output power of 126.92 kW. The maximum total PV generation is 21.52% of the total peak demand. Fig 5.1 shows the diagram of the modified IEEE 34-bus distribution network and the interconnection of PVs, DGs, and EV clusters. Here, the switchable lines are shown as dashed lines. The characteristics of the

dispatchable DG units are shown in Table 5.1. Table 5.2 shows the operation cost of DG1-DG3 for each segment of the linearized cost curve. The hourly electricity price is considered for the feeder. As shown in Fig. 5.1, four EV clusters are considered. EV cluster 1 has a three-phase interconnection, while EV clusters 2, 3, and 4 are connected to the grid on phases A, B, and C, respectively. Table 5.3 shows the characteristics of the EV clusters. The following cases are considered:

Case 1 – Deterministic operation of the distribution network

Case 2 – Scenario-based stochastic operation of the distribution network

Case 3 – Robust operation of the distribution network

Case 4 – Data-driven distributionally robust operation of the distribution network

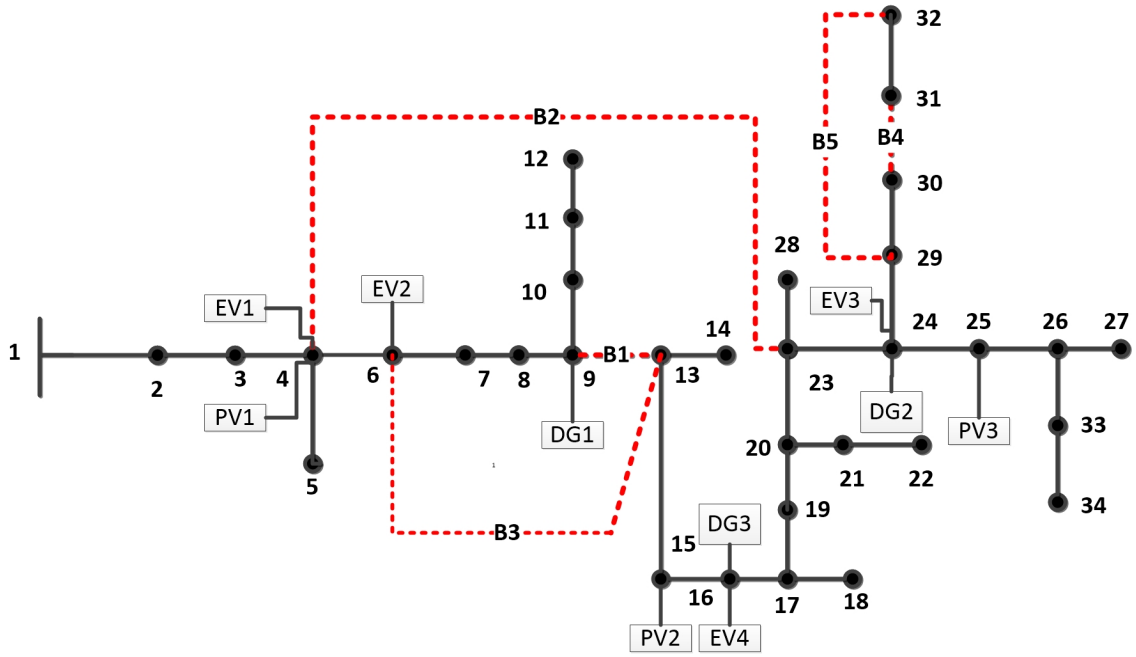

Figure 5.1: Modified IEEE 34-bus distribution network

Table 5.1: Dispatchable DG units' characteristics

DG	Bus	P^{min} (kW)	P^{max} (kW)	Q^{min} (kVAR)	Q^{max} (kVAR)
1	4	0	150	-75	75
2	6	0	100	-50	50
3	24	0	50	-25	25

Table 5.2: The marginal cost of each segment for DGs ($/kWh)

DG	$w_{i,1}$	$w_{i,2}$	$w_{i,3}$	$w_{i,4}$
1	0.18	0.22	0.26	0.30
2	0.17	0.24	0.31	0.38
3	0.15	0.25	0.35	0.45

5.3.1.1 Case 1 - Deterministic operation of the distribution network

In this case, the deterministic solutions of the distribution network operation problem with and without EV interconnections are investigated. The operation cost of the distribution network without EV interconnection is $4530.19 and the operation cost increases to $5336.82 when EV clusters are interconnected to the distribution network. Fig. 5.2 shows the dispatch of feeder, PVs, DGs and charging and discharging power of EVs on phase A. The total energy provided by the feeder and DGs is 11860 kWh. Tables 5.4 and 5.5 show the state of the switchable lines in the network without and with EV interconnection respectively.

Table 5.3: Characteristics of EV clusters in the IEEE 34-bus system

EV	Number of vehicles	Bus	P^{max} (kW)	E^{min} (kWh)	E^{max} (kWh)
1	40	4	888	360	3600
2	25	6	185	75	750
3	40	24	296	120	1200
4	30	16	222	90	900

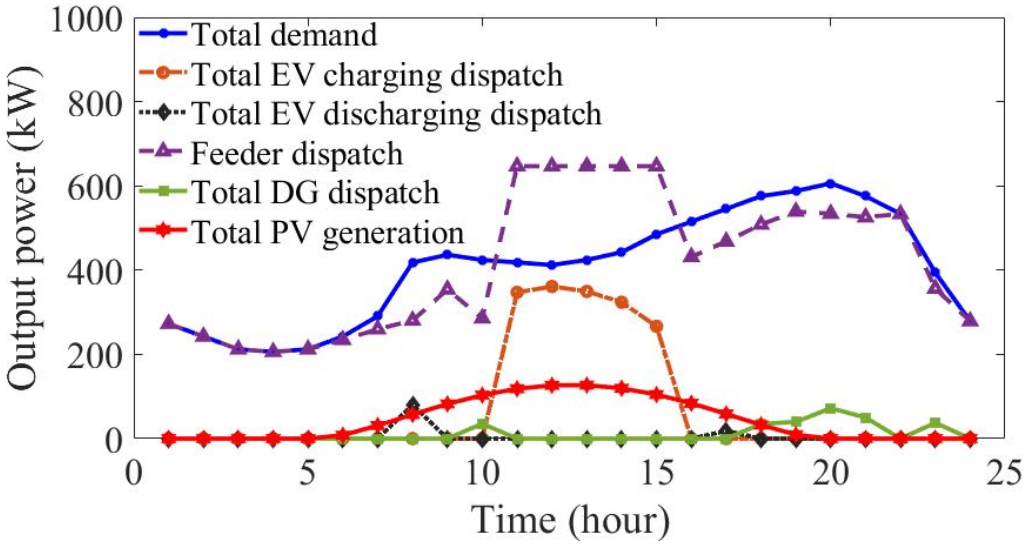

Figure 5.2: The dispatch of feeder, DGs, PVs, and the charging and discharging power of EVs on phase A in Case 1.

Table 5.4: The status of switchable branches in Case 1 without EV interconnection

Switchable branch	Hours (24 hours)
B1	1 1 1 1 1 1 1 1 1 1 1 1 1 1 1 1 1 1 1 1 1 1 1 1
B2	0 0 0 0 0 0 0 0 0 0 0 0 0 0 0 0 0 0 0 0 0 0 0 0
B3	0 0 0 0 0 0 0 0 0 0 0 0 0 0 0 0 0 0 0 0 0 0 0 0
B4	1 1 1 1 1 1 1 1 1 1 1 1 1 1 1 1 1 1 1 1 1 1 1 1
B5	0 0 0 0 0 0 0 0 0 0 0 0 0 0 0 0 0 0 0 0 0 0 0 0

5.3.1.2 Case 2 – Scenario-based stochastic operation of the distribution network

In this case, the uncertainty associated with the PV generation and EV clusters are considered using 40 scenarios. The expected operation cost of the distribution network is increased to \$5364.58 compared to the deterministic solution as a result of the imposed uncertainties in the operation horizon. The switching states of the switchable lines are shown in Table 5.6. As shown in this table, the branch connecting buses 4 and 23 is closed and the branch connecting buses 9 to 13 is opened. The expected dispatch of feeder, PVs, DGs and charging and discharging power of EVs on phase A is shown in Fig. 5.3. Here, the total

Table 5.5: The status of switchable branches in Case 1 with EV interconnection

Switchable branches	Hours (24 hours)
B1	0 0 1 1 0 0 0 0 0 0 0 0 0 0 0 0 0 0 0 0 0 0 0 0
B2	1 1 0 0 1 1 1 1 1 1 1 1 1 1 1 1 1 1 1 1 1 1 1 1
B3	0 0 0 0 0 0 0 0 0 0 0 0 0 0 0 0 0 0 0 0 0 0 0 0
B4	1 1 1 1 1 1 1 1 1 1 1 1 1 1 1 1 1 1 1 1 1 1 1 1
B5	0 0 0 0 0 0 0 0 0 0 0 0 0 0 0 0 0 0 0 0 0 0 0 0

Table 5.6: The status of switchable branches in Case 2

Switchable branch	Hours (24 hours)
B1	0 0 0 0 0 0 0 0 0 0 0 0 0 0 0 0 0 0 0 0 0 0 0 0
B2	1 1 1 1 1 1 1 1 1 1 1 1 1 1 1 1 1 1 1 1 1 1 1 1
B3	0 0 0 0 0 0 0 0 0 0 0 0 0 0 0 0 0 0 0 0 0 0 0 0
B4	1 1 1 1 1 1 1 1 1 1 1 1 1 1 1 1 1 1 1 1 1 1 1 1
B5	0 0 0 0 0 0 0 0 0 0 0 0 0 0 0 0 0 0 0 0 0 0 0 0

expected energy provided by the feeder and DGs is 11885 kWh which is increased compare to that in Case 1.

5.3.1.3 Case 3 – Robust operation of the distribution network

In this section, a two-stage robust optimization problem is formulated and solved using the C&CG algorithm. The non-linear terms in the sub-problem are linearized using McCormick envelopes. The uncertainty sets for the PV generation and EV cluster characteristics are formed using the upper and lower bounds of the empirical data. Fig. 5.4, shows the worst-case dispatch of feeder, PVs, DGs, and charging and discharging power of EVs on phase A. In this case, the total energy output of DGs and feeder is increased to 12392 kWh, which is larger than those in Cases 1 and 2. The operation cost of the distribution network is \$11834.53 which is more than those in Cases 1 and 2. As expected, the solution to the robust optimization problem is more conservative compared to the solution to the SP and deterministic problems. The switching states of the switchable branches in the distribution

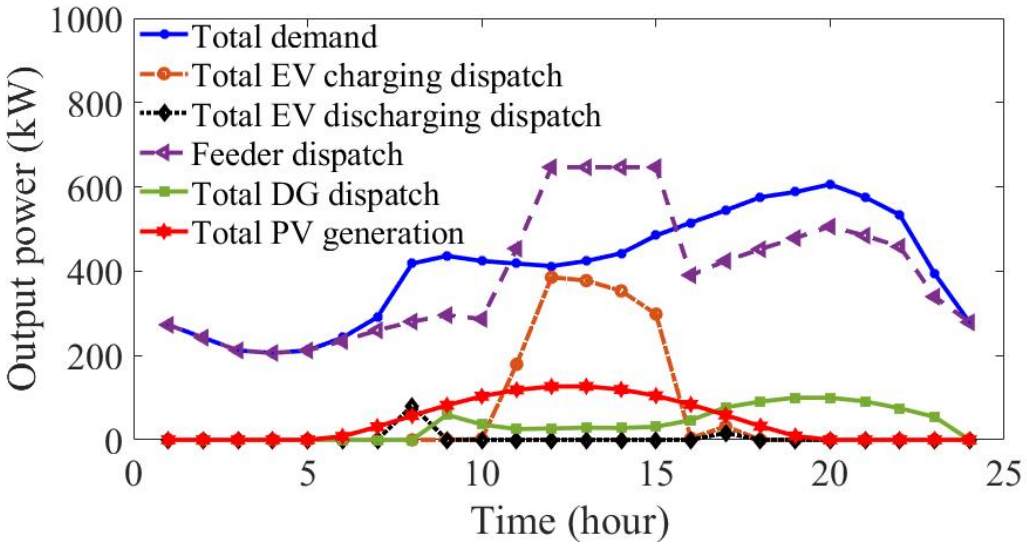

Figure 5.3: The expected dispatch of feeder, DGs, PVs, and charging and discharging power of EVs on phase A in Case 2.

system are the same as those in Case 2, except for hours 5 and 7, where branch 1 is closed and branches 2 and 3 are opened. The total demand curtailment is 348.3650 kWh which is more than those in Cases 1 and 2.

5.3.1.4 Case 4 – Data-driven distributionally robust operation of the distribution network

In this section, the worst-case probability distributions of uncertain variables are procured given the 40 sample data for each variable. Fig. 5.5, shows the expected dispatch of feeder, PVs, DGs, and charging and discharging power of EVs for phase A, considering the worst-case probability of each scenario. The total expected energy output of feeder and DGs in this case is 12117 kWh which is less than that in Case 3 and more than that in Cases 1 and 2. The switching states of distribution branches are given in Table 5.7. Here, without switchable branches, the maximum voltage deviation during the operation horizon on phases A, B, and C, is 0.052; however, with switching capability, such deviation will decrease to 0.016. In this case, the impacts of the size of the historical data and selected confidence level, V2G capability in EV clusters, and the out-of-sample performance of DRO are investigated in the IEEE-34 distribution network.

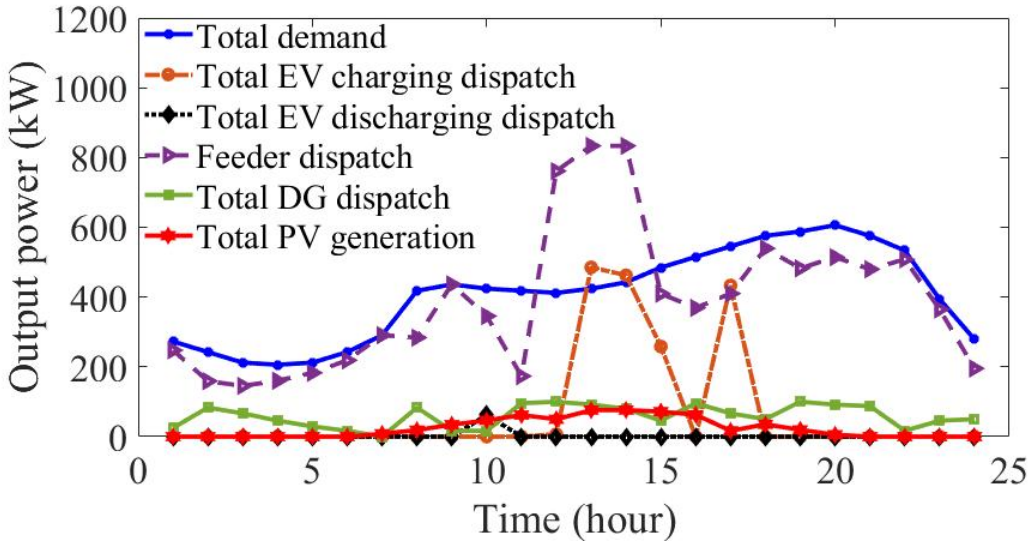

Figure 5.4: The worst-case dispatch of feeder, DGs, PVs, and charging and discharging of EVs in Case 3 on phase A.

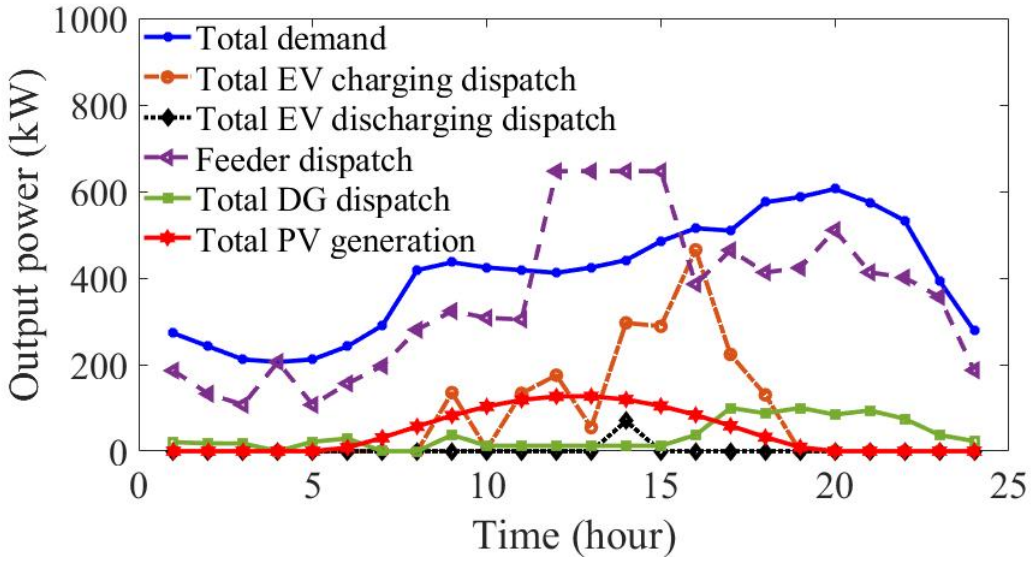

Figure 5.5: The expected dispatch of feeder, DGs, PVs, and charging and discharging of EVs on phase A in Case 4, considering the worst-case probability distribution of uncertain variables.

a) The impacts of sample size and confidence level

Table 5.8, shows the impact of the number of samples on the total in-sample operation cost of

Table 5.7: The status of switchable branches in Case 4

Switchable branches	Hours (24 hours)
B1	0 0 0 0 0 0 0 0 0 0 0 0 0 0 0 0 0 0 0 0 0 0 0 0
B2	0 0 0 0 0 0 0 0 0 0 0 0 0 0 0 0 0 0 0 0 0 0 0 0
B3	1 1 1 1 1 1 1 1 1 1 1 1 1 1 1 1 1 1 1 1 1 1 1 1
B4	1 1 1 1 1 1 1 1 1 1 1 1 1 1 1 1 1 1 1 1 1 0 1 0
B5	0 0 0 0 0 0 0 0 0 0 0 0 0 0 0 0 0 0 0 0 0 1 0 1

the distribution network in this case. The results are compared to those presented in Case 2. As shown in this table the expected operation cost of the distribution network as the solution to the data-driven DRO problem, converges to the solution to the SP problem as the size of sample data increases. As shown in Table 5.8, the solution to the formulated DRO problem i.e., the expected operation cost of the distribution network, for different sizes of sample data, is greater than the solution to the SP problem. This shows that solving the DRO problem provides a more conservative solution compared to the SP solutions. Furthermore, it is shown in this case that the solution to the SP problem i.e., the expected operation cost of the distribution network, increases as the number of samples increases; however, the solution to the DRO problem decreases as the number of samples increases. The solution to the DRO problem is less conservative compared to the solution to the RO problem. Here, the expected operation cost of the distribution network is \$8019.10 that is increased to \$11834.53 when the distribution network operation problem is solved as a RO problem. Table 5.9 shows the solution time with different sizes of sample data in Cases 2 and 4. As shown in this table, the solution time for solving the DRO problem (Case 4) is higher than that for the SP problem (Case 2). Furthermore, as the number of samples increases the solution time increases.

The total demand curtailments on all phases are shown in Table 5.10. The total demand curtailments on phases A, B, and C are increased by 41.638 kWh, 87.714 kWh, and 27.534 kWh in this case compared to those in Case 1. Furthermore, the demand curtailments on phases A, B, and C are increased by 40.608 kWh, 84.6 kWh, and 26.80 kWh in this case compared to those in Case 2. The demand curtailments on all phases, in this case, are less than those in Case 3.

Table 5.8: The expected operation cost ($) in Cases 2 and 4 with different sizes of sample data

Case	Size of sample data				
	20	40	60	80	100
Case 2	5544.47	5364.58	5331.19	5307.90	5320.40
Case 4	8019.10	7922.62	7915.80	7924.46	7907.78

Table 5.9: Solution times for Cases 2 and 4 with different sizes of sample data

Case	Size of sample data				
	20	40	60	80	100
Case 2	00:00:32	00:00:52	00:01:27	00:01:59	00:02:32
Case 4	00:03:52	01:42:58	24:42:57	31:19:39	33:47:54

As the size of the sample data increases, the Wasserstein radius α decreases; however, the Wasserstein radius is also affected by the confidence level β. As the confidence level increases the Wasserstein radius increases. Table 5.11, shows the impact of the confidence level on the solution of the DRO problem (i.e., the expected operation cost of the distribution network) for 40 data samples. As the confidence level increases, the increase in the Wasserstein radius will lead to considering the probability distributions of uncertain variables that are further away from the probability distribution of the empirical data which results in the higher expected operation costs.

b) The impacts of V2G capability in EV clusters

In this section the impacts of the V2G capability of the EVs on the operation cost are

Table 5.10: The total curtailment on each phase in all cases

Cases	Total Curtailment (kWh)		
	Phase A	Phase B	Phase C
Case 1	0	0	0
Case 2	1.03	3.114	0.731
Case 3	97.254	194.332	56.779
Case 4	41.638	87.714	27.534

Table 5.11: The expected operation cost in Case 4 with different confidence levels

Confidence level	Wasserstein radius	Cost ($)
0.99	5.758	7922.62
0.95	4.644	7920.70
0.9	4.072	7914.41
0.8	3.404	7908.74
0.7	2.944	7896.95
0.6	2.568	7847.02
0.5	2.234	7815.14

Table 5.12: Distribution network operation cost with and without the V2G capability

Cases	Cost ($)	
	With V2G	Without V2G
Case 1	5336.82	5378.49
Case 2	5364.58	5405.30
Case 3	10670.90	11834.53
Case 4	7922.618	7964.053

investigated. Table 5.12 presents the operation cost for all cases with and without V2G capability for EV clusters. As shown in this table, the operation cost will decrease as EVs are equipped with the V2G capability. Fig 5.6 shows the total available energy in EV clusters with V2G capability.

c) Out-of-sample performance

In order to evaluate the out of sample performance of SP and DRO problems, the dispatch of the distribution feeder is considered as a first-stage decision which is not dependent on samples and scenarios. The out-of-sample performance of SP and DRO solutions are shown in Table 5.13. Here, the out-of-sample performance of DRO solution is better than that for SP as the operation cost of the distribution network using DRO formulation is less than that using SP for out-of-sample EV and PV generation data. Fig. 5.7 demonstrates the distribution of out-of-sample cost for 40 sample data in Cases 2 and 4. As shown in this figure, the probability distribution of out-of-sample operation cost using DRO is concentrated than the solution to the SP problem. This implies that the solution to DRO problem is more

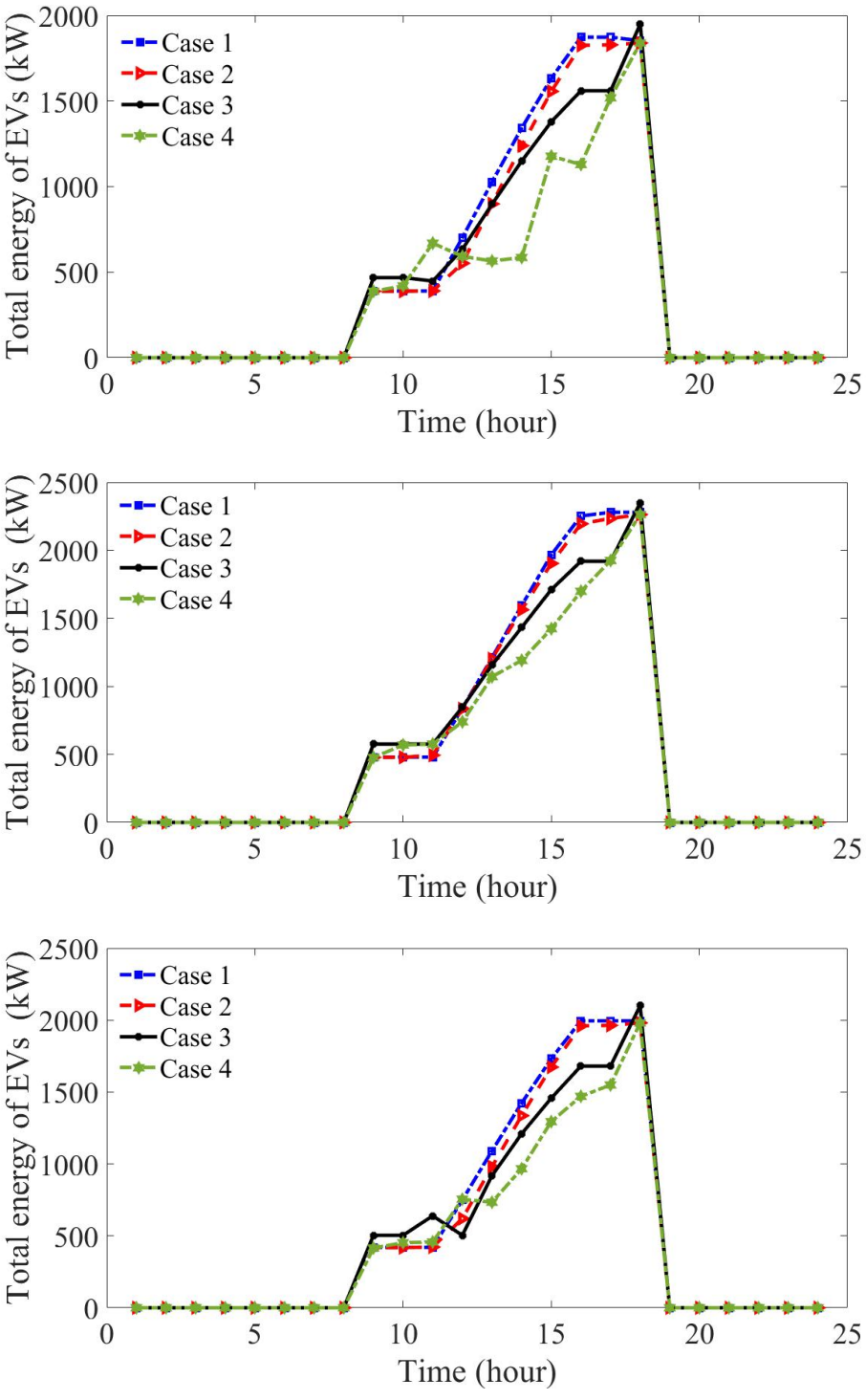

(c)

Figure 5.6: The total available energy in EV clusters in Cases 1 and 3 and the total expected available energy in Cases 2 and 4 connected to (a) phase A, (b) phase B and (c) phase C in

Table 5.13: The out-of-sample expected operation costs ($) in Cases 2 and 4 with different sizes of sample data

Cases	Size of sample data			
	40	60	80	100
Case 2	5094.03	5096.25	5090.45	5098.52
Case 4	5015.10	4914.99	5008.95	5040.27

robust compared to the solution to the SP problem.

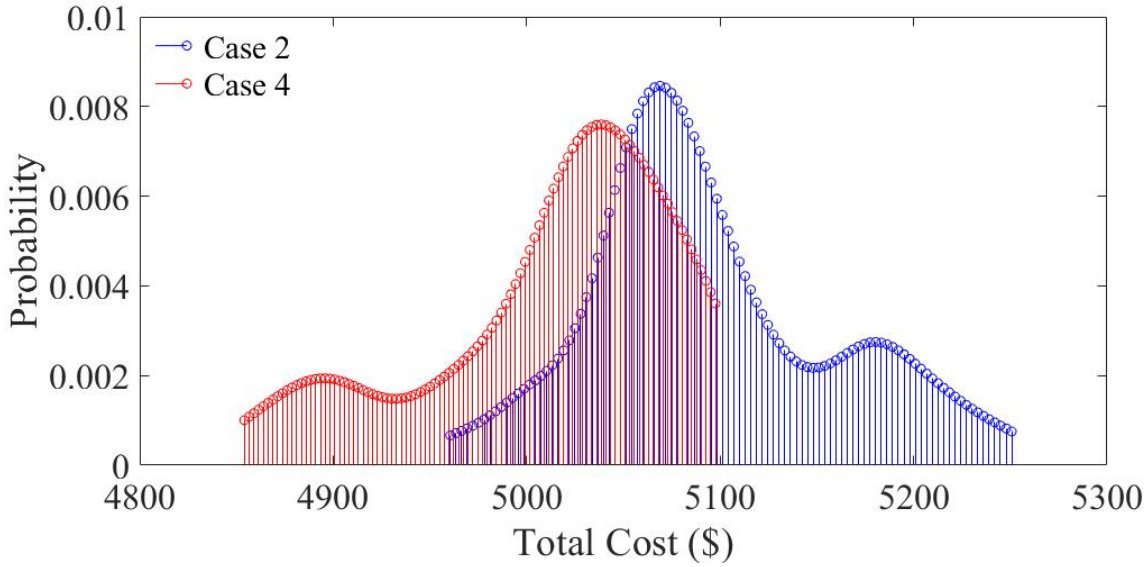

Figure 5.7: Out-of-sample distribution of operation cost in Case 2 and Case 4.

5.3.2 IEEE 123-bus system

The modified IEEE 123-bus test system with switchable lines, is shown in Fig. 5.8. The peak real and reactive demands on phase A are 1420 kW and 775 kVar, the peak real and reactive demands on phase B are 915 kW and 515 kVar, and the peak real and reactive demands on phase C are 1155 kW and 635 kVar, respectively. Table 5.14 shows the

characteristics of three-phase DG units. The marginal costs at each segment of the DG units' cost curves are shown in Table 5.15 and the hourly price of electricity at the distribution feeder is similar to that for the IEEE 34-bus distribution system. The characteristics of the EV clusters are given in Table 5.16. The maximum total solar PV generation is 36.1% of the total peak demand. The total PV generation and demand profiles are shown in Fig. 5.9. The maximum total EV demand is 46.6% of the total peak demand. Similar to the IEEE 34-bus network four case studies are considered.

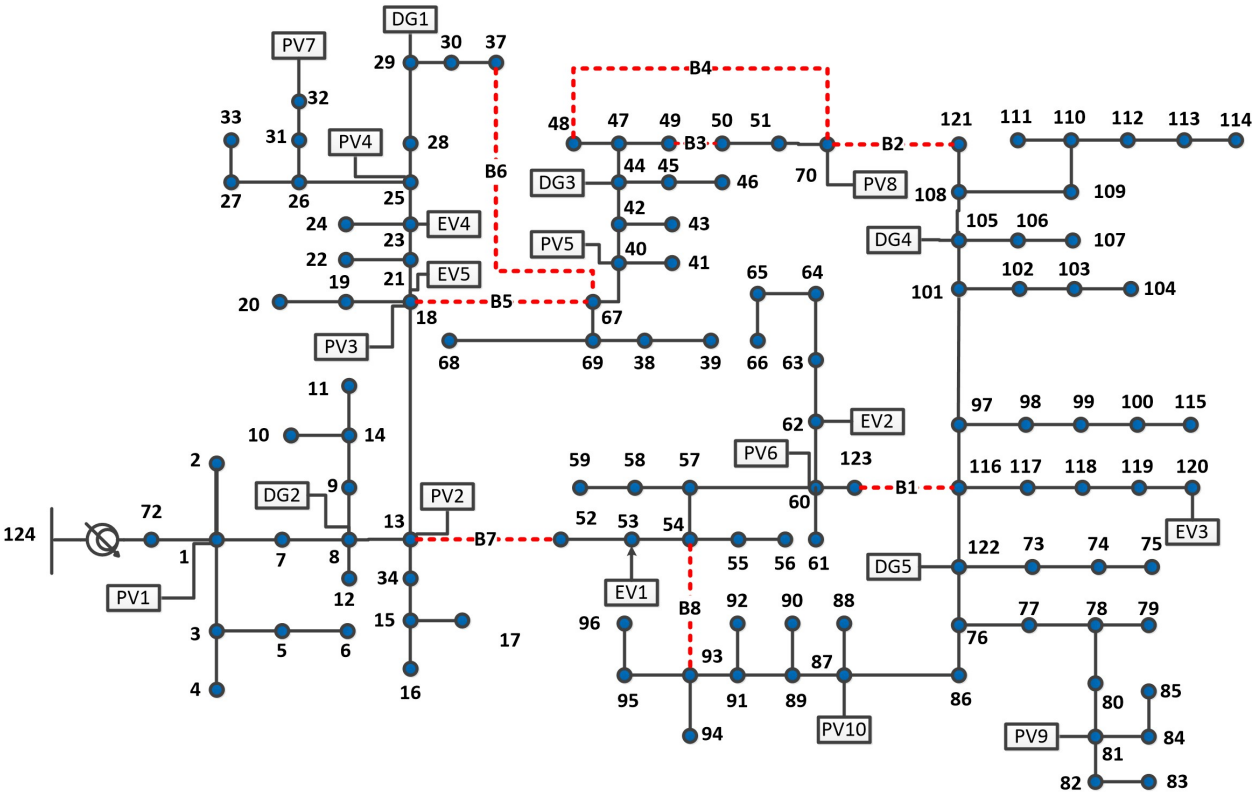

Figure 5.8: The modified IEEE 123-bus system.

5.3.2.1 Case 1 – Deterministic operation of the distribution network

In this case, once the EV interconnection is ignored the operation cost of the distribution

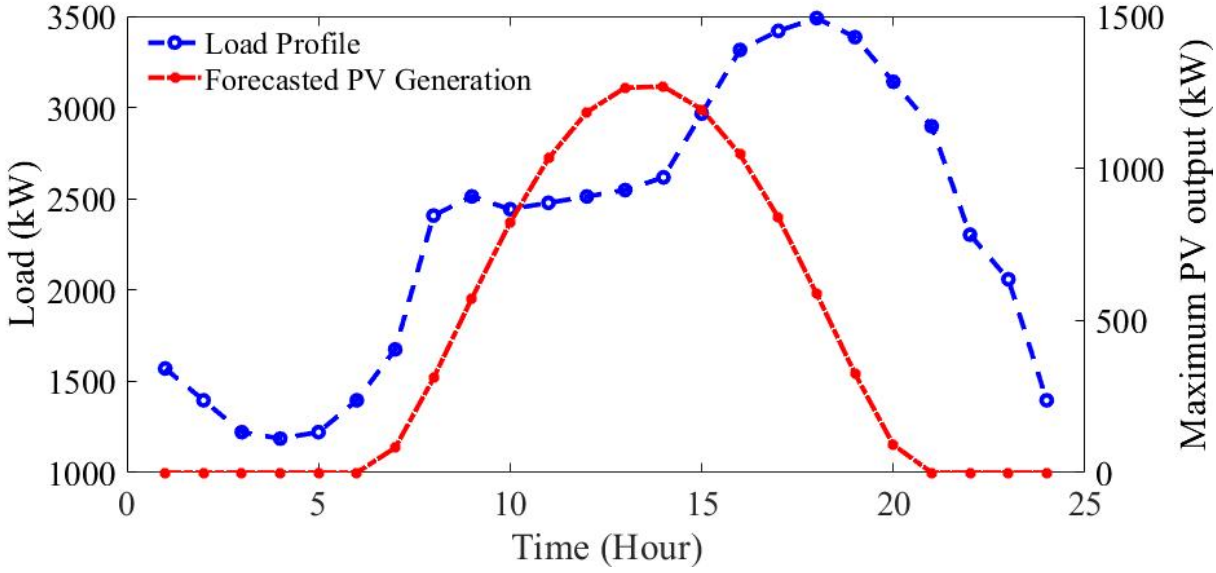

Figure 5.9: PV generation and demand profiles for IEEE 123-bus system

Table 5.14: Characteristics of DG units in the IEEE 123-bus system

DG	Bus	P^{min} (kW)	P^{max} (kW)	Q^{min} (kVAR)	Q^{max} (kVAR)
1	29	0	200	-100	100
2	8	0	200	-100	100
3	44	0	100	-60	60
4	105	0	120	-60	60

network is \$8183.75. The interconnection of EVs to the distribution network will increase the operation cost to \$9545.05. Table 5.17 shows the switching states of the switchable branches considering the EV interconnection.

5.3.2.2 Case 2 – Scenario-based stochastic operation of the distribution network

In this case, the expected operation cost for 40 scenarios is \$9576.46, and the switching states of the switchable branches are shown in Table 5.18. Similar to the previous case study, the expected operation cost is higher compared to operation cost in Case 1 (solution to the deterministic problem).

Table 5.15: The marginal cost of each segment of DGs in the IEEE 123-bus system ($/kWh)

DG	$w_{i,1}$	$w_{i,2}$	$w_{i,3}$	$w_{i,4}$
1	0.18	0.22	0.26	0.30
2	0.17	0.24	0.3	0.38
3	0.15	0.25	0.35	0.45
4	0.15	0.25	0.35	0.45

Table 5.16: Characteristics of EV fleets in IEEE 123-bus system

EV	Number of vehicles	Bus	P^{max} (kW)	E^{min} (kWh)	E^{max} (kWh)
1	75	18	555	225	2250
2	60	23	444	180	1800
3	90	62	666	270	270
4	150	53	1110	450	4500
5	60	123	444	180	1800

Table 5.17: The status of switchable branches with EV interconnection in Case 1 for the IEEE 123-bus system

Switchable branches	Hours (24 hours)
B1	0 0 0 0 0 0 1 0 0 0 0 0 0 0 0 0 0 0 0 0 0 0 0 0
B2	1 1 1 1 1 1 0 1 1 1 1 1 1 1 1 1 1 1 1 1 1 1 1 1
B3	0 1 0 0 0 0 1 0 1 1 1 1 1 0 1 1 1 1 1 1 1 1 1 1
B4	1 0 1 1 1 1 0 1 0 0 0 0 0 1 0 0 0 0 0 0 0 0 0 0
B5	0 1 1 1 1 1 1 1 1 1 1 1 1 1 1 1 1 1 1 1 0 0 0 0
B6	1 0 0 0 0 0 0 0 0 0 0 0 0 1 0 0 0 0 0 0 1 1 1 1
B7	0 1 0 1 1 1 1 1 0 1 1 1 0 1 0 0 1 0 1 0 0 1 1 1
B8	1 0 1 0 0 0 0 0 1 0 0 0 1 0 1 1 0 1 0 1 1 0 0 0

Table 5.18: The status of switchable branches in Case 2 for the IEEE 123-bus system

Switchable branches	Hours (24 hours)
B1	0 1 1 1 1 1 1 1 1 1 1 1 1 1 1 1 1 1 1 1 1 1 1 1
B2	1 0 0 0 0 0 0 0 0 0 0 0 0 0 0 0 0 0 0 0 0 0 0 0
B3	1 1 1 1 1 1 1 1 1 1 1 1 1 1 1 1 1 1 1 1 1 1 1 1
B4	0 0 0 0 0 0 0 0 0 0 0 0 0 0 0 0 0 0 0 0 0 0 0 0
B5	0 1 1 1 1 1 1 1 1 1 1 1 1 1 1 1 1 1 1 1 1 1 1 1
B6	1 0 0 0 0 0 0 0 0 0 0 0 0 0 0 0 0 0 0 0 0 0 0 0
B7	0 1 1 1 1 1 1 1 1 1 1 1 1 1 1 1 1 1 1 1 1 1 1 1
B8	1 0 0 0 0 0 0 0 0 0 0 0 0 0 0 0 0 0 0 0 0 0 0 0

Table 5.19: The status of switchable branches in Case 3 for the IEEE 123-bus system

Switchable branches	Hours (24 hours)
B1	0 0 0 0 0 0 1 0 0 0 0 0 0 0 0 0 0 0 0 0 0 0 0 0
B2	1 1 1 1 1 1 0 1 1 1 1 1 1 1 1 1 1 1 1 1 1 1 1 1
B3	0 1 0 0 0 0 1 0 1 1 1 1 1 0 1 1 1 1 1 1 1 1 1 1
B4	1 0 1 1 1 1 0 1 0 0 0 0 0 1 0 0 0 0 0 0 0 0 0 0
B5	0 0 0 0 0 0 0 0 0 0 0 0 0 0 0 0 0 0 0 0 0 0 0 0
B6	1 1 1 1 1 1 1 1 1 1 1 1 1 1 1 1 1 1 1 1 1 1 1 1
B7	0 1 1 1 1 1 1 1 0 1 1 1 1 1 1 1 1 1 1 1 1 1 0 0
B8	1 0 0 0 0 0 0 0 1 0 0 0 0 0 0 0 0 0 0 0 0 0 1 1

5.3.2.3 Case 3 – Robust operation of the distribution network

In the RO problem formulation, the uncertainty sets for solar PV generation and EVs are determined using the upper and lower values of the empirical data. The total operation cost is \$24067.32, which is higher than the operation costs in Cases 1 and 2. The states of the switchable branches are given in Table 5.19.

5.3.2.4 Case 4 – Data-Driven Distributionally robust operation of the distribution network

In this case, the expected operation cost of the distribution network considering the worst-case probability distribution of the uncertain variables with 40 data samples, is \$17305.01. The expected operation cost of the distribution network in this case (the solution to the DRO problem) is higher than those in Cases 1 and 2, and less than that in Case 3. The total demand curtailments in Cases 1-4 are shown in Table 5.20. As shown in this table, the total demand curtailments on all phases in Cases 1 and 2 are zero. The total demand curtailment in Case 3 is the highest and the total demand curtailment in Case 4 is higher than those in Cases 1 and 2. Table 5.21, demonstrates the sates of the switchable branches in this case and Table 5.22 shows the expected operation cost of the distribution network as the number of data samples increases from 20 to 100. As shown in Table 5.22, with the increase in the number of samples, the value of the objective function of the DRO problem is decreasing and gets closer to that of the SP problem. Moreover, the solution to the SP problem increases with the increase in the number of sample data. However, similar to the previous case study,

Table 5.20: Total demand curtailments on all phases in the IEEE 123-bus system

Cases	Total Curtailment (kWh)		
	Phase A	Phase B	Phase C
Case 1	0	0	0
Case 2	0	0	0
Case 3	567.919	0	172.346
Case 4	388.970	14.867	11.528

Table 5.21: The status of the switchable branches in Case 4 for the IEEE 123-bus system

Switchable branches	Hours (24 hours)
B1	1 0 1 0 0 0 0 0 1 0 0 0 0 0 0 0 0 0 1 0 0 0 0 1
B2	0 1 0 1 1 1 1 1 0 1 1 1 1 1 1 1 1 1 0 1 1 1 1 0
B3	1 1 1 0 0 1 1 1 0 0 1 0 0 1 1 1 0 0 1 1 1 0 1 1
B4	0 0 0 1 1 0 0 0 1 1 0 1 1 0 0 0 1 1 0 0 0 1 0 0
B5	0 0 0 0 0 0 0 0 0 0 1 1 0 0 0 1 0 1 0 0 0 1 0 0
B6	1 1 1 1 1 1 1 1 1 1 0 0 1 1 1 1 1 0 1 1 1 0 1 1
B7	1 1 1 0 1 0 1 1 1 1 0 0 0 1 0 0 0 0 1 0 0 0 0 1
B8	0 0 0 0 0 1 0 0 0 0 1 1 1 0 1 1 1 1 0 1 1 1 1 0

the value of the objective function in the DRO problem i.e., the expected operation cost of the distribution network decreases as the number of data samples increases.

Considering 40 data samples, the expected operation cost of the distribution network with V2G capability for the interconnected EVs is $17305.01. The expected operation cost increases to $17612.28 once the EV clusters do not have the V2G capability. The total operation cost of the distribution network with and without V2G capability of EVs in all cases are shown in Table 5.23.

5.4 Conclusion

In this chapter, the data-driven distributionally robust operation of the distribution network with high penetration of PV generation and EV interconnection is evaluated. The proposed formulation captures the uncertainty in PV generation and the characteristics of the interconnected EV clusters. A solution algorithm based on the C&CG approach is

Table 5.22: The expected operation cost of the IEEE 123-bus system with different numbers of empirical data samples

Cases	Size of Historical Data				
	20	40	60	80	100
Case 2	14591	14706	14675	14767	14901
Case 4	17310	17305	17298	17290	17288

Table 5.23: The operation cost of the IEEE 123-bus system with and without V2G capability in EVs

Cases	Distribution network operation cost ($)	
	With V2G capability	Without V2G capability
Case 1	9545.05	9879.51
Case 2	14705.52	15000.06
Case 3	24067.32	27475.95
Case 4	17305.01	17612.28

used to solve the proposed formulation. It is shown that the expected operation cost of the distribution network using the proposed DRO formulation converges to the solution of the SP problem as the number of data samples increases. Moreover, increasing the confidence level will increase the Wasserstein radius and therefore, increase the operation of the distribution network. The solution to the DRO problem is compared to those of SP and RO problems. It is shown that the operation cost of the distribution network is highest once the operation problem is formulated as a RO problem. The solution to the distributionally robust operation of the distribution network is less conservative compared to the solution to the RO problem and therefore, the operation cost of the distribution network using the DRO formulation is less than that using the RO formulation. The demand curtailment of the distribution network is compared to the SP and RO solutions. It is shown that the demand curtailment is the highest, once the distribution network operation problem is formulated as a RO problem. Furthermore, the out-of-sample performance of the DRO problem is compared to that of the SP problem. It is shown that the distributionally robust operation of the distribution network would lead to a more conservative solution once it is exposed to unseen uncertainties.

Therefore the out-of-sample performance of the DRO solution is better than that for the SP. The impact of V2G on the operation cost of the distribution network is further investigated. It is shown that the V2G capability of EV clusters will reduce the operation cost of the distribution network.

Chapter 6

Data-Driven Distributionally Robust Operation of Distribution Networks with Ramping Flexibility

The increase in the generation capacity of the variable renewable resources and electricity demand introduces new operational challenges to the unbalanced three-phase distribution networks. This chapter addresses the uncertainty associated with the ramping of net demand using a data-driven approach. A continuous-time optimization problem is reformulated to a linear programming problem using Bernstein polynomials. A distributionally robust optimization problem is formulated to capture the worst-case probability distribution of the net demand, which includes the demand and the PV generation. The solution to the distributionally robust operation of the unbalanced distribution network is compared to that of the stochastic programming problem in which the uncertainty associated with the net demand ramp is captured using scenarios. The developed formulated problem is validated using a modified IEEE 13-bus unbalanced distribution system. The impact of ramp limits of the main feeder on the expected operation cost of the distribution network is investigated. This chapter proposes a data-driven approach to handle the uncertainty in the ramping requirement of the net demand using limited empirical data. The proposed data-driven distributionally robust operation scheme for the distribution networks combines the economic benefits of SP and RO problems by considering the worst-case probability of the net demand ramping using limited available empirical ramping samples. The contributions of this chapter are listed as follows:

- The unbalanced distribution network operation problem is formulated as a distributionally robust optimization problem considering the worst-case probability of the net demand ramping requirements.
- The in-sample and out-of-sample performances of the proposed method are compared

with the SP counterpart of the formulated problem.

- The feeder and DGs ramping costs are considered and the impact of the feeder ramping limit on the expected operation cost of the distribution network is evaluated.

The rest of this chapter is organized as follows; section 6.1 presents the continuous-time formulation of the unbalanced distribution network operation problem. The presented problem is further reformulated as a discrete optimization problem using Bernstein polynomial and the distributionally robust counterpart of the problem is presented in this section. Section 6.2 presents the numerical results and the conclusion is presented in Section 6.3.

6.1 Problem Formulation

6.1.1 Notation

In this chapter, $n \in \mathcal{F}$, $g \in \mathcal{G}$, $i, j \in \mathcal{B}$, $v \in \mathcal{V}$, $d \in \mathcal{D}$, $\tau \in \mathcal{H}$, $\varphi \in \Phi$, and $m \in \mathcal{M}$ represent the indices for feeder, distributed generation, bus (node), PV, demand, time step, phase of the distribution network and segment in the piece-wise linear cost function of the DG, respectively. The introduced indices belong to the corresponding sets; furthermore, the set of branches is defined as $\mathcal{L} = \{(i, j) \mid i, j \in \mathcal{B}, i \neq j\}$. The variables $p_i^{(.),\varphi}(t)$ and $q_i^{(.),\varphi}(t)$ represent the real and reactive power of a unit connected to bus i, respectively. Furthermore, variables $p_{ij}^{\varphi}(t)$ and $q_{ij}^{\varphi}(t)$ represent the real and reactive power flow from node i to node j respectively. The variable $ps_i^{g,m,\varphi}(t)$ is the power output at segment m; and the positive variables $r_i^{(.),n,\varphi}(t)$ and $r_i^{(.),g,m,\varphi}(t)$ are the deployed ramping services of the distribution feeder and DGs respectively. The variable $v_i^{\varphi}(t)$ is the squared voltage on phase φ at node i. The parameters presented in the problem formulation are described as follows. Here, $\rho_n(t)$ is the hourly price of electricity, $\omega_{g,m}$ is the marginal cost and $\overline{ps}_i^{g,m,\varphi}$ is the maximum power in segment m of DG unit g; $\beta_n(t)$ and $\eta_{g,m}$ are the ramping costs of the feeder and DG. Furthermore, $\overline{V}$ and $\underline{V}$ are the upper and lower limits of the voltage, $\tilde{R}_{ij}$ is the resistance, and $\tilde{X}_{ij}$ is the reactance of the branch ij. Moreover, κ_{ij}^{φ} is the availability of phase φ, and $\overline{S}_{ij}^{\varphi}$ is the apparent power capacity of the branch. The parameters $\overline{Q}_i^{v,\varphi}$, $\overline{P}_i^{g,\varphi}$ and $\overline{Q}_i^{g,\varphi}$ are the maximum reactive power of PV unit, maximum real and maximum reactive power of DG units respectively. Finally, PF is the acceptable power factor of the distribution feeder.

6.1.2 Day-ahead continuous-time operation of the distribution network

The day-ahead continuous-time operation of the unbalanced distribution system is formulated as (6.1)-(6.20). The objective function is given in (6.1), where the first two components represent the expected operation cost of the feeder and distributed generation units (DGs), respectively. The last two components represent the ramping costs of the feeder and distributed generation considering the worst-case probability of the net demand ramping. The operation cost of the DG unit is considered as a quadratic function that is linearized using piece-wise linearization technique as shown in (6.2) and (6.3). The nodal real and reactive power balance constraints are shown in (6.4) and (6.5) respectively.

$$\min_{\boldsymbol{p},\boldsymbol{q},\boldsymbol{v},\boldsymbol{r}} \max_{\mathbb{P}} \mathbb{E}_{\mathbb{P}} \sum_{i} \sum_{\varphi} \left(\sum_{n} \int_{0}^{T} \rho_n(t) \cdot p_i^{n,\varphi}(t) dt + \sum_{g} \sum_{m} \int_{0}^{T} \omega_{g,m} \cdot ps_i^{g,m,\varphi}(t) dt + \right.$$
$$\left. \sum_{n} \int_{0}^{T} \beta_n(t) \cdot (r_i^{1,n,\varphi}(t) + r_i^{2,n,\varphi}(t)) dt + \sum_{g} \sum_{m} \int_{0}^{T} \eta_{g,m} \cdot (r_i^{1,g,m,\varphi}(t) + r_i^{2,g,m,\varphi}(t)) dt \right) \quad (6.1)$$

$$ps_i^{g,m,\varphi}(t) \leq \overline{ps}_i^{g,m,\varphi} \quad (6.2)$$

$$p_i^{g,\varphi}(t) = \sum_{m} ps_i^{g,m,\varphi}(t) \quad (6.3)$$

$$\sum_{(i,j)\in\mathcal{L}} p_{ij}^{\varphi}(t) + \sum_{n\in\mathcal{F}} p_i^{n,\varphi}(t) + \sum_{g\in\mathcal{G}} p_i^{g,\varphi}(t) = \sum_{d\in\mathcal{D}} \hat{p}_i^{d,\varphi}(t) - \sum_{v\in\mathcal{V}} \hat{p}_i^{v,\varphi}(t) \quad (6.4)$$

$$\sum_{(i,j)\in\mathcal{L}} q_{ij}^{\varphi}(t) + \sum_{n\in\mathcal{F}} q_i^{n,\varphi}(t) + \sum_{g\in\mathcal{G}} q_i^{g,\varphi}(t) = \sum_{d\in\mathcal{D}} \hat{q}_i^{d,\varphi}(t) - \sum_{v\in\mathcal{V}} q_i^{v,\varphi}(t) \quad (6.5)$$

$$v_j^{\varphi}(t) = v_i^{\varphi}(t) - 2 \cdot \left(\tilde{R}_{ij} \cdot p_{ij}^{\varphi}(t) + \tilde{X}_{ij} \cdot q_{ij}^{\varphi}(t) \right) \quad (6.6)$$

$$\underline{V}^2 \leq v_i^{\varphi}(t) \leq \overline{V}^2 \quad (6.7)$$

$$-\sqrt{2} \cdot \kappa_{ij}^{\varphi} \cdot \overline{S}_{ij}^{\varphi} \leq p_{ij}^{\varphi}(t) + q_{ij}^{\varphi}(t) \leq \sqrt{2} \cdot \kappa_{ij}^{\varphi} \cdot \overline{S}_{ij}^{\varphi} \quad (6.8)$$

$$-\sqrt{2}\cdot\kappa_{ij}^{\varphi}\cdot\overline{S}_{ij}^{\varphi}\leq p_{ij}^{\varphi}\left(t\right)-q_{ij}^{\varphi}\left(t\right)\leq\sqrt{2}\cdot\kappa_{ij}^{\varphi}\cdot\overline{S}_{ij}^{\varphi} \tag{6.9}$$

$$-\kappa_{ij}^{\varphi}\cdot\overline{S}_{ij}^{\varphi}\leq p_{ij}^{\varphi}\left(t\right)\leq\kappa_{ij}^{\varphi}\cdot\overline{S}_{ij}^{\varphi} \tag{6.10}$$

$$-\kappa_{ij}^{\varphi}\cdot\overline{S}_{ij}^{\varphi}\leq q_{ij}^{\varphi}\left(t\right)\leq\kappa_{ij}^{\varphi}\cdot\overline{S}_{ij}^{\varphi} \tag{6.11}$$

$$\sum_{n}\frac{dp_{i}^{n,\varphi}\left(t\right)}{dt}+\sum_{g}\frac{dp_{i}^{g,\varphi}\left(t\right)}{dt}=\sum_{d}\frac{d\hat{p}_{i}^{d,\varphi}\left(t\right)}{dt}-\sum_{v}\frac{d\hat{p}_{i}^{v,\varphi}\left(t\right)}{dt} \tag{6.12}$$

$$\frac{dp_{i}^{n,\varphi}\left(t\right)}{dt}=r_{i}^{1,n,\varphi}\left(t\right)-r_{i}^{2,n,\varphi}\left(t\right) \tag{6.13}$$

$$\frac{dp_{i}^{g,m,\varphi}\left(t\right)}{dt}=r_{i}^{1,g,m,\varphi}\left(t\right)-r_{i}^{2,g,m,\varphi}\left(t\right) \tag{6.14}$$

$$r_{i}^{1,n,\varphi}\left(t\right),r_{i}^{2,n,\varphi}\left(t\right),r_{i}^{1,g,m,\varphi}\left(t\right),r_{i}^{2,g,m,\varphi}\left(t\right)\geq0 \tag{6.15}$$

$$-\overline{Q}_{i}^{v,\varphi}\leq q_{i}^{v,\varphi}\left(t\right)\leq\overline{Q}_{i}^{v,\varphi} \tag{6.16}$$

$$0\leq p_{i}^{g,\varphi}\left(t\right)\leq\overline{P}_{i}^{g,\varphi} \tag{6.17}$$

$$-\overline{Q}_{i}^{g,\varphi}\leq q_{i}^{g,\varphi}\left(t\right)\leq\overline{Q}_{i}^{g,\varphi} \tag{6.18}$$

$$q_{i}^{n,\varphi}\left(t\right)\leq\tan(\cos^{-1}PF)\cdot p_{i}^{n,\varphi}\left(t\right) \tag{6.19}$$

$$-\tan(\cos^{-1}PF)\cdot p_{i}^{n,\varphi}\left(t\right)\leq q_{i}^{n,\varphi}\left(t\right) \tag{6.20}$$

The nodal voltages on both sides of a branch satisfy (6.6) and (6.7). The real and reactive power flow of each branch satisfies a circular constraint which is linearized using (6.8)-(6.11) [97]. Similar constraints are used for the real and reactive power of the distribution feeder. The relationship between the provided ramping services by the feeder and DGs, with the required ramping of the net demand is shown in (6.12), where the net demand at bus i is the demand power minus the PV generation, i.e., $\hat{p}_i^{net,\varphi}(t) = \hat{p}_i^{d,\varphi}(t) - \hat{p}_i^{v,\varphi}(t)$. The ramping trajectory of the feeder is represented by the difference of two positive variables, $r_i^{1,n,\varphi}(t)$ and $r_i^{2,n,\varphi}(t)$, as shown in (6.13), and (6.15). A similar constraint is considered for the DG units shown in (6.14). The reactive power of PVs and the real and reactive power of DGs are bounded by the capacity of the units as shown in (6.16)-(6.18). The reactive power of the feeder is limited by the acceptable power factor as shown in (6.19) and (6.20).

6.1.3 Reformulation of continuous-time operation of distribution network

The formulated continuous-time operation of the distribution network (6.1)-(6.20) is reformulated using the Bernstein Polynomial (BP) and its properties. The 1-dimensional, nth order BP($P_m(t)$) is formulated as (6.21) for $t \in [t_i, t_f]$, where, t_i and t_f are the initial and final time of the continuous trajectory (i.e. Bezeir Curve). Here, $p^{k,m}$ is the kth Bernstein coefficient, and $B_{k,m}$ is the BP basis given in (6.22). The BP properties (6.23)-(6.25) are used to convert the continuous time trajectories into a time-independent Bezeir curve control points [109].

$$P_m(t) = \sum_{k=0}^{m} p^{k,m} B_{k,m}(t) \tag{6.21}$$

$$B_{k,m}(t) = \binom{m}{k} \frac{(t-t_i)^k (t-t_f)^{m-k}}{(t_f-t_i)^m} \tag{6.22}$$

$$\min_{k\in\{0,\dots,m\}} p^{k,m} \leq P_m(t) \leq \max_{k\in\{0,\dots,m\}} p^{k,m} \tag{6.23}$$

$$\dot{P}_{m-1}(t) = \sum_{k=0}^{m-1} \dot{p}^{k,m-1} B_{k,m-1}(t) \tag{6.24}$$

$$\int_{t_i}^{t_f} P_m(t)dt = \frac{t_f - t_i}{m+1} \sum_{k=0}^{m} p^{k,m} \tag{6.25}$$

For the time interval $\tau \in [t_i, t_f]$, the continuous-time variable $p_i^{(.),\varphi}(t)$ is written using the equivalent discrete-time variable $p_{i,\tau}^{(.),\varphi,k}$, where each time interval τ is one hour, and the order of BP is 3, i.e. $m = 3$. Therefore $k = 0, 1, 2, 3$ and the problem is reformulated to (6.26), (6.2)-(6.11), (6.27)-(6.29) and (6.15)-(6.20) by replacing each continuous-time variable $X_i^{(.)}(t)$ with its corresponding control points $X_i^{(.),k}$.

$$\begin{aligned}\min_{\boldsymbol{p,q,v,r}} \max_{\mathbb{P}} \mathbb{E}_{\mathbb{P}} \sum_i \sum_\varphi \sum_\tau \sum_k \Bigg(& \sum_n \rho_{i,\tau}^n p_{i,\tau}^{n,\varphi,k} + \\ & \sum_g \sum_m \omega_{g,m} \cdot ps_{i,\tau}^{g,m,\varphi,k} + \sum_n \beta_{i,\tau}^n \cdot (r_{i,\tau}^{1,n,\varphi,k} + r_{i,\tau}^{2,n,\varphi,k}) \\ & + \sum_g \sum_m \eta_{g,m} \cdot (r_{i,\tau}^{1,g,m,\varphi,k} + r_{i,\tau}^{2,g,m,\varphi,k}) \Bigg)\end{aligned} \tag{6.26}$$

$$\begin{bmatrix} p_{i,\tau}^{n,\varphi,1} - p_{i,\tau}^{n,\varphi,0} \\ p_{i,\tau}^{n,\varphi,2} - p_{i,\tau}^{n,\varphi,1} \\ p_{i,\tau}^{n,\varphi,3} - p_{i,\tau}^{n,\varphi,2} \end{bmatrix} + \begin{bmatrix} p_{i,\tau}^{g,m,\varphi,1} - p_{i,\tau}^{g,m,\varphi,0} \\ p_{i,\tau}^{g,m,\varphi,2} - p_{i,\tau}^{g,m,\varphi,1} \\ p_{i,\tau}^{g,m,\varphi,3} - p_{i,\tau}^{g,m,\varphi,2} \end{bmatrix} = \begin{bmatrix} \hat{p}_{i,\tau}^{d,\varphi,1} - \hat{p}_{i,\tau}^{d,\varphi,0} \\ \hat{p}_{i,\tau}^{d,\varphi,2} - \hat{p}_{i,\tau}^{d,\varphi,1} \\ \hat{p}_{i,\tau}^{d,\varphi,3} - \hat{p}_{i,\tau}^{d,\varphi,2} \end{bmatrix} - \begin{bmatrix} \hat{p}_{i,\tau}^{v,\varphi,1} - \hat{p}_{i,\tau}^{v,\varphi,0} \\ \hat{p}_{i,\tau}^{v,\varphi,2} - \hat{p}_{i,\tau}^{v,\varphi,1} \\ \hat{p}_{i,\tau}^{v,\varphi,3} - \hat{p}_{i,\tau}^{v,\varphi,2} \end{bmatrix} \tag{6.27}$$

$$3 \cdot \begin{bmatrix} p_{i,\tau}^{n,\varphi,1} - p_{i,\tau}^{n,\varphi,0} \\ p_{i,\tau}^{n,\varphi,2} - p_{i,\tau}^{n,\varphi,1} \\ p_{i,\tau}^{n,\varphi,3} - p_{i,\tau}^{n,\varphi,2} \end{bmatrix} = \begin{bmatrix} r_{i,\tau}^{1,n,\varphi,0} - r_{i,\tau}^{2,n,\varphi,0} \\ r_{i,\tau}^{1,n,\varphi,1} - r_{i,\tau}^{2,n,\varphi,1} \\ r_{i,\tau}^{1,n,\varphi,2} - r_{i,\tau}^{2,n,\varphi,2} \end{bmatrix} \tag{6.28}$$

$$3 \cdot \begin{bmatrix} p_{i,\tau}^{g,m,\varphi,1} - p_{i,\tau}^{g,m,\varphi,0} \\ p_{i,\tau}^{g,m,\varphi,2} - p_{i,\tau}^{g,m,\varphi,1} \\ p_{i,\tau}^{g,m,\varphi,3} - p_{i,\tau}^{g,m,\varphi,2} \end{bmatrix} = \begin{bmatrix} r_{i,\tau}^{1,g,m,\varphi,0} - r_{i,\tau}^{2,g,m,\varphi,0} \\ r_{i,\tau}^{1,g,m,\varphi,1} - r_{i,\tau}^{2,g,m,\varphi,1} \\ r_{i,\tau}^{1,g,m,\varphi,2} - r_{i,\tau}^{2,g,m,\varphi,2} \end{bmatrix} \tag{6.29}$$

To capture the uncertainty in net demand ramping requirements, a data-driven distributionally robust optimization problem is formulated. Here, the empirical data includes the samples of net demand ramp rates in (6.30) where the forecast error of total net demand is given in (6.31). The unknown probability distribution $\mathbb{P}$ of the net ramping is in the ambiguity set

$\mathcal{P}$ with a certain confidence level. The ambiguity set is formed as a Wasserstein ball with radius ϵ around the empirical probability distribution [65]- [110].

$$\tilde{\mathcal{R}}_{\tau}^{\varphi} = \begin{bmatrix} \tilde{\xi}_{\tau}^{\varphi,m1} - \tilde{\xi}_{\tau}^{\varphi,m0} \\ \tilde{\xi}_{\tau}^{\varphi,m2} - \tilde{\xi}_{\tau}^{\varphi,m1} \\ \tilde{\xi}_{\tau}^{\varphi,m3} - \tilde{\xi}_{\tau}^{\varphi,m2} \end{bmatrix} \tag{6.30}$$

$$\tilde{\xi}_{\tau}^{\varphi,k} = \sum_{i \in \mathcal{B}} \left(\tilde{p}_{i,\tau}^{net,\varphi,k} - \hat{p}_{i,\tau}^{net,\varphi,k} \right) \tag{6.31}$$

To reformulate (6.26), the affine adjustments for ramping requirement of feeder and DGs on each phase φ, are defined as (6.32)-(6.35) where $\tilde{\mathcal{R}}_{\tau}^{\varphi}$ represents the forecast error of the total net demand ramping requirement.

$$\begin{bmatrix} \tilde{p}_{i,\tau}^{g,m,\varphi,1} - \tilde{p}_{i,\tau}^{g,m,\varphi,0} \\ \tilde{p}_{i,\tau}^{g,m,\varphi,2} - \tilde{p}_{i,\tau}^{g,m,\varphi,1} \\ \tilde{p}_{i,\tau}^{g,m,\varphi,3} - \tilde{p}_{i,\tau}^{g,m,\varphi,2} \end{bmatrix} = \begin{bmatrix} p_{i,\tau}^{g,m,\varphi,1} - p_{i,\tau}^{g,m,\varphi,0} \\ p_{i,\tau}^{g,m,\varphi,2} - p_{i,\tau}^{g,m,\varphi,1} \\ p_{i,\tau}^{g,m,\varphi,3} - p_{i,\tau}^{g,m,\varphi,2} \end{bmatrix} - \alpha_{i,\tau}^{g,\varphi} \cdot \tilde{\mathcal{R}}_{\tau}^{\varphi} \tag{6.32}$$

$$\begin{bmatrix} \tilde{p}_{i,\tau}^{n,\varphi,1} - \tilde{p}_{i,\tau}^{n,\varphi,0} \\ \tilde{p}_{i,\tau}^{n,\varphi,2} - \tilde{p}_{i,\tau}^{n,\varphi,1} \\ \tilde{p}_{i,\tau}^{n,\varphi,3} - \tilde{p}_{i,\tau}^{n,\varphi,2} \end{bmatrix} = \begin{bmatrix} p_{i,\tau}^{n,\varphi,1} - p_{i,\tau}^{n,\varphi,0} \\ p_{i,\tau}^{n,\varphi,2} - p_{i,\tau}^{n,\varphi,1} \\ p_{i,\tau}^{n,\varphi,3} - p_{i,\tau}^{n,\varphi,2} \end{bmatrix} - \alpha_{i,\tau}^{n,\varphi} \cdot \tilde{\mathcal{R}}_{\tau}^{\varphi} \tag{6.33}$$

$$0 \leq \alpha_{i,\tau}^{n,\varphi}, \alpha_{i,\tau}^{g,\varphi} \leq 1 \tag{6.34}$$

$$\sum_{n} \alpha_{i,\tau}^{n,\varphi} + \sum_{g} \alpha_{i,\tau}^{g,\varphi} = 1 \tag{6.35}$$

With the presented affine adjustments, the total expected cost of feeder and DGs and the total expected cost of the ramping of feeder and DGs, can be represented as a function of net demand ramping uncertainty. Therefore (6.26) is formulated as $\max_{\mathbb{P} \in \mathcal{P}} \mathbb{E}_{\mathbb{P}} \left[\mathcal{L}^{\varphi}(x^{\varphi}, \mathcal{R}^{\varphi}) \right]$, and the generalized exact linear reformulation of (6.26) is shown in (6.36)-(6.39), where, a_{ν}^{φ} and b_{ν}^{φ} are the linear functions of x^{φ} [65]. The formulated DRO problem is a linear programming problem that includes (6.36)-(6.39), (6.27)-(6.29), and the discrete-time form of (6.2)-(6.11)

and (6.15)-(6.20).

$$\inf_{\lambda^{\varphi}, s_l^{\varphi}, \gamma_{l\nu}^{\varphi}} \sum_{\varphi \in \Phi} \left(\lambda^{\varphi} \epsilon + \frac{1}{N} \sum_{l=1}^{N} s_l^{\varphi} \right) \tag{6.36}$$

$$b_{\nu}^{\varphi} + \langle a_{\nu}^{\varphi}, \tilde{\mathcal{R}}_l^{\varphi} \rangle + \langle \gamma_{l\nu}^{\varphi}, d - C\tilde{\mathcal{R}}_l^{\varphi} \rangle \leq s_l^{\varphi}, \quad \forall l \leq N,\ \nu \leq K \tag{6.37}$$

$$\left\| C^{\top} \gamma_{l\nu}^{\varphi} - a_l^{\varphi} \right\|_* \leq \lambda^{\varphi}, \quad \forall l \leq N,\ \nu \leq K \tag{6.38}$$

$$\gamma_{l\nu}^{\varphi} \geq 0 \tag{6.39}$$

6.2 Numerical Results

In this section, the modified IEEE 13-bus unbalanced distribution network is considered as a test case. Fig. 6.1 shows the network diagram. Here DGs and PVs are three-phase generation units. The capacity of DG1 and DG2 is 300 kW and the capacity of DG3 is 350 kW. Four PV units with the capacity of 250 kW are installed. The total peak demand on phases A, B, and C are 1175 kW, 1039 kW, and 1252 kW, respectively. The maximum reactive power demand on phases A, B, and C, are 616 $kVAr$, 665 $kVAr$, and 771 $kVAr$, respectively. The control points of the PV and demand profiles formed by the sample data are calculated. Fig. 6.2 shows the forecasted PV generation and demand profile and the corresponding control points. The ramping cost of the feeder is three times the electricity price, and the ramping costs of the DGs are three times the cost of the DGs for each segment. The feeder capacity is 3300 kVA with the minimum acceptable power factor of 0.82. The simulations are performed on a PC with an Intel 2.6 GHz Core i7 processor and 16 GB of memory and CPLEX 12.8 is used as a solver.

6.2.1 Distributionally robust operation with ramping costs

The performance of the proposed DRO problem formulation for various sample data sizes is evaluated, and the results are compared with the results of the SP counterpart. Table 6.1 demonstrates the in-sample and out-of-sample performance of DRO and SP problems. As it is shown by increasing the number of sample data, the Wasserstein radius ϵ and the

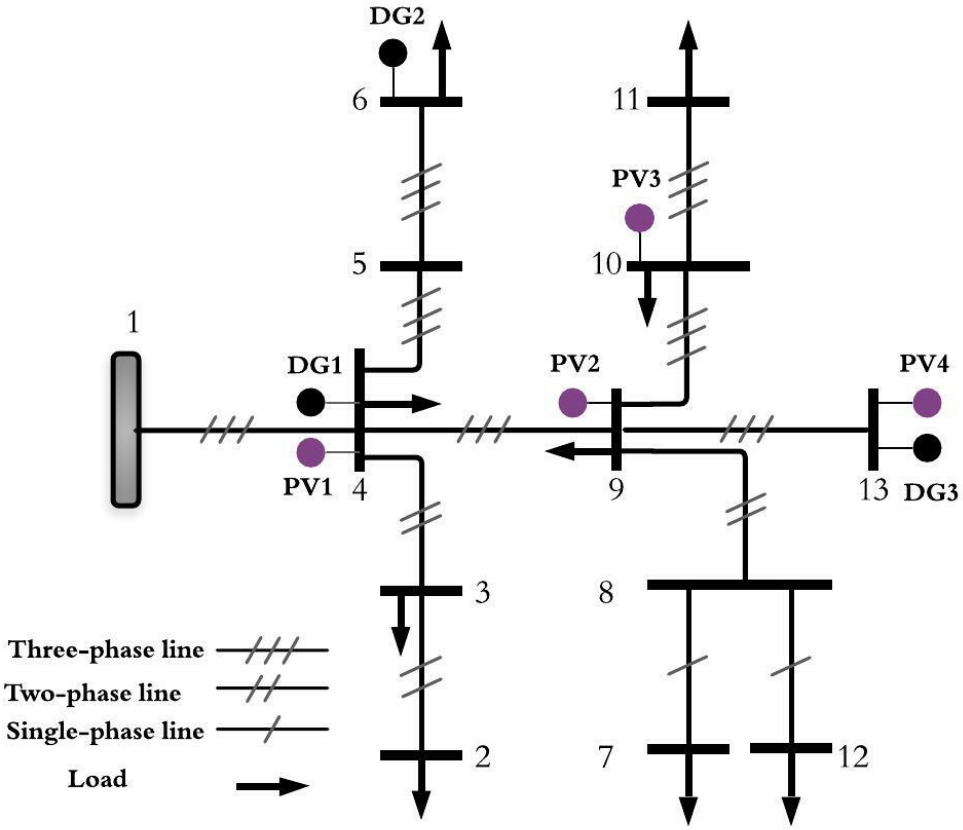

Figure 6.1: Modified IEEE 13-bus system

total expected operation cost of DRO for in-sample data are decreasing. Furthermore, the objective of the DRO problem (network expected operation cost) is higher than the solution to the SP problem with the same number of sample data. The total expected operation cost for 100 samples is increased from \$8075.26 to \$10445.12 once the ramping cost is considered in the SP problem. Furthermore, the total expected operation cost is increased from \$8409.59 when ramping costs of DG and feeder are ignored, to \$10873.47 once the ramping costs are considered in the DRO problem.

To evaluate the out-of-sample performance of the DRO and SP problem formulations, a new set of testing sample data is generated to represent the unseen scenarios, and the power dispatch of the feeder is fixed. The results in Table 6.1 demonstrate that the out-of-sample performance in DRO provides lower expected operation cost, which proves the better

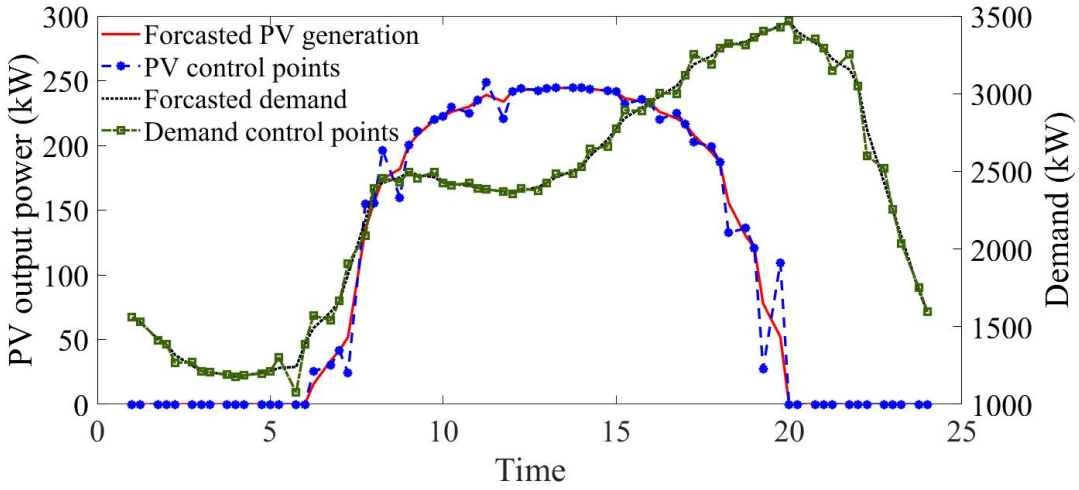

Figure 6.2: Forecasted PV generation and demand

Table 6.1: The In-sample and Out-of-sample performance of DRO and SP

		DRO [$]		SP [$]	
N	ϵ	In-sample	Out-of-sample	In-sample	Out-of-sample
20	2.96	10949.92	11044.79	10459.22	11591.77
40	1.77	10947.70	11022.23	10481.29	11586.87
60	1.40	10923.49	11049.96	10463.12	11623.36
80	1.21	10907.28	11059.48	10457.74	11628.81
100	1.08	10873.47	11044.64	10445.12	11618.34

performance of the DRO solution when facing unseen scenarios. The probability distribution of the out-of-sample operation cost of the DRO problem is compared with those for the SP problem for 100 samples in Fig. 6.3. As shown here, the probability distribution of the operation cost of the solution to the DRO problem has a lower standard deviation (281.88) compared to the SP (331.38), which indicates more robustness of the DRO solution when facing the unseen scenarios.

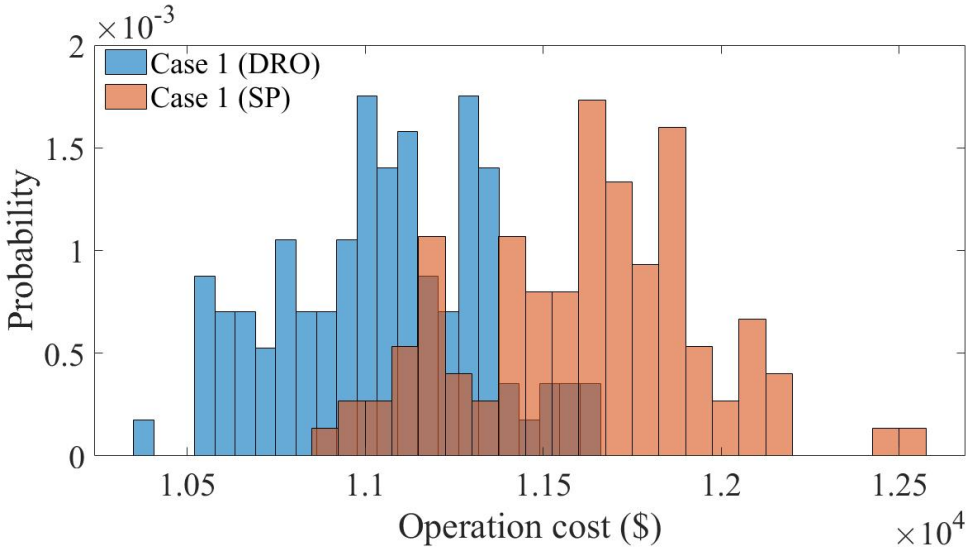

Figure 6.3: Out-of-sample performance of the operation cost

6.2.2 Limited ramp rate of the distribution feeder

Here, the impact of limiting the feeder ramp rate on the expected operation cost of the distribution network is investigated once the distribution network operation is formulated as a DRO problem for 100 sample data. As shown in Fig. 6.4, by increasing the feeder ramp rate limit, the expected operation cost of the distribution network is decreasing. The expected operation cost for ramping rates above 300 $kW/(20min)$ is \$10873.47. The maximum expected operation cost is \$13450.85 as the ramp rate limit reaches 34 $kW/(20min)$.

6.3 Conclusion

In this chapter, a distributionally robust continuous-time operation of the unbalanced distribution network considering the worst-case probability of the net demand ramp samples was proposed. The BPs and their properties are used to reformulate the continuous-time problem formulation into a tractable discrete-time problem. The discrete-time problem is then reformulated using the Wasserstein metric-based distributionally robust optimization problem to capture the worst-case probability of the net demand ramping. The numerical results are shown for a modified IEEE 13-bus unbalanced distribution system. It is shown that once the ramping rate of the feeder is limited, the expected operation cost of the distribution network increases. Furthermore, the simulation outcomes show that the solution

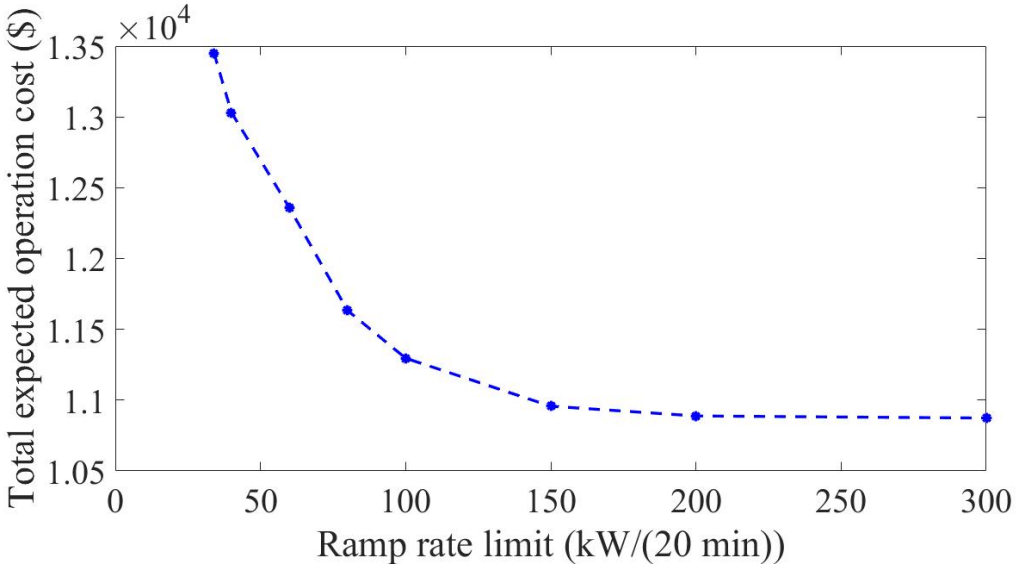

Figure 6.4: Impact of ramping limit on the total expected operation cost

to the DRO problem has superior out-of-sample performance compared to the solution of the SP problem.

Chapter 7

Adaptive Robust Distributed Operation of Distribution Network with Interconnected Microgrids

This paper proposes a framework for the day-ahead operation of the unbalanced distribution network with multiple microgrids considering the worst-case realization of demand and solar Photovoltaic generation in distribution network and microgrids. The problem is formulated as a two-stage optimization problem in which switching in the distribution network is procured at the first stage, and the distribution network and microgrids operation problems are solved at the second stage. The formulated problem is decomposed and solved using the column and constraint generation (C&CG) approach. The interactions between microgrids and distribution network is captured using the alternating direction method of multipliers (ADMM) method. The proposed approach is applied to a modified IEEE 34-bus system with two interconnected microgrids. The impact of islanding in microgrids and the switching in distribution network on the overall operation cost and power loss of the distribution network were investigated. The key contributions of this chapter are as follows:

- An adaptive robust distributed operation of distribution network with interconnected microgrids is proposed and solved using C&CG algorithm. The master problem and subproblems are formulated as MISOCP problems.

- The first-stage decisions are the switching states of the distribution network branches while the second-stage decisions include the worst-case realization of the uncertain solar PV generation and demand. The consensus among the dual form of the second stage problems is ensured using the ADMM approach where the dual variables are the shared variables among the microgrid and distribution network second-stage problems.

- The impacts of islanding and grid-connected operation modes of MGs and switching capability of the distribution networks are evaluated on the overall operation cost of

the system.

The rest of the chapter is organized as follows: section 7.1 presents the problem formulation, and the detailed descriptions of the objective function and constraints. The proposed solution methodology is presented in section 7.2. The numerical results are discussed in section 7.3. Finally, the conclusion is presented in section 7.4.

Nomenclature

Sets and Indices:

- $n, \mathcal{F}$ Index and set of feeder.
- $g, \mathcal{G}$ Index and set of distributed generation units.
- $i, j, \mathcal{B}$ Index and set of buses.
- $v, \mathcal{V}$ Index and set of solar photovoltaic generation.
- $d, \mathcal{D}$ Index and set of demand.
- $t, \mathcal{T}$ Index and set of time.
- $m, \mathcal{M}$ Index and set of the segments in piece-wise linear cost function of DGs.
- φ, Φ Index of PV generation unit.
- MG Index of microgrid.
- DS Index of distribution network.
- Λ_i^{DS} Set of buses in the neighborhood of bus i in the distribution network.
- Λ_i^{MG} Set of buses in the neighborhood of bus i in the microgrids.
- Λ_i^{CC} Set of buses in microgrids the neighborhood of bus i in the distribution network.
- $\mathcal{L}^{DS}$ Set of branches in the distribution network.
- $\mathbb{C}_s$ Set of closed branches.
- $\mathbb{O}_s$ Set of open branches.

Variables:

- $p_{i,t}^{(.),\varphi}$ Real power of the units connected to bus i.
- $q_{i,t}^{(.),\varphi}$ Reactive power of the units connected to bust i.
- $p_{ij,t}^{\varphi}$ Real power flow from node i to j.
- $q_{ij,t}^{\varphi}$ Reactive power flow from node i to j.
- $l_{ij,t}^{\varphi}$ Square of current magnitudes from node i to j.
- $v_{i,t}^{\varphi}$ Square of voltage magnitudes at node i.
- $ps_{i,t}^{m,g,\varphi}$ Power in segment m of the distributed generation g of the cost curve.
- $\gamma_{e,t}^{(.),\varphi}$ Binary variable representing the uncertainty in demand and PVs.
- $y_{ij,t}$ Binary variable shows the status of connection of branches in the distribution network.
- $Y_{ij,t}$ Auxiliary binary variables.

Parameters:

- $\overline{P}_{i,t}^{(.),\varphi}$ Maximum real power of the units connected to bust i.
- $\overline{Q}_{i,t}^{(.),\varphi}$ Maximum reactive power of the units connected to bust i.
- $\underline{Q}_{i,t}^{(.),\varphi}$ Minimum reactive power of the units connected to bust i.
- $\overline{I}_{ij,t}^{\varphi}$ Maximum Square of current magnitudes from node i to j.
- $\overline{V}_{i,t}^{\varphi}, \underline{V}_{i,t}^{\varphi}$ Maximum and minimum square of voltage magnitudes limits at node i.
- $\overline{ps}_{i,t}^{m,g,\varphi}$ Maximum real power in segment m of the distributed generation g of the cost curve.
- $\boldsymbol{\rho}_{ij}^{\varphi}$ Binary parameters indicates the status of the connection of lines on each phase.
- $C_i^{m,g}$ Marginal cost of the unit i in segment m.

– $\overline{S}_{i,t}^{(.),\varphi}$ Maximum apparent power of the PV units connected to bust i.

– PF Power factor.

– k Iteration counter in the C&CG algorithm.

– τ Iteration counter in the ADMM algorithm.

7.1 Problem Formulation

The proposed problem is formulated as a two-stage optimization problem. The first stage determines the topology of the distribution network by identifying the status of the switchable branches [111]. The second-stage aims to minimize the total operation cost of distribution network and MGs considering the worst-case realization of the solar PV generation and demand. The second-stage problem is solved in a distributed manner using ADMM by formulating the dual form of the problem for distribution network and MGs and ensure the consensus among the shared dual variables in each sub-problem. The day-ahead operation of the unbalanced distribution system with interconnected MGs is formulated in (7.1)-(7.25). The first term in (7.1) represents the objective of the first-stage problem. The second term represents the objective function of the second-stage problem in which the worst-case realization of the solar PV generation and demand were considered. In the objective function of the second-stage problem, the first three components represent the operation cost of the feeder, the operation cost of the distributed generation units (DGs), and the load shedding penalty in the distribution system. The last two components represent the operation cost of the distributed generation units and load shedding penalties in MGs. The piece-wise linearized form of the operation cost of DG units is shown in (7.4) and (7.5). Here, C_d^{DS} and C_d^{MG} are the load shedding penalties in the distribution network and MGs, respectively. The real and reactive power balances at each bus are enforced by (7.6) and (7.7) respectively, where, $\mathcal{L}_l^f$ is the set of buses at the sending end of a line and $\mathcal{L}_l^t$ is the set of buses at the receiving end of the bus. The bus voltages on both sides of a branch satisfy (7.8)-(7.9) and the voltage at each bus is limited by (7.11). Here, $\widetilde{\boldsymbol{R}}_l$ and $\widetilde{\boldsymbol{X}}_l$ are the resistance and inductive reactance matrices of the unbalanced branch l that are defined in [99]. The big-M method is used to relax the power flow constraint once phase p_{ij}^{φ} and/or

distribution branch $y_{ij,t}$ does not exist. The real and reactive power at the sending end of a branch is limited by (7.10) which is further reformulated as a second-order conic constraint. The current flow in distribution branch is limited by (7.12). The relationship between the real and reactive power of PV generation is given by (7.13) which is formulated as a second-order conic constraint [112]. The real power output of PV unit is limited by (7.14), where, $\gamma_{i,t}^{v,\varphi,DS}$ is a binary variable. The maximum solar PV generation is within a polyhedral set defined as (7.26) where, $\overline{P}_{i,t}^{v,\varphi,(.)}$ and $\Delta P_{i,t}^{v,\varphi,(.)}$ are the maximum forecasted solar PV generation and the deviation from the maximum solar PV generation. The status of the switches in the first-stage problem is determined in a way that the radial topology of the distribution network is ensured. The constraints (7.2) and (7.3) ensure the radial topology of the distribution network with network switching decisions [111]. The real and reactive power outputs of the DG unit are enforced by (7.15)-(7.16). The real power of the demand is enforced by (7.19), where, the uncertainty in the demand is represented similar to the uncertainty in PV generation as shown in (7.27). The reactive power of the distribution feeder is constrained by (7.17)-(7.18) considering the acceptable power factor at the feeder. It is worth noting that similar formulation (7.4)-(7.5) and (7.8)-(7.16) is written for MGs. The real and reactive power balance at each bus in the MGs are enforced by (7.23) and (7.24). The voltage at two sides of the coupling tie-lines between the distribution network and MGs satisfy (7.25).

$$\begin{aligned}\min_{y_{ij,t}} \mathbf{0} + \max_{\boldsymbol{\gamma}_{i,t}^{(.),\varphi,(.)}} \min_{\mathbf{p},\mathbf{q},\mathbf{U}} \Bigg(& \sum_{i\in\mathcal{B}^{DS}} \sum_{n\in\mathcal{F}} \sum_{\varphi\in\Phi} \sum_{t\in\mathcal{T}} \rho_{i,t} \cdot p_{i,t}^{n,\varphi} + \\ & \sum_{i\in\mathcal{B}^{DS}} \sum_{\varphi\in\Phi} \sum_{t\in\mathcal{T}} \sum_{g\in\mathcal{G}} \sum_{m\in\mathcal{M}} C_i^{m,g} \cdot ps_{i,t}^{m,g,\varphi} + \\ & \sum_{i\in\mathcal{B}^{DS}} \sum_{\varphi\in\Phi} \sum_{t\in\mathcal{T}} C_d^{DS} \cdot \left(\overline{p}_{i,t}^{d,\varphi} - p_{i,t}^{d,\varphi}\right) + \\ & \sum_{i\in\mathcal{B}^{MG}} \sum_{\varphi\in\Phi} \sum_{t\in\mathcal{T}} \sum_{g\in\mathcal{G}} \sum_{m\in\mathcal{M}} C_i^{m,g} \cdot ps_{i,t}^{m,g,\varphi} + \\ & \sum_{i\in\mathcal{B}^{MG}} \sum_{\varphi\in\Phi} \sum_{t\in\mathcal{T}} C_d^{MG} \cdot \left(\overline{p}_{i,t}^{d,\varphi} - p_{i,t}^{d,\varphi}\right) \Bigg) \end{aligned} \tag{7.1}$$

s.t.

$$\sum_{ij\in\mathcal{L}^{DS}} y_{ij,t} = K - 1 \tag{7.2}$$

$$\sum_{s\in\mathbb{S}}\left(\prod_{ij\in\mathbb{C}_s} y_{ij,t}\cdot\prod_{ij\in\mathbb{O}_s}\left(1-y_{ij,t}\right)\right)=1 \tag{7.3}$$

$$ps_{i,t}^{m,g,\varphi}\le\overline{ps}_{i,t}^{m,g,\varphi}\qquad\forall i\in\mathcal{B}^{DS} \tag{7.4}$$

$$p_{i,t}^{m,g,\varphi}=\sum_{m} ps_{i,t}^{m,g,\varphi}\qquad\forall i\in\mathcal{B}^{DS} \tag{7.5}$$

$$\sum_{j\in\Lambda_i^{DS}}(p_{ij,t}^{\varphi}-\tilde{R}_{ij}^{DS}\cdot l_{ij,t}^{\varphi})-\sum_{j\in\Lambda_i^{CC}}p_{ij,t}^{\varphi}+\sum_{n\in\mathcal{F}}p_{i,t}^{n,\varphi}$$
$$+\sum_{g\in\mathcal{G}}p_{i,t}^{g,\varphi}=\sum_{d\in\mathcal{D}}p_{i,t}^{d,\varphi}-\sum_{v\in\mathcal{V}}p_{i,t}^{v,\varphi};\quad\forall i\in\mathcal{B}^{DS} \tag{7.6}$$

$$\sum_{j\in\Lambda_i^{DS}}(q_{ij,t}^{\varphi}-\tilde{X}_{ij}^{DS}\cdot l_{ij,t}^{\varphi})-\sum_{j\in\Lambda_i^{CC}}q_{ij,t}^{\varphi}+\sum_{n\in\mathcal{F}}q_{i,t}^{n,\varphi}$$
$$+\sum_{g\in\mathcal{G}}q_{i,t}^{g,\varphi}=\sum_{d\in\mathcal{D}}q_{i,t}^{d,\varphi}-\sum_{v\in\mathcal{V}}q_{i,t}^{v,\varphi};\quad\forall i\in\mathcal{B}^{DS} \tag{7.7}$$

$$v_{j,t}^{\varphi}-v_{i,t}^{\varphi}+2\cdot\left(\tilde{R}_{ij}^{DS}\cdot p_{ij,t}^{\varphi}+\tilde{X}_{ij}^{DS}\cdot q_{ij,t}^{\varphi}\right)-((\tilde{R}_{ij}^{DS})^2+(\tilde{X}_{ij}^{DS})^2)\cdot l_{ij,t}^{\varphi}$$
$$\le\boldsymbol{M}\cdot(2-\boldsymbol{\rho}_l^{\varphi}-y_{ij,t});\quad\forall i\in\mathcal{B}^{DS},j\in\Lambda_i^{DS} \tag{7.8}$$

$$v_{j,t}^{\varphi}-v_{i,t}^{\varphi}+2\cdot\left(\tilde{R}_{ij}^{DS}\cdot p_{ij,t}^{\varphi}+\tilde{X}_{ij}^{DS}\cdot q_{ij,t}^{\varphi}\right)-((\tilde{R}_{l}^{DS})^2+(\tilde{X}_{l}^{DS})^2)\cdot l_{ij,t}^{\varphi}$$
$$\ge-\boldsymbol{M}\cdot(2-\boldsymbol{\rho}_l^{\varphi}-y_{ij,t});\quad\forall i\in\mathcal{B}^{DS},j\in\Lambda_i^{DS} \tag{7.9}$$

$$\left\|\begin{matrix}2p_{ij,t}^{\varphi}\\2q_{ij,t}^{\varphi}\\l_{ij,t}^{\varphi}-v_{i,t}^{\varphi}\end{matrix}\right\|_2\le l_{ij,t}^{\varphi}+v_{ij,t}^{\varphi}\qquad\forall i\in\mathcal{B}^{DS},j\in\Lambda_i^{DS} \tag{7.10}$$

$$\underline{V}^2\le v_{i,t}^{\varphi}\le\overline{V}^2\qquad\forall i\in\mathcal{B}^{DS} \tag{7.11}$$

$$0\le l_{ij,t}^{\varphi}\le(\overline{I}_{ij}^{\varphi})^2\qquad\forall i\in\mathcal{B}^{DS},j\in\Lambda_i^{DS} \tag{7.12}$$

$$(p_{i,t}^{v,\varphi})^2+(q_{i,t}^{v,\varphi})^2\le(\overline{S}_{i,t}^{v,\varphi})^2\qquad\forall i\in\mathcal{B}^{DS} \tag{7.13}$$

$$0 \leq p_{i,t}^{v,\varphi} \leq \hat{P}_i^{v,\varphi} + \gamma_{i,t}^{v,\varphi} \tilde{P}_i^{v,\varphi} \qquad \forall i \in \mathcal{B}^{DS} \tag{7.14}$$

$$0 \leq p_{i,t}^{g,\varphi} \leq \overline{P}_i^{g,\varphi} \qquad \forall i \in \mathcal{B}^{DS} \tag{7.15}$$

$$-\overline{Q}_i^{g,\varphi} \leq q_{i,t}^{g,\varphi} \leq \overline{Q}_i^{g,\varphi} \qquad \forall i \in \mathcal{B}^{DS} \tag{7.16}$$

$$q_{i,t}^{n,\varphi} \leq \tan(\cos^{-1} PF) \cdot p_{i,t}^{n,\varphi} \qquad \forall i \in \mathcal{B}^{DS} \tag{7.17}$$

$$-\tan(\cos^{-1} PF) \cdot p_{i,t}^{n,\varphi} \leq q_{i,t}^{n,\varphi} \qquad \forall i \in \mathcal{B}^{DS} \tag{7.18}$$

$$0 \leq p_{i,t}^{d,\varphi} \leq \hat{P}_i^{d,\varphi} + \gamma_{i,t}^{d,\varphi} \tilde{P}_i^{d,\varphi} \qquad \forall i \in \mathcal{B}^{DS} \tag{7.19}$$

$$Y_{ij,t} \leq (y_{ij,t})_{ij \in \mathbb{O}_s} \qquad \forall ij \in \mathcal{L}^{DS} \tag{7.20}$$

$$Y_{ij,t} \leq (y_{ij,t})_{ij \in \mathbb{C}_s} \qquad \forall ij \in \mathcal{L}^{DS} \tag{7.21}$$

$$Y_{ij,t} \geq (y_{ij,t})_{ij \in \mathbb{C}_s} + (y_{ij,t})_{ij \in \mathbb{O}_s} - 1 \qquad \forall ij \in \mathcal{L}^{DS} \tag{7.22}$$

$$\sum_{j \in \Lambda_i^{MG}} (p_{ij,t}^{\varphi} - \tilde{R}_{ij}^{MG} \cdot l_{ij,t}^{\varphi}) + \sum_{g \in \mathcal{G}} p_{i,t}^{g,\varphi} + \sum_{j \in \Lambda_I^{CC}} (p_{ij,t}^{\varphi} - \tilde{R}_{ij}^{CC} \cdot l_{ij,t}^{\varphi}) = \sum_{d \in \mathcal{D}} p_{i,t}^{d,\varphi} - \sum_{v \in \mathcal{V}} p_{i,t}^{v,\varphi} \quad \forall i \in \mathcal{B}^{MG} \tag{7.23}$$

$$\sum_{j \in \Lambda_i^{MG}} (q_{ij,t}^{\varphi} - \tilde{X}_{ij}^{MG} \cdot l_{ij,t}^{\varphi}) + \sum_{g \in \mathcal{G}} q_{i,t}^{g,\varphi} + \sum_{j \in \Lambda_i^{CC}} (q_{ij,t}^{\varphi} - \tilde{X}_{ij}^{CC} \cdot l_{ij,t}^{\varphi}) = \sum_{d \in \mathcal{D}} q_{i,t}^{d,\varphi} - \sum_{v \in \mathcal{V}} q_{i,t}^{v,\varphi} \quad \forall i \in \mathcal{B}^{MG} \tag{7.24}$$

$$v_{j,t}^{\varphi} - v_{i,t}^{\varphi} + 2 \cdot \left(\tilde{R}_{ij} \cdot p_{ij,t}^{\varphi} + \tilde{X}_{ij} \cdot q_{ij}^{\varphi} \right) - (\tilde{R}_{ij}^2 + \tilde{X}_{ij}^2) \cdot l_{ij,t}^{\varphi} = 0 \qquad \forall i \in \mathcal{B}^{DS}, j \in \mathcal{B}^{MG} \cap \Lambda_i^{CC} \tag{7.25}$$

$$\Omega_1 = \begin{cases} p_{i,t}^{v,\varphi,(.)} = \left[\overline{P}_{i,t}^{v,\varphi,(.)} - \Delta P_{i,t}^{v,\varphi,(.)}, \overline{P}_{i,t}^{v,\varphi,(.)} + \Delta P_{i,t}^{v,\varphi,(.)}\right] \\ \hat{P}_{i,t}^{v,\varphi,(.)} = \overline{P}_{i,t}^{v,\varphi,(.)} - \Delta P_{i,t}^{v,\varphi,(.)} \\ \tilde{P}_{i,t}^{v,\varphi,(.)} = 2 \cdot \Delta P_{i,t}^{v,\varphi,(.)} \end{cases} \tag{7.26}$$

$$\Omega_2 = \begin{cases} p_{i,t}^{d,\varphi,(.)} = \left[\overline{P}_{i,t}^{d,\varphi,(.)} - \Delta P_{i,t}^{d,\varphi,(.)}, \overline{P}_{i,t}^{d,\varphi,(.)} + \Delta P_{i,t}^{d,\varphi,(.)}\right] \\ \hat{P}_{i,t}^{d,\varphi,(.)} = \overline{P}_{i,t}^{d,\varphi,(.)} - \Delta P_{i,t}^{d,\varphi,(.)} \\ \tilde{P}_{i,t}^{d,\varphi,(.)} = 2 \cdot \Delta P_{i,t}^{d,\varphi,(.)} \end{cases} \tag{7.27}$$

7.2 Solution Methodology

The proposed (C&CG) algorithm leverages ADMM algorithm to determine the consensus among the formulated dual problems. For the sake of simplicity, the abstract form of the problem formulation is presented here. The proposed C&CG algorithm is described as follows:

1) Step 1 - Initialization: Initialize the upper and lower bounds and the iteration counter k in the C&CG as as $LB = -\infty$, $UB = \infty$, $k = 0$

2) Step 2 - Solve the master problem: Solve the problem (7.28)-(7.39) and update the lower bound.

$$\min_{\boldsymbol{x}} \ \boldsymbol{c}^\top \boldsymbol{x} + \eta \tag{7.28}$$

s.t.

$$\boldsymbol{A}\boldsymbol{x} = \boldsymbol{d} \tag{7.29}$$

$$\eta \geq \boldsymbol{b}_1^\top \boldsymbol{z}_1^\omega + \boldsymbol{b}_2^\top \boldsymbol{z}_2^\omega; \forall \omega \leq k \tag{7.30}$$

$$\boldsymbol{D}_1 \boldsymbol{z}_1^\omega \leq \boldsymbol{g}_1; \forall \omega \leq k \tag{7.31}$$

$$\boldsymbol{H}_1 \boldsymbol{z}_1^\omega + \boldsymbol{H}_1^{cc} \boldsymbol{z}^{cc,\omega} = \boldsymbol{f}_1; \forall \omega \leq k \tag{7.32}$$

$$\|\boldsymbol{G}_1 \boldsymbol{z}_1^\omega\| \leq \boldsymbol{h}_1^\top \boldsymbol{z}_1^\omega; \forall \omega \leq k \tag{7.33}$$

$$\boldsymbol{N}_1 \boldsymbol{\xi}_{\omega,1}^* + \boldsymbol{F}_1 \boldsymbol{z}_1^\omega \leq \boldsymbol{q}_1; \quad \forall \omega \leq k \tag{7.34}$$

$$\boldsymbol{D}_2\boldsymbol{z}_2^{\omega} \leq \boldsymbol{g}_2; \forall \omega \leq k \tag{7.35}$$

$$\boldsymbol{H}_2\boldsymbol{z}_2^{\omega} + \boldsymbol{H}_2^{cc}\boldsymbol{z}^{cc,\omega} = \boldsymbol{f}_2; \forall \omega \leq k \tag{7.36}$$

$$\|\boldsymbol{G}_2\boldsymbol{z}_2^{\omega}\| \leq \boldsymbol{h}_2^{\top}\boldsymbol{z}_2^{\omega}; \forall \omega \leq k \tag{7.37}$$

$$\boldsymbol{N}_2\boldsymbol{\xi}_{\omega,2}^{*} + \boldsymbol{F}_2\boldsymbol{z}_2^{\omega} \leq \boldsymbol{q}_2; \quad \forall \omega \leq k \tag{7.38}$$

$$\boldsymbol{S}_1\boldsymbol{z}_1^{\omega} + \boldsymbol{S}_2\boldsymbol{z}_2^{\omega} = 0; \quad \forall \omega \leq k \tag{7.39}$$

Here, $\boldsymbol{x}$ represents the vector of first-stage decision variables, and $\boldsymbol{z}_1$ and $\boldsymbol{z}_2$ represents the second-stage recourse decision variables, i.e. $p_{i,t}^{(.),\varphi,(.)}$, $q_{i,t}^{(.),\varphi,(.)}$, $p_{ij,t}^{\varphi,(.)}$, $q_{ij,t}^{\varphi,(.)}$, $v_{i,t}^{\varphi,(.)}$, $l_{ij,t}^{\varphi,(.)}$ in the distribution network and MGs respectively. The constraint (7.29) represents (7.2) and (7.20)-(7.22); constraint (7.30) represent the total operation cost of distribution network and MGs given in (7.1). Constraint (7.31) represents the constraints (7.4), (7.5), (7.8), (7.9), (7.11), (7.12), (7.14)-(7.19). Constraint (7.32) represents (7.6) and (7.7). Constraint (7.33), represents (7.10) and (7.14) and constraint (7.34) represents (7.15) and (7.20). Similarly, Constraints (7.35)-(7.38) are describing the similar constraints for MGs. Constraint (7.39) represents the constraint (7.25). The lower bound is updated in each iteration using (7.40).

$$LB = \boldsymbol{c}^{\top}\boldsymbol{x} + \hat{\eta}^{k+1} \tag{7.40}$$

3) Step 3 - Solve subproblem: To solve the subproblem (7.41)-(7.50), the problem is re-written as (7.51)-(7.57) using the duality theory. McCormick envelopes are used to linearize $\boldsymbol{\xi_1}^{\top}\boldsymbol{\pi}_5$ and $\boldsymbol{\xi_2}^{\top}\boldsymbol{\pi}_{10}$ [100]. Here $\pi_{(.)}$ are the dual variables, where, $\pi_1, ..., \pi_5$ are dual variables for distribution network constraints and $\pi_6, ..., \pi_{10}$ are dual variables for MG constraints. π_{11} is the dual variable for complicating constraint.

$$\underset{\boldsymbol{\xi}}{max}\underset{z_1,z_2}{min}(\boldsymbol{b}_1^{\top}\boldsymbol{z}_1 + \boldsymbol{b}_2^{\top}\boldsymbol{z}_2) \tag{7.41}$$

s.t.

$$\boldsymbol{D}_1\boldsymbol{z}_1 \leq \boldsymbol{g}_1 \qquad : \boldsymbol{\pi}_1 \tag{7.42}$$

$$\boldsymbol{H}_1\boldsymbol{z}_1 + \boldsymbol{H}_1^{cc}\boldsymbol{z}^{cc} = \boldsymbol{f}_1 \qquad : \boldsymbol{\pi}_2 \tag{7.43}$$

$$\|\boldsymbol{G}_1\boldsymbol{z}_1\|_2 \leq \boldsymbol{h}_1^\top \boldsymbol{z}_1 \qquad : \boldsymbol{\pi}_3, \boldsymbol{\pi}_4 \tag{7.44}$$

$$\boldsymbol{F}_1\boldsymbol{z}_1 \leq \boldsymbol{N}_1\boldsymbol{\xi}_1 \qquad : \boldsymbol{\pi}_5 \tag{7.45}$$

$$\boldsymbol{D}_2\boldsymbol{z}_2 \leq \boldsymbol{g}_2 \qquad : \boldsymbol{\pi}_6 \tag{7.46}$$

$$\boldsymbol{H}_2\boldsymbol{z}_2 + \boldsymbol{H}_2^{cc}\boldsymbol{z}^{cc} = \boldsymbol{f}_2 \qquad : \boldsymbol{\pi}_7 \tag{7.47}$$

$$\|\boldsymbol{G}_2\boldsymbol{z}_2\|_2 \leq \boldsymbol{h}_2^\top \boldsymbol{z}_2 \qquad : \boldsymbol{\pi}_8, \boldsymbol{\pi}_9 \tag{7.48}$$

$$\boldsymbol{F}_2\boldsymbol{z}_2 \leq \boldsymbol{N}_2\boldsymbol{\xi}_2 \qquad : \boldsymbol{\pi}_{10} \tag{7.49}$$

$$\boldsymbol{S}_1\boldsymbol{z}_1 + \boldsymbol{S}_2\boldsymbol{z}_2 = 0 \qquad : \boldsymbol{\pi}_{11} \tag{7.50}$$

$$\Theta \quad = \quad \max_{\boldsymbol{\xi}} \Big(\boldsymbol{g}_1^\top \boldsymbol{\pi}_1 \; + \; \boldsymbol{f}_1^\top \boldsymbol{\pi}_2 \; + \; \boldsymbol{N}_1^\top \boldsymbol{\xi}_1^\top \boldsymbol{\pi}_5 \; + \; \boldsymbol{g}_2^\top \boldsymbol{\pi}_6 \; + \; \boldsymbol{f}_2^\top \boldsymbol{\pi}_7 \; + \; \boldsymbol{N}_2^\top \boldsymbol{\xi}_2^\top \boldsymbol{\pi}_{10} \Big) \tag{7.51}$$

$$\boldsymbol{D}_1^\top \boldsymbol{\pi}_1 + \boldsymbol{H}_1^\top \boldsymbol{\pi}_2 + \boldsymbol{F}_1^\top \boldsymbol{\pi}_4 + \boldsymbol{S}_1^\top \boldsymbol{\pi}'_{11} \leq \boldsymbol{b}_1 \tag{7.52}$$

$$\boldsymbol{D}_2^\top \boldsymbol{\pi}_5 + \boldsymbol{H}_2^\top \boldsymbol{\pi}_7 + \boldsymbol{F}_2^\top \boldsymbol{\pi}_{10} + \boldsymbol{S}_2^\top \boldsymbol{\pi}_{11} \leq \boldsymbol{b}_2 \tag{7.53}$$

$$\boldsymbol{H}_1^{cc} \boldsymbol{\pi}_2 + \boldsymbol{H}_2^{cc} \boldsymbol{\pi}_7 = 0 \tag{7.54}$$

$$\boldsymbol{\pi}'_{11} - \boldsymbol{\pi}_{11} = 0 \tag{7.55}$$

$$\|\boldsymbol{\pi}_3\|_2 \leq \boldsymbol{\pi}_4 \tag{7.56}$$

$$\|\boldsymbol{\pi}_8\|_2 \leq \boldsymbol{\pi}_9 \tag{7.57}$$

4) Step 3A - The problem (7.51)-(7.57) can be decomposed into two sub-problems one for distribution network and one for MGs; where, the first three terms in the objective function and constraints (7.52) and (7.56) represent the dual counter-part for the primal problem of the distribution network. The rest of the terms in the objective function and constraints (7.53) and (7.59) represent the dual counter-part of the primal problem in

the MGs. The complicating constraints (7.54) and (7.55) are relaxed and the augmented Lagrangian function is defined as the objective function (7.58).

$$\boldsymbol{L} = \Bigg(\Big(\boldsymbol{g}_1^\top \boldsymbol{\pi}_1 + \boldsymbol{f}_1^\top \boldsymbol{\pi}_2 + \boldsymbol{N}_1^\top \boldsymbol{\xi}_1^\top \boldsymbol{\pi}_5 + \boldsymbol{g}_2^\top \boldsymbol{\pi}_6 + \boldsymbol{f}_2^\top \boldsymbol{\pi}_7 + \boldsymbol{N}_2^\top \boldsymbol{\xi}_2^\top \boldsymbol{\pi}_{10}\Big) + \\ \boldsymbol{\lambda}_1(\boldsymbol{H}_1^{cc}\boldsymbol{\pi}_2 + \boldsymbol{H}_2^{cc}\boldsymbol{\pi}_7) + \boldsymbol{\lambda}_2(\boldsymbol{\pi}'_{11} - \boldsymbol{\pi}_{11}) + \frac{\boldsymbol{\alpha}}{2}\left\|\boldsymbol{H}_1^{cc}\boldsymbol{\pi}_2 + \boldsymbol{H}_2^{cc}\boldsymbol{\pi}_7\right\|_2^2 + \frac{\boldsymbol{\alpha}}{2}\left\|\boldsymbol{\pi}'_{11} - \boldsymbol{\pi}_{11}\right\|_2^2\Bigg) \quad (7.58)$$

Therefore, the problem in (7.51)-(7.57) is reformulated as the problem given in (7.59)-(7.63)

$$\underset{\boldsymbol{\xi},\boldsymbol{\pi}_{(.)}}{max}(\boldsymbol{L}) \quad (7.59)$$

$$\boldsymbol{D}_1^\top \boldsymbol{\pi}_1 + \boldsymbol{H}_1^\top \boldsymbol{\pi}_2 + \boldsymbol{F}_1^\top \boldsymbol{\pi}_4 + \boldsymbol{S}_1^\top \boldsymbol{\pi}'_{11} \leq \boldsymbol{b}_1 \quad (7.60)$$

$$\boldsymbol{D}_2^\top \boldsymbol{\pi}_5 + \boldsymbol{H}_2^\top \boldsymbol{\pi}_7 + \boldsymbol{F}_2^\top \boldsymbol{\pi}_{10} + \boldsymbol{S}_2^\top \boldsymbol{\pi}_{11} \leq \boldsymbol{b}_2 \quad (7.61)$$

$$\|\boldsymbol{\pi}_3\|_2 \leq \boldsymbol{\pi}_4 \quad (7.62)$$

$$\|\boldsymbol{\pi}_8\|_2 \leq \boldsymbol{\pi}_9 \quad (7.63)$$

5) Step 3B - Using the ADMM algorithm, the variables $\boldsymbol{\pi}_2$, $\boldsymbol{\pi}_7$, $\boldsymbol{\pi}_{11}$, $\boldsymbol{\pi'}_{11}$, $\boldsymbol{\lambda}_1$ and $\boldsymbol{\lambda}_2$ are updated in iteration $\boldsymbol{\tau}$ as shown in (7.64)-(7.67).

$$\boldsymbol{\pi}_2^{\tau+1}, \boldsymbol{\pi}_{11}^{\tau+1} := \underset{\boldsymbol{\xi},\boldsymbol{\pi_1},\ldots,\boldsymbol{\pi_5},\boldsymbol{\pi 11}}{\arg\max}\ \boldsymbol{L_1}(\boldsymbol{\lambda_1^\tau}, \boldsymbol{\lambda_2^\tau}, \boldsymbol{\pi_2}, \boldsymbol{\pi_{11}}, \boldsymbol{\pi_7^\tau}, \boldsymbol{\pi'^\tau_{11}}) \quad (7.64)$$

$$\boldsymbol{\pi}_7^{\tau+1}, \boldsymbol{\pi'}_{11}^{\tau+1} := \underset{\boldsymbol{\xi},\boldsymbol{\pi_6},\ldots,\boldsymbol{\pi_{10}},\boldsymbol{\pi'_{11}}}{\arg\max}\ \boldsymbol{L_2}(\boldsymbol{\lambda_1^\tau}, \boldsymbol{\lambda_2^\tau}, \boldsymbol{\pi_2^\tau}, \boldsymbol{\pi_{11}^\tau}, \boldsymbol{\pi_7}, \boldsymbol{\pi'_{11}}) \quad (7.65)$$

$$\boldsymbol{\lambda}_1^{\tau+1} = \boldsymbol{\lambda}_1^\tau + \boldsymbol{\alpha}(\boldsymbol{H}_1^{cc}\boldsymbol{\pi}_2^{\tau+1} + \boldsymbol{H}_2^{cc}\boldsymbol{\pi}_7^{\tau+1}) \quad (7.66)$$

$$\boldsymbol{\lambda}_2^{\tau+1} = \boldsymbol{\lambda}_2^\tau + \boldsymbol{\alpha}(\boldsymbol{\pi'}_{11}^{\tau+1} - \boldsymbol{\pi}_{11}^{\tau+1}) \quad (7.67)$$

Using ADMM method, the problem (7.59)-(7.63) is decomposed and solved in an iteratively. First, the problem (7.64) which is expanded in (7.69)-(7.71) for distribution network is solved using the Lagrangian function $\boldsymbol{L_1}$ in (7.68) and the dual variables (i.e. $\boldsymbol{\pi}_2$, $\boldsymbol{\pi}_{11}$,$\boldsymbol{\lambda}_1$) are

procured. Next, the problem (7.65) which is expanded in (7.73)-(7.75) is solved for MGs to procure the dual variables (i.e. $\boldsymbol{\pi}_7$, $\boldsymbol{\pi'}_{11}$, $\boldsymbol{\lambda}_2$) considering the Lagrangian function $\boldsymbol{L_2}$ formulated in (7.72). Next, the lagrangian multipliers $\boldsymbol{\lambda_1}$ and $\boldsymbol{\lambda_2}$ are updated using (7.66) and (7.67) respectively. Next, proceed to *Step 3C*.

$$\boldsymbol{L_1} = \Bigg(\boldsymbol{g}_1^\top \boldsymbol{\pi}_1 + \boldsymbol{f}_1^\top \boldsymbol{\pi}_2 + \boldsymbol{N}_1^\top \boldsymbol{\xi}_1^\top \boldsymbol{\pi}_5 + \boldsymbol{\lambda}_1 \boldsymbol{H}_1^{cc} \boldsymbol{\pi}_2 + \boldsymbol{\lambda}_2 \boldsymbol{\pi}_{11} + \frac{\boldsymbol{\alpha}}{2} \left[\left\| \boldsymbol{H}_1^{cc} \boldsymbol{\pi}_2 + \boldsymbol{H}_2^{cc} \hat{\boldsymbol{\pi}}_7 \right\|_2^2 + \left\| \boldsymbol{\pi}_{11} - \hat{\boldsymbol{\pi}'}_{11} \right\|_2^2 \right] \Bigg) \tag{7.68}$$

$$\underset{\boldsymbol{\xi_1}, \boldsymbol{\pi_1}, \ldots, \boldsymbol{\pi_5}, \boldsymbol{\pi'_{11}}}{max} (\boldsymbol{L}_1) \tag{7.69}$$

s.t.

$$\boldsymbol{D}_1^\top \boldsymbol{\pi}_1 + \boldsymbol{H}_1^\top \boldsymbol{\pi}_2 + \boldsymbol{F}_1^\top \boldsymbol{\pi}_4 + \boldsymbol{S}_1^\top \boldsymbol{\pi}'_{11} \leq 0 \tag{7.70}$$

$$\left\| \boldsymbol{\pi}_3 \right\|_2 \leq \boldsymbol{\pi}_4 \tag{7.71}$$

and

$$\boldsymbol{L_2} = \Bigg(\boldsymbol{g}_2^\top \boldsymbol{\pi}_6 + \boldsymbol{f}_2^\top \boldsymbol{\pi}_7 + \boldsymbol{N}_2^\top \boldsymbol{\xi}_2^\top \boldsymbol{\pi}_{10} + \boldsymbol{\lambda}_1 \boldsymbol{H}_2^{cc} \boldsymbol{\pi}_7 - \boldsymbol{\lambda}_2 \boldsymbol{\pi'}_{11} + \frac{\boldsymbol{\alpha}}{2} \left[\left\| \boldsymbol{H}_1^{cc} \hat{\boldsymbol{\pi}}_2 + \boldsymbol{H}_2^{cc} \boldsymbol{\pi}_7 \right\|_2^2 + \left\| \hat{\boldsymbol{\pi}}_{11} - \boldsymbol{\pi'}_{11} \right\|_2^2 \right] \Bigg) \tag{7.72}$$

$$\underset{\boldsymbol{\xi_2}, \boldsymbol{\pi_6}, \ldots, \boldsymbol{\pi_{10}}, \boldsymbol{\pi_{11}}}{max} (\boldsymbol{L}_2) \tag{7.73}$$

s.t.

$$\boldsymbol{D}_2^\top \boldsymbol{\pi}_5 + \boldsymbol{H}_2^\top \boldsymbol{\pi}_7 + \boldsymbol{F}_2^\top \boldsymbol{\pi}_{10} + \boldsymbol{S}_2^\top \boldsymbol{\pi}_{11} \leq 0 \tag{7.74}$$

$$\left\| \boldsymbol{\pi}_8 \right\|_2 \leq \boldsymbol{\pi}_9 \tag{7.75}$$

6) Step 3C - Check the convergence criteria: The convergence criteria (7.76) is checked. If the convergence criteria is not satisfied, go back to *Step 3B*. Otherwise, update the upper

bound of the C&CG loop (7.77) and go to *Step 4*.

$$\boldsymbol{r}^{\tau} = max\left[\|\boldsymbol{H}_1^{cc}\hat{\boldsymbol{\pi}}_2^{\tau} + \boldsymbol{H}_2^{cc}\boldsymbol{\pi}_7^{\tau}\|_{\infty} + \left\|\boldsymbol{\pi'}_{11}^{\tau} - \boldsymbol{\pi}_{11}^{\tau}\right\|_{\infty} \right] \leq \varepsilon_2 \tag{7.76}$$

$$UB = min\{UB, \boldsymbol{L_1}^{*(k+1)} + \boldsymbol{L_2}^{*(k+1)}\} \tag{7.77}$$

7) Step 4 - Check the convergence criterion of C&CG algorithm: If $UB - LB \geq \varepsilon_1$, then go to *Step 5*, otherwise terminate the algorithm.

8) Step 5 - Generate columns and constraints: Add constraints (7.30)-(7.39) to the master problem and go to *Step 2*.

Algorithm 2 The proposed algorithm

initialization the C&CG loop: $k = 0$, $\varepsilon \leq 10^{-3}$, $LB = -\infty$ and $UB = \infty$.
while $UB - LB \geq \varepsilon_1$ **do**
  Solve master problem (7.28)-(7.39).
  Update the LB using (7.40).
  initialization the ADMM loop: ε_2, λ_1, λ_2, τ and α.
  while $\boldsymbol{r}^{\tau} \geq \varepsilon_2$ **do**
    Solve subproblem given in (7.69)-(7.71).
    update the parameters $\boldsymbol{\pi}_2$ and $\boldsymbol{\pi}_{11}$ using (7.64)
    Solve subproblem given in (7.73)-(7.75).
    update the parameters $\boldsymbol{\pi}_7$ and $\boldsymbol{\pi}'_{11}$ using (7.65)
    update the $\boldsymbol{\lambda}_1$ and $\boldsymbol{\lambda}_2$ using (7.66)-(7.67)
  end while
  Update the UB as given in (7.77).
  Generate column and constraints (7.30)-(7.39) and set $k = k + 1$.
end while

7.3 Numerical Results

The simulation are conducted on a a PC with 2.60 GHZ Core-i7 CPU and 16.0 GB memory. The problem formulation is modeled in Python/Pyomo and Gurobi solver is used

to solve the MISOCP problem.

7.3.1 Characteristics of the test system

The modified IEEE 34-bus unbalanced distribution network is considered as a test case. Two single-phase microgrids, MG1 and MG2 are connected to the phase A of the distribution network through tie-lines on buses 12 and 26 as shown in the Fig. 7.1, respectively.Three-phase and single-phase loads are connected to the network, where the maximum real and reactive forecasted demands on phase A, phase B, and phase C are (606 kW, 357 $kVar$), (584 kW, 344 $kVAr$), and (579 kW, 343 $kVar$), respectively. Three 3-phase PV generation units with maximum forecasted output power of 126.92 kW are considered. The peak real and reactive demand of MG1 is 420 kW and 200 $kVar$, respectively. MG1 includes two single-phase PV units each with maximum forecasted generation of 42.3 kW, and two distributed generation units. The peak real and reactive demand of MG2 is 180 kW and 90 $kVar$, respectively. MG2 includes two single-phase PV units each with maximum forecasted generation of 42.3 kW and two distributed generation units. The characteristics of the dispatchable DG units and solar PV generation units for the distribution network and microgrids are given in Table 7.1 and Table 7.2, respectively. The marginal costs of the DGs for each segment in the linearized cost curve are given in Table 7.3. The operation cost of all DGs in MGs and distribution network are considered to be the same. The hourly electricity price is considered as the marginal cost of the distribution feeder to provide power in the day-ahead operation of the distribution network. In Fig 7.1, the switchable lines are shown as red dashed lines. The lower and upper bounds of the polyhedral uncertainty sets are considered to be [0.9, 1.1] of the maximum forecasted values for the solar PV generation and demand. The initial values for $\boldsymbol{\lambda}_1$ and $\boldsymbol{\lambda}_2$ are 1.4 and the initial value for $\boldsymbol{\alpha}$ is 0.9.

7.3.2 Performance of Proposed Optimization Framework

The error tolerance $\boldsymbol{\varepsilon}_2$ for the ADMM is 10^{-3} and error tolerance $\boldsymbol{\varepsilon}_1$ for the C&CG algorithm is 10^{-1}. Here, the C&CG algorithm is converged after 3 iteration, while ADMM algorithm convergence in the subproblem is highly depends on the parameters' initialization. Here, the ADMM algorithm in the subproblem is converged in 63 iteration. The residuals

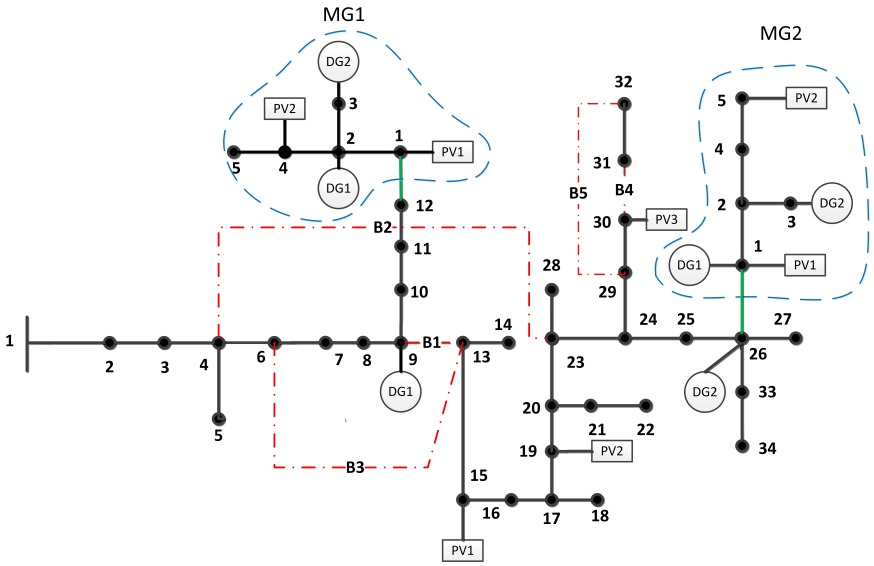

Figure 7.1: Schematic of modified IEEE 34-bus distribution network with two microgrids

Table 7.1: Characteristics of the dispatchable DG units in the DS, MG1 and MG2

System	DG	Bus	$P^{max}[kW]$	$Q^{min}[kVar]$	$Q^{max}[kVar]$
DS	1	9	500	-250	250
	2	26	400	-200	200
MG1	1	2	450	-225	225
	2	3	350	-170	170
MG2	1	1	300	-150	150
	2	3	150	-70	70

Table 7.2: Characteristics of solar PV units in the DS, MG1 and MG2

System	PV	Bus	$P^{max}[kW]$	$Q^{min}[kVar]$	$Q^{max}[kVar]$
DS	1	15	130	-65	65
	2	19	130	-65	65
	3	30	130	-65	65
MG1	1	1	45	-20	20
	2	4	45	-20	20
MG2	1	1	45	-20	20
	2	5	45	-20	20

Table 7.3: The marginal cost of each segment for DGs ($/kWh)

DG	C_i^1	C_i^2	C_i^3	C_i^4
1	0.18	0.22	0.26	0.30
2	0.17	0.23	0.28	0.36

calculated in (7.76) are shown in Fig. 7.2 for the last iteration of C&CG algorithm. The switching status of the switchable branches in the distribution network is shown in Table 7.4. The switching capability decreases the total power loss and improves the voltage profile in the distribution system. However, ignoring the switching capability will reduce the computation time and the C&CG algorithm is converged in two iterations. Without the switching capability, the total power loss on phase A, phase B and phase C in distribution network are 342.45 kW, 224.36 kW, 230.17 kW respectively. Considering the switching capability will reduce the distribution network loss to 339.03 kW, 218.60 kW, 225.28 kW on phase A, phase B and phase C, respectively. Fig. 7.3 shows the dispatch of the feeder, DG and solar PVs generation units and interconnected tie-lines between MG1 and MG2 with the distribution network on phase A. The power exchanged between microgrids and distribution feeder reduces the operation cost and improves the voltage profile in the distribution network. As shown in Fig. 7.3, at hours 2, 3, 4, 5, 18, 19, 20 and 21 the MGs delivering power to the distribution network and for the rest of the hours the distribution network supplies part of the load of the microgrids. Fig. 7.4 and Fig. 7.5 illustrate the dispatch of feeder, DG and solar PV generation units on phases B and C respectively. In Fig. 7.5, on phase B, at hour 18, the hourly price of the electricity at the feeder in \$0.27/kWh, the marginal costs of DG1 and DG2 in the distribution network are \$0.26/kWh \$0.28/kWh respectively. Therefore, DG1 generates more power (i.e. 258.64 kW), compare to DG2 (i.e. 81.07 kW) and feeder (i.e. 174.37 kW). Similarly, in Fig. 7.6, on phase C, at hour 18, DG1 generates more power compared to DG2 and the feeder. Furthermore, the MGs are single-phase and connected to phase A, therefore there are no power exchange between phase B and phase C of the distribution network with MG1 and MG2. With switching capability, the total operation cost of whole network (distribution system and MGs) is \$6236.31, however, the total operation cost of the network without the switching capability will increase to \$6237.09.

7.3.3 Operation of Microgrids in Island Mode

In this section the performance of the proposed optimization approach is compared with the case in which the microgrids are operating in island mode. The total operation cost in this

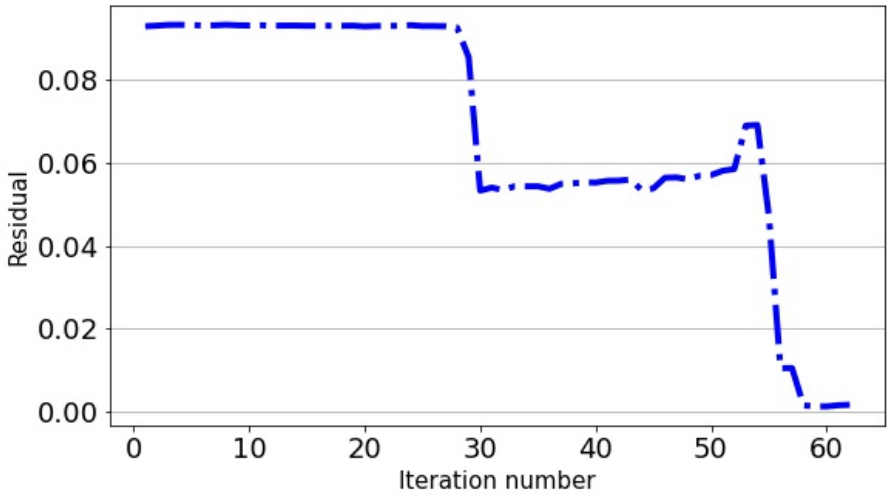

Figure 7.2: The ADMM convergence criteria

Table 7.4: The status of switchable branches

Switchable branch	Hours (24 hours)
B1	1 1 1 1 0 1 1 1 1 1 1 1 1 1 1 1 1 1 1 1 0 1 1
B2	0 0 0 0 1 0 0 0 0 0 0 0 0 0 0 0 0 0 0 0 0 0 0
B3	0 0 0 0 0 0 0 0 0 0 0 0 0 0 0 0 0 0 0 0 0 1 0 0
B4	0 0 0 0 0 0 0 0 0 0 0 0 0 0 0 0 0 0 0 0 0 0 0 0
B5	1 1 1 1 1 1 1 1 1 1 1 1 1 1 1 1 1 1 1 1 1 1 1

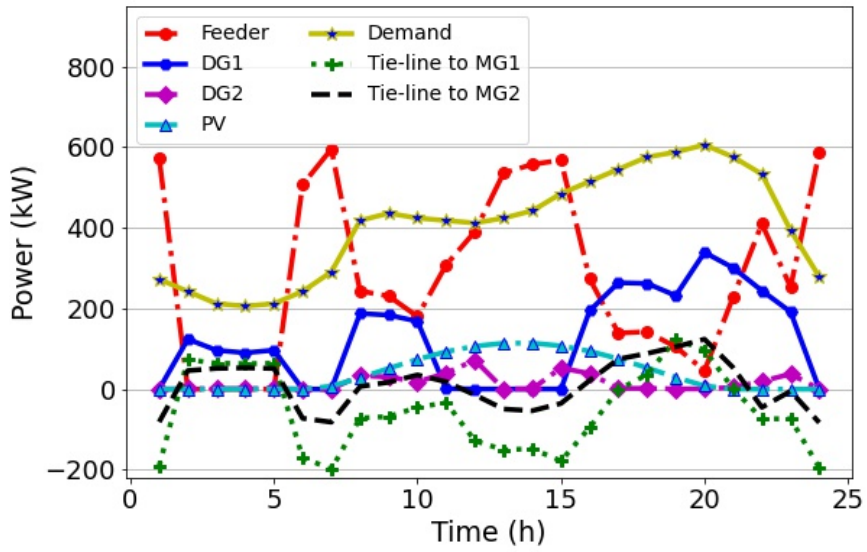

Figure 7.3: The power dispatch of feeder, DGs, PVs, Tie-lines and demand on phase A.

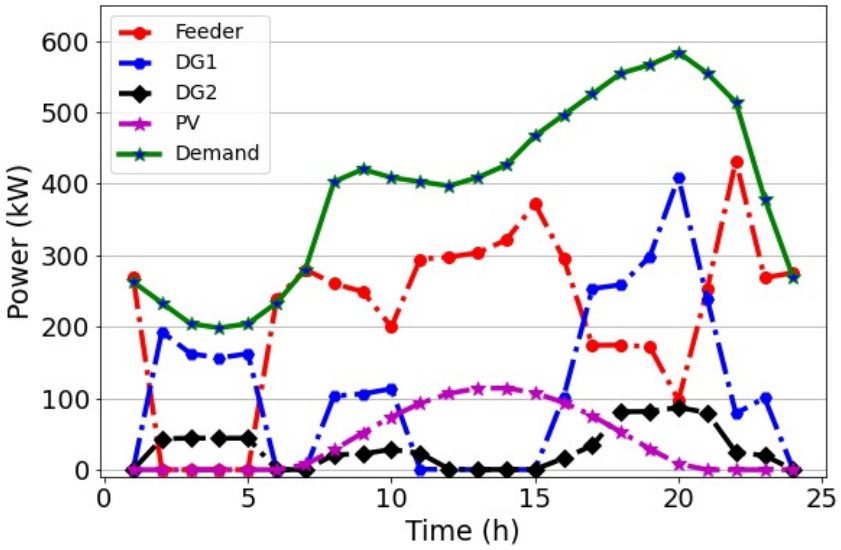

Figure 7.4: The power dispatch of feeder, DGs, PVs and demand on phase B.

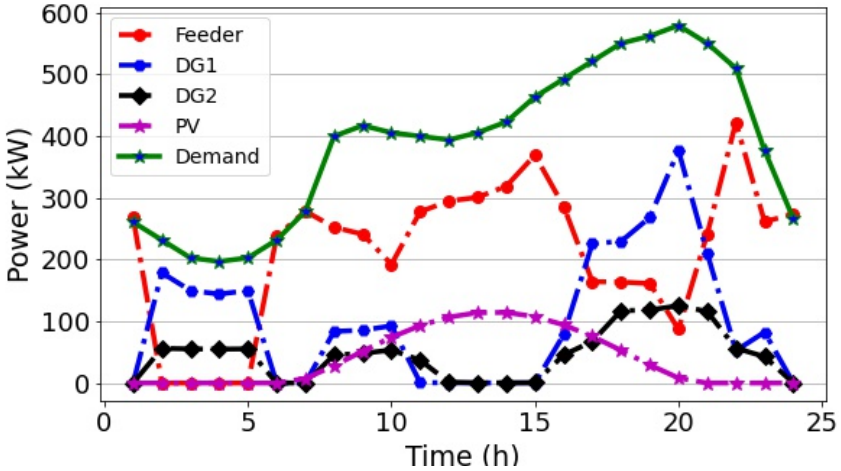

Figure 7.5: The power dispatch of feeder, DGs, PVs and demand on phase C.

case is increased to \$6338.22 which is more than the total operation cost in grid-connected operating mode of MGs (i.e. \$6236.31). Fig. 7.6 shows the voltage profile in the distribution network, at hour 19 in the island operation of MGs with switching and the grid-connected mode with and without switching capability in the distribution network. With switching capability, the voltage deviation from the nominal voltage 1.0 p.u., in the grid-connected operation mode is lower compare to the islanded operation mode. Furthermore the voltage deviation from the nominal voltage with switching capability is lower compare to the case ignoring the switching capability. The voltage profile for the rest of the operation horizon have similar pattern.

Fig. 7.7 shows the DGs and PV dispatch in MG1 and MG2 in islanding and grid-connected operating modes. At hour 7 while MG1 and MG2 are connected to the grid, the dispatch of DGs are zero because the electricity price of the feeder (i.e \$0.13) is less than the marginal cost of the DGs. Therefore the demand in MG1 is supplied by the distribution network as shown in Fig 7.3. In this figure, the negative value of the power flow on tie-lines means the direction of the power is from the distribution network to the microgrids. However in the islanding operation mode, the demand in the microgrids are supplied by the DGs and PVs (i.e. the dispatch of DG1 at hour 7 in grid-connected mode is 87.22 kW and dispatch of the DG2 is 109.62 kW) which results in higher total operation cost.

7.4 Conclusion

This chapter presents an adaptive robust distributed optimization framework for the operation of the unbalanced distribution network with interconnected microgrids. The problem is formulated as a multi-stage optimization problem where, the network topology is determined in the first stage and the operation costs of the MGs and distribution network are minimized considering the worst-case realization of the uncertain variables in the second stage. The second-stage problem is solved in a distributed fashion using the ADMM algorithm. The first stage and second stage problems are formulated as MISOCP problems. The presented solution algorithms are applied to a modified IEEE 34-bus unbalanced distribution network with two single-phase interconnected MGs. The performance and the results are evaluated in the grid-connected and island operation modes of the MGs. It shown that the

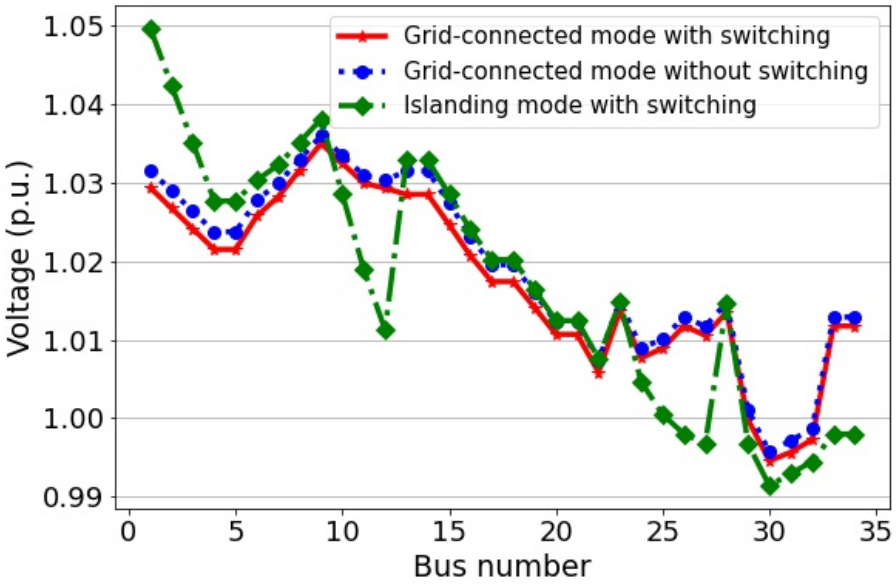

Figure 7.6: The voltage profile of the distribution network on phase A, in grid connected mode with and without switching capability and in islanding operation mode with switching capability at hour 19.

total operation cost is decreased and the voltage profile is improved in the grid-connected operating mode of MGs. Furthermore, the switching capability of distribution network improves the voltage profile, network loss and operation cost of the distribution network.

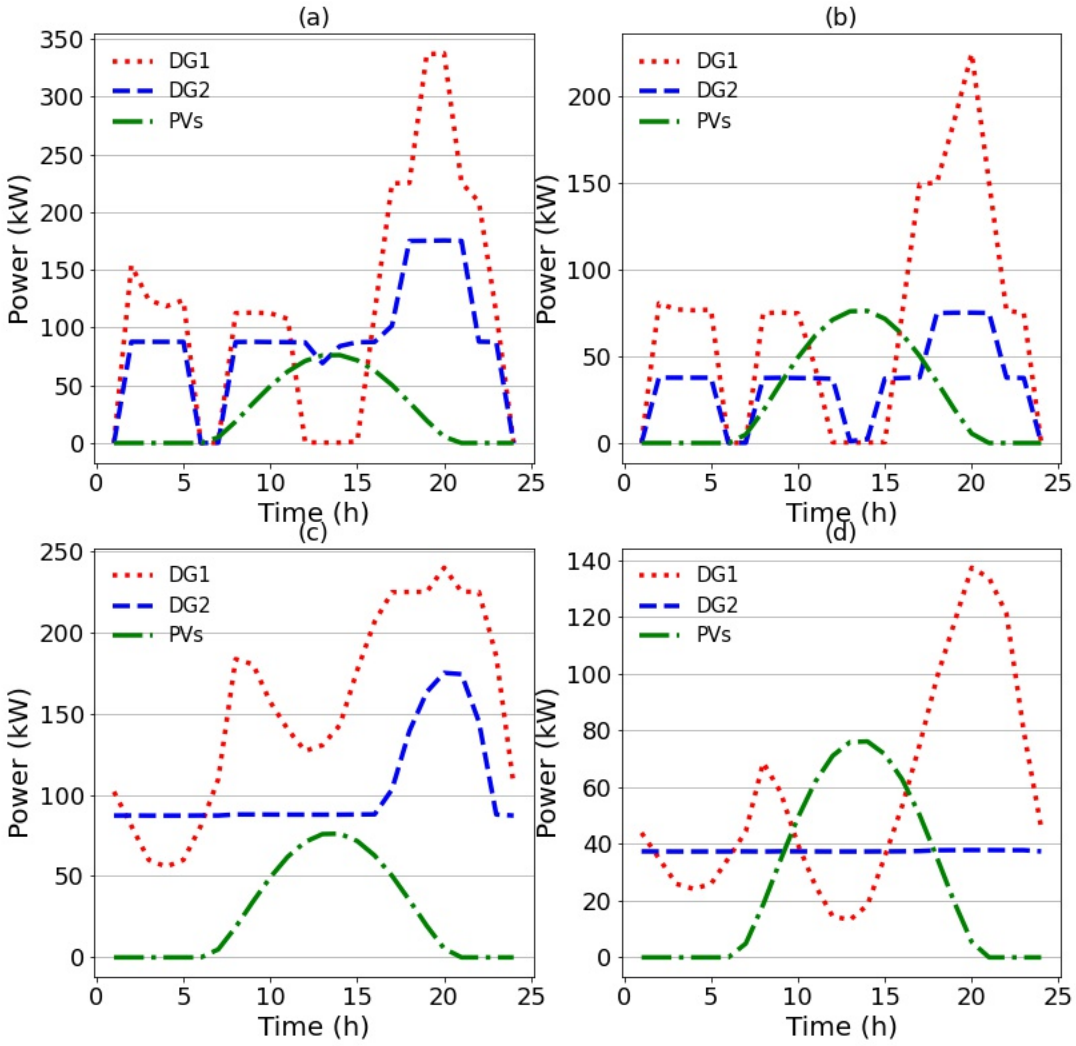

Figure 7.7: The power dispatch of DGs and PVs in microgrids in islanding and grid-connected mode. (a) MG1 in grid-connected mode (b) MG2 in grid-connected mode (c) MG1 in islanding mode (d) MG2 in islanding mode

BIBLIOGRAPHY

[1] IRENA, "Future of solar photovoltaic: Deployment, investment, technology, grid integration and socio-economic aspects (a global energy transformation: paper)„" Abu Dhabi, Tech. Rep., 2019. 1

[2] W. Warwick, T. Hardy, M. Hoffman, and J. Homer, "Electricity distribution system baseline report," *Pacific Northwest National Laboratory, Tech Rep PNNL*, vol. 25178, 2016. 1

[3] U. S., EIA, "Annual energy outlook 2019 with projections to 2050," 2019. 1

[4] "Global EV Outlook 2019," https://www.iea.org/reports/global-ev-outlook-2019, 2019. 1

[5] R. Torquato, D. Salles, C. O. Pereira, P. C. M. Meira, and W. Freitas, "A comprehensive assessment of pv hosting capacity on low-voltage distribution systems," *IEEE Transactions on Power Delivery*, vol. 33, no. 2, pp. 1002–1012, 2018. 3

[6] D. Zhu, A. K. Jain, R. Broadwater, and F. Bruna, "Feeder voltage profile design for energy conservation and pv hosting capacity enhancement," *Electric Power Systems Research*, vol. 164, pp. 263–271, 2018. 3

[7] F. Ding and B. Mather, "On distributed pv hosting capacity estimation, sensitivity study, and improvement," *IEEE Transactions on Sustainable Energy*, vol. 8, no. 3, pp. 1010–1020, 2016. 3

[8] D. Chathurangi, U. Jayatunga, S. Perera, A. Agalgaonkar, and T. Siyambalapitiya, "A nomographic tool to assess solar pv hosting capacity constrained by voltage rise in low-voltage distribution networks," *International Journal of Electrical Power & Energy Systems*, vol. 134, p. 107409, 2022. 3

[9] S. Hashemi and J. Østergaard, "Efficient control of energy storage for increasing the pv hosting capacity of lv grids," *IEEE Transactions on Smart Grid*, vol. 9, no. 3, pp. 2295–2303, 2016. 3

[10] S. Hashemi, J. Østergaard, T. Degner, R. Brandl, and W. Heckmann, "Efficient control of active transformers for increasing the pv hosting capacity of lv grids," *IEEE Transactions on Industrial Informatics*, vol. 13, no. 1, pp. 270–277, 2016. 3

[11] A. Dubey and S. Santoso, "On estimation and sensitivity analysis of distribution circuit's photovoltaic hosting capacity," *IEEE Transactions on Power Systems*, vol. 32, no. 4, pp. 2779–2789, 2016. 3

[12] X. Xu, J. Li, Z. Xu, J. Zhao, and C. S. Lai, "Enhancing photovoltaic hosting capacity—a stochastic approach to optimal planning of static var compensator devices in distribution networks," *Applied energy*, vol. 238, pp. 952–962, 2019. 3

[13] M. Alanazi, M. Mahoor, and A. Khodaei, "Co-optimization generation and transmission planning for maximizing large-scale solar pv integration," *International Journal of Electrical Power & Energy Systems*, vol. 118, p. 105723, 2020. 3

[14] A. Ali, K. Mahmoud, and M. Lehtonen, "Maximizing hosting capacity of uncertain photovoltaics by coordinated management of oltc, var sources and stochastic evs," *International Journal of Electrical Power & Energy Systems*, vol. 127, p. 106627, 2021. 3

[15] T. Niknam, M. Zare, and J. Aghaei, "Scenario-based multiobjective volt/var control in distribution networks including renewable energy sources," *IEEE Transactions on Power Delivery*, vol. 27, no. 4, pp. 2004–2019, 2012. 3

[16] Z. Wang, B. Chen, J. Wang, J. Kim, and M. M. Begovic, "Robust optimization based optimal dg placement in microgrids," *IEEE Transactions on Smart Grid*, vol. 5, no. 5, pp. 2173–2182, 2014. 4

[17] R. Seguin, J. Woyak, D. Costyk, J. Hambrick, and B. Mather, "High-penetration pv integration handbook for distribution engineers," National Renewable Energy Lab.(NREL), Golden, CO (United States), Tech. Rep., 2016. 4

[18] L. Bird, J. Cochran, and X. Wang, "Wind and solar energy curtailment: Experience and practices in the united states," National Renewable Energy Lab.(NREL), Golden, CO (United States), Tech. Rep., 2014. 4

[19] A. Mills, "Understanding variability and uncertainty of photovoltaics for integration with the electric power system," 2009. 4

[20] T. Ding, C. Li, Y. Yang, J. Jiang, Z. Bie, and F. Blaabjerg, "A two-stage robust optimization for centralized-optimal dispatch of photovoltaic inverters in active distribution networks," *IEEE Transactions on Sustainable Energy*, vol. 8, no. 2, pp. 744–754, 2016. 4

[21] Y. P. Agalgaonkar, B. C. Pal, and R. A. Jabr, "Stochastic distribution system operation considering voltage regulation risks in the presence of pv generation," *IEEE Transactions on Sustainable Energy*, vol. 6, no. 4, pp. 1315–1324, 2015. 4

[22] K. Coogan, M. J. Reno, S. Grijalva, and R. J. Broderick, "Locational dependence of pv hosting capacity correlated with feeder load," in *2014 IEEE PES T&D Conference and Exposition*, 2014, pp. 1–5. 4

[23] A. Navarro-Espinosa and L. F. Ochoa, "Increasing the pv hosting capacity of lv networks: Oltc-fitted transformers vs. reinforcements," in *2015 IEEE Power Energy Society Innovative Smart Grid Technologies Conference (ISGT)*, 2015, pp. 1–5. 4

[24] S. Sakar, M. E. Balci, S. H. A. Aleem, and A. F. Zobaa, "Increasing pv hosting capacity in distorted distribution systems using passive harmonic filtering," *Electric Power Systems Research*, vol. 148, pp. 74–86, 2017. 4

[25] S. Lakshmi and S. Ganguly, "Modelling and allocation planning of voltage-sourced converters to improve the rooftop pv hosting capacity and energy efficiency of distribution networks," *IET Generation, Transmission & Distribution*, vol. 12, no. 20, pp. 4462–4471, 2018. 4

[26] R. Mahroo-Bakhtiari, M. Izadi, A. Safdarian, and M. Lehtonen, "Distributed load management scheme to increase pv hosting capacity in lv feeders," *IET Renewable Power Generation*, vol. 14, no. 1, pp. 125–133, 2019. 4

[27] J. F. Sousa, C. L. Borges, and J. Mitra, "Pv hosting capacity of lv distribution networks using smart inverters and storage systems: a practical margin," *IET Renewable Power Generation*, vol. 14, no. 8, pp. 1332–1339, 2020. 5

[28] S. Wang, Y. Dong, L. Wu, and B. Yan, "Interval overvoltage risk based pv hosting capacity evaluation considering pv and load uncertainties," *IEEE Transactions on Smart Grid*, vol. 11, no. 3, pp. 2709–2721, 2020. 5

[29] J. Zhao, J. Wang, Z. Xu, C. Wang, C. Wan, and C. Chen, "Distribution network electric vehicle hosting capacity maximization: A chargeable region optimization model," *IEEE Transactions on Power Systems*, vol. 32, no. 5, pp. 4119–4130, 2017. 5

[30] O. Hafez and K. Bhattacharya, "Integrating ev charging stations as smart loads for demand response provisions in distribution systems," *IEEE Transactions on Smart Grid*, vol. 9, no. 2, pp. 1096–1106, 2016. 5

[31] P. Papadopoulos, S. Skarvelis-Kazakos, I. Grau, L. M. Cipcigan, and N. Jenkins, "Predicting electric vehicle impacts on residential distribution networks with distributed generation," in *2010 IEEE Vehicle Power and Propulsion Conference*. IEEE, 2010, pp. 1–5. 5

[32] M. H. Amini, M. P. Moghaddam, and O. Karabasoglu, "Simultaneous allocation of electric vehicles' parking lots and distributed renewable resources in smart power distribution networks," *Sustainable cities and society*, vol. 28, pp. 332–342, 2017. 5

[33] L. Hua, J. Wang, and C. Zhou, "Adaptive electric vehicle charging coordination on distribution network," *IEEE Transactions on Smart Grid*, vol. 5, no. 6, pp. 2666–2675, 2014. 5

[34] A. Chaouachi, E. Bompard, G. Fulli, M. Masera, M. De Gennaro, and E. Paffumi, "Assessment framework for ev and pv synergies in emerging distribution systems," *Renewable and Sustainable Energy Reviews*, vol. 55, pp. 719–728, 2016. 5

[35] H. Kikusato, Y. Fujimoto, S.-i. Hanada, D. Isogawa, S. Yoshizawa, H. Ohashi, and Y. Hayashi, "Electric vehicle charging management using auction mechanism for

reducing pv curtailment in distribution systems," *IEEE Transactions on Sustainable Energy*, vol. 11, no. 3, pp. 1394–1403, 2019. 5

[36] Y. Guo, J. Xiong, S. Xu, and W. Su, "Two-stage economic operation of microgrid-like electric vehicle parking deck," *IEEE Transactions on Smart Grid*, vol. 7, no. 3, pp. 1703–1712, 2015. 5

[37] K. Mahmud, M. J. Hossain, and G. E. Town, "Peak-load reduction by coordinated response of photovoltaics, battery storage, and electric vehicles," *IEEE Access*, vol. 6, pp. 29 353–29 365, 2018. 5, 6

[38] Z. Akhtar, M. Opatovsky, B. Chaudhuri, and S. Y. R. Hui, "Comparison of point-of-load versus mid-feeder compensation in lv distribution networks with high penetration of solar photovoltaic generation and electric vehicle charging stations," *IET Smart Grid*, vol. 2, no. 2, pp. 283–292, 2019. 5, 6

[39] S. Weckx and J. Driesen, "Load balancing with ev chargers and pv inverters in unbalanced distribution grids," *IEEE transactions on Sustainable Energy*, vol. 6, no. 2, pp. 635–643, 2015. 5, 6

[40] C. Sabillon, J. F. Franco, M. J. Rider, and R. Romero, "Joint optimal operation of photovoltaic units and electric vehicles in residential networks with storage systems: A dynamic scheduling method," *International Journal of Electrical Power & Energy Systems*, vol. 103, pp. 136–145, 2018. 5, 6

[41] M. R. Islam, H. Lu, G. Fang, L. Li, and M. J. Hossain, "Optimal dispatch of electrical vehicle and pv power to improve the power quality of an unbalanced distribution grid," in *2019 International Conference on High Performance Big Data and Intelligent Systems (HPBD&IS)*. IEEE, 2019, pp. 258–263. 5, 6

[42] R. Fachrizal, U. H. Ramadhani, J. Munkhammar, and J. Widén, "Combined pv–ev hosting capacity assessment for a residential lv distribution grid with smart ev charging and pv curtailment," *Sustainable Energy, Grids and Networks*, vol. 26, p. 100445, 2021. 6

[43] J. Zhao, T. Zheng, and E. Litvinov, "Variable resource dispatch through do-not-exceed limit," *IEEE Transactions on Power Systems*, vol. 30, no. 2, pp. 820–828, 2014. 6

[44] Z. Li, F. Qiu, and J. Wang, "Data-driven real-time power dispatch for maximizing variable renewable generation," *Applied energy*, vol. 170, pp. 304–313, 2016. 6

[45] ——, "Multi-period do-not-exceed limit for variable renewable generation dispatch considering discrete recourse controls," *arXiv preprint arXiv:1608.05273*, 2016. 6

[46] IEA, "Global ev outlook 2021: Accelerating ambitions despite pandemic," 2021. 7

[47] U. EIA, "Annual energy outlook 2020: with projections to 2050," 2020. 7

[48] M. S. Kumar and S. T. Revankar, "Development scheme and key technology of an electric vehicle: An overview," *Renewable and Sustainable Energy Reviews*, vol. 70, pp. 1266–1285, 2017. 7

[49] A. Dubey and S. Santoso, "Electric vehicle charging on residential distribution systems: Impacts and mitigations," *IEEE Access*, vol. 3, pp. 1871–1893, 2015. 7

[50] N. B. Arias, S. Hashemi, P. B. Andersen, C. Træholt, and R. Romero, "Distribution system services provided by electric vehicles: recent status, challenges, and future prospects," *IEEE Transactions on Intelligent Transportation Systems*, 2019. 7

[51] K. Clement-Nyns, E. Haesen, and J. Driesen, "The impact of charging plug-in hybrid electric vehicles on a residential distribution grid," *IEEE Transactions on power systems*, vol. 25, no. 1, pp. 371–380, 2009. 7

[52] Z. Ma, N. Yang, S. Zou, and Y. Shao, "Charging coordination of plug-in electric vehicles in distribution networks with capacity constrained feeder lines," *IEEE Transactions on Control Systems Technology*, vol. 26, no. 5, pp. 1917–1924, 2017. 7

[53] E. Akhavan-Rezai, M. F. Shaaban, E. F. El-Saadany, and F. Karray, "Managing demand for plug-in electric vehicles in unbalanced lv systems with photovoltaics," *IEEE Transactions on Industrial Informatics*, vol. 13, no. 3, pp. 1057–1067, 2017. 7

[54] H. Lu, J. Hossain, M. R. Islam, and L. Li, "Multiobjective optimization technique for mitigating unbalance and improving voltage considering higher penetration of electric vehicles and distributed generation," *IEEE Systems Journal*, 2020. 7

[55] K. Chaudhari, A. Ukil, K. N. Kumar, U. Manandhar, and S. K. Kollimalla, "Hybrid optimization for economic deployment of ess in pv-integrated ev charging stations," *IEEE Transactions on Industrial Informatics*, vol. 14, no. 1, pp. 106–116, 2017. 8

[56] S. Faridimehr, S. Venkatachalam, and R. B. Chinnam, "A stochastic programming approach for electric vehicle charging network design," *IEEE Transactions on Intelligent Transportation Systems*, vol. 20, no. 5, pp. 1870–1882, 2018. 8

[57] B. Zhang, Q. Yan, and M. Kezunovic, "Placement of ev charging stations integrated with pv generation and battery storage," in *2017 Twelfth International Conference on Ecological Vehicles and Renewable Energies (EVER)*. IEEE, 2017, pp. 1–7. 8

[58] Y.-T. Liao and C.-N. Lu, "Dispatch of ev charging station energy resources for sustainable mobility," *IEEE Transactions on Transportation Electrification*, vol. 1, no. 1, pp. 86–93, 2015. 8

[59] X. Bai and W. Qiao, "Robust optimization for bidirectional dispatch coordination of large-scale v2g," *IEEE Transactions on Smart Grid*, vol. 6, no. 4, pp. 1944–1954, 2015. 8

[60] S. Pirouzi, J. Aghaei, M. A. Latify, G. R. Yousefi, and G. Mokryani, "A robust optimization approach for active and reactive power management in smart distribution networks using electric vehicles," *IEEE Systems Journal*, vol. 12, no. 3, pp. 2699–2710, 2017. 8

[61] S. Minniti, A. Haque, N. Paterakis, and P. Nguyen, "A hybrid robust-stochastic approach for the day-ahead scheduling of an ev aggregator," in *2019 IEEE Milan PowerTech*. IEEE, 2019, pp. 1–6. 9

[62] A. Akbari-Dibavar, K. Zare, and S. Nojavan, "A hybrid stochastic-robust optimization approach for energy storage arbitrage in day-ahead and real-time markets," *Sustainable Cities and Society*, vol. 49, p. 101600, 2019. 9

[63] A. Bagheri, J. Wang, and C. Zhao, "Data-driven stochastic transmission expansion planning," *IEEE Transactions on Power Systems*, vol. 32, no. 5, pp. 3461–3470, 2016. 9

[64] C. Zhao and Y. Guan, "Data-driven stochastic unit commitment for integrating wind generation," *IEEE Transactions on Power Systems*, vol. 31, no. 4, pp. 2587–2596, 2015. 9

[65] R. Zhu, H. Wei, and X. Bai, "Wasserstein metric based distributionally robust approximate framework for unit commitment," *IEEE Transactions on Power Systems*, vol. 34, no. 4, pp. 2991–3001, 2019. 9, 88, 121

[66] R. Xie, W. Wei, M. E. Khodayar, J. Wang, and S. Mei, "Planning fully renewable powered charging stations on highways: A data-driven robust optimization approach," *IEEE transactions on transportation electrification*, vol. 4, no. 3, pp. 817–830, 2018. 9

[67] Z. Zhongming, L. Linong, Y. Xiaona, Z. Wangqiang, L. Wei *et al.*, "Solar generation was 3% of us electricity in 2020, but we project it will be 20% by 2050," 2021. 10

[68] P. Gagnon, R. Margolis, J. Melius, C. Phillips, and R. Elmore, "Rooftop solar photovoltaic technical potential in the united states. a detailed assessment," National Renewable Energy Lab.(NREL), Golden, CO (United States), Tech. Rep., 2016. 10

[69] F. Rahimi and S. Mokhtari, "A new distribution system operator construct," *Open Access Technology International (OATI). Available online: https://www. gridwiseac. org/pdfs/workshop_091014/a_new_ dist_sys_optr_construct_paper. pdf (accessed on 12 October 2018)*, 2014. 10

[70] J. Wang, J. Wang, C. Liu, and J. P. Ruiz, "Stochastic unit commitment with sub-hourly dispatch constraints," *Applied energy*, vol. 105, pp. 418–422, 2013. 10

[71] A. Nikoobakht, J. Aghaei, M. Shafie-Khah, and J. P. Catalão, "Minimizing wind power curtailment using a continuous-time risk-based model of generating units and bulk energy storage," *IEEE Transactions on Smart Grid*, vol. 11, no. 6, pp. 4833–4846, 2020. 10, 11

[72] Y. Yang, J. Wang, X. Guan, and Q. Zhai, "Subhourly unit commitment with feasible energy delivery constraints," *Applied energy*, vol. 96, pp. 245–252, 2012. 10

[73] M. Parvania and A. Scaglione, "Unit commitment with continuous-time generation and ramping trajectory models," *IEEE Transactions on Power Systems*, vol. 31, no. 4, pp. 3169–3178, 2015. 10

[74] A. Nikoobakht, J. Aghaei, M. Shafie-Khah, and J. P. Catalão, "Continuous-time co-operation of integrated electricity and natural gas systems with responsive demands under wind power generation uncertainty," *IEEE Transactions on Smart Grid*, vol. 11, no. 4, pp. 3156–3170, 2020. 11

[75] B. Zhou, J. Fang, X. Ai, W. Yao, and J. Wen, "Flexibility-enhanced continuous-time scheduling of power system under wind uncertainties," *IEEE Transactions on Sustainable Energy*, vol. 12, no. 4, pp. 2306–2320, 2021. 11

[76] C. Lowery and M. O'Malley, "Impact of wind forecast error statistics upon unit commitment," *IEEE Transactions on Sustainable Energy*, vol. 3, no. 4, pp. 760–768, 2012. 11

[77] H. Zou, S. Mao, Y. Wang, F. Zhang, X. Chen, and L. Cheng, "A survey of energy management in interconnected multi-microgrids," *IEEE Access*, vol. 7, pp. 72 158–72 169, 2019. 11

[78] L. Che, X. Zhang, M. Shahidehpour, A. Alabdulwahab, and A. Abusorrah, "Optimal interconnection planning of community microgrids with renewable energy sources," *IEEE Transactions on Smart Grid*, vol. 8, no. 3, pp. 1054–1063, 2015. 11

[79] Z. Wang, B. Chen, J. Wang, M. M. Begovic, and C. Chen, "Coordinated energy management of networked microgrids in distribution systems," *IEEE Transactions on Smart Grid*, vol. 6, no. 1, pp. 45–53, 2014. 11

[80] J. Wang and X. Lu, "Sustainable and resilient distribution systems with networked microgrids [point of view]," *Proceedings of the IEEE*, vol. 108, no. 2, pp. 238–241, 2020. 11

[81] H. Ji, C. Wang, P. Li, F. Ding, and J. Wu, "Robust operation of soft open points in active distribution networks with high penetration of photovoltaic integration," *IEEE Transactions on Sustainable Energy*, vol. 10, no. 1, pp. 280–289, 2018. 12

[82] B. Zhang, Q. Li, L. Wang, and W. Feng, "Robust optimization for energy transactions in multi-microgrids under uncertainty," *Applied Energy*, vol. 217, pp. 346–360, 2018. 12

[83] S. Lu, W. Gu, S. Zhou, S. Yao, and G. Pan, "Adaptive robust dispatch of integrated energy system considering uncertainties of electricity and outdoor temperature," *IEEE Transactions on Industrial Informatics*, vol. 16, no. 7, pp. 4691–4702, 2019. 12

[84] S. Wang, H. Gangammanavar, S. D. Ekşioğlu, and S. J. Mason, "Stochastic optimization for energy management in power systems with multiple microgrids," *IEEE Transactions on Smart Grid*, vol. 10, no. 1, pp. 1068–1079, 2017. 12, 13

[85] P. P. Vergara, J. C. López, M. J. Rider, H. R. Shaker, L. C. da Silva, and B. N. Jørgensen, "A stochastic programming model for the optimal operation of unbalanced three-phase islanded microgrids," *International Journal of Electrical Power & Energy Systems*, vol. 115, p. 105446, 2020. 12

[86] B. Zeng and L. Zhao, "Solving two-stage robust optimization problems using a column-and-constraint generation method," *Operations Research Letters*, vol. 41, no. 5, pp. 457–461, 2013. 12, 19, 69

[87] C. Zhang, Y. Xu, Z. Y. Dong, and R. Zhang, "Multi-objective adaptive robust voltage/var control for high-pv penetrated distribution networks," *IEEE Transactions on Smart Grid*, vol. 11, no. 6, pp. 5288–5300, 2020. 12

[88] D. K. Molzahn, F. Dörfler, H. Sandberg, S. H. Low, S. Chakrabarti, R. Baldick, and J. Lavaei, "A survey of distributed optimization and control algorithms for electric power systems," *IEEE Transactions on Smart Grid*, vol. 8, no. 6, pp. 2941–2962, 2017. 13

[89] W. Zheng, W. Wu, B. Zhang, H. Sun, and Y. Liu, "A fully distributed reactive power optimization and control method for active distribution networks," *IEEE Transactions on Smart Grid*, vol. 7, no. 2, pp. 1021–1033, 2015. 13

[90] A. Rajaei, S. Fattaheian-Dehkordi, M. Fotuhi-Firuzabad, and M. Moeini-Aghtaie, "Decentralized transactive energy management of multi-microgrid distribution systems based on admm," *International Journal of Electrical Power & Energy Systems*, vol. 132, p. 107126, 2021. 13

[91] N. Nikmehr, "Distributed robust operational optimization of networked microgrids embedded interconnected energy hubs," *Energy*, vol. 199, p. 117440, 2020. 13

[92] L. Gan, N. Li, U. Topcu, and S. H. Low, "Exact convex relaxation of optimal power flow in radial networks," *IEEE Transactions on Automatic Control*, vol. 60, no. 1, pp. 72–87, 2014. 13

[93] Y. Chen, Y. Li, J. Xiang, and X. Shen, "An optimal power flow formulation with socp relaxation in radial network," in *2018 IEEE 14th International Conference on Control and Automation (ICCA)*. IEEE, 2018, pp. 921–926. 13

[94] B. Kocuk, S. S. Dey, and X. A. Sun, "Strong socp relaxations for the optimal power flow problem," *Operations Research*, vol. 64, no. 6, pp. 1177–1196, 2016. 13, 14

[95] Q. Li and V. Vittal, "Non-iterative enhanced sdp relaxations for optimal scheduling of distributed energy storage in distribution systems," *IEEE Transactions on Power Systems*, vol. 32, no. 3, pp. 1721–1732, 2016. 13, 14

[96] L. Gan and S. H. Low, "Convex relaxations and linear approximation for optimal power flow in multiphase radial networks," in *2014 Power Systems Computation Conference*. IEEE, 2014, pp. 1–9. 13

[97] X. Chen, W. Wu, and B. Zhang, "Robust restoration method for active distribution networks," *IEEE Transactions on Power Systems*, vol. 31, no. 5, pp. 4005–4015, 2015. 16, 35, 92, 119

[98] M. Feizi and M. Khodayar, "Dispatchability limits for pv generation in unbalanced distribution network with evs," in *IEEE Power and Energy Society General Meeting (PESGM)*. IEEE, 2020, pp. 1–5. 28

[99] B. Chen, C. Chen, J. Wang, and K. L. Butler-Purry, "Sequential service restoration for unbalanced distribution systems and microgrids," *IEEE Transactions on Power Systems*, vol. 33, no. 2, pp. 1507–1520, 2017. 35, 65, 130

[100] J. Luedtke, M. Namazifar, and J. Linderoth, "Some results on the strength of relaxations of multilinear functions," *Mathematical programming*, vol. 136, no. 2, pp. 325–351, 2012. 36, 41, 135

[101] G. Tal, M. A. Nicholas, J. Davies, and J. Woodjack, "Charging behavior impacts on electric vehicle miles traveled: who is not plugging in?" *Transportation Research Record*, vol. 2454, no. 1, pp. 53–60, 2014. 43

[102] S. R. Shukla, S. Paudyal, and M. R. Almassalkhi, "Efficient distribution system optimal power flow with discrete control of load tap changers," *IEEE Transactions on Power Systems*, vol. 34, no. 4, pp. 2970–2979, 2019. 65

[103] H. Ji, C. Wang, P. Li, J. Zhao, G. Song, F. Ding, and J. Wu, "An enhanced socp-based method for feeder load balancing using the multi-terminal soft open point in active distribution networks," *Applied Energy*, vol. 208, pp. 986–995, 2017. 65

[104] Y. Zheng, J. Zhao, Y. Song, F. Luo, K. Meng, J. Qiu, and D. J. Hill, "Optimal operation of battery energy storage system considering distribution system uncertainty," *IEEE Transactions on Sustainable Energy*, vol. 9, no. 3, pp. 1051–1060, 2017. 65

[105] A. Thiele, T. Terry, and M. Epelman, "Robust linear optimization with recourse," *Rapport technique*, pp. 4–37, 2009. 66

[106] A. Mitsos, B. Chachuat, and P. I. Barton, "Mccormick-based relaxations of algorithms," *SIAM Journal on Optimization*, vol. 20, no. 2, pp. 573–601, 2009. 70

[107] (access 10/11/2021) Nrel nsrdb data viewer. [Online]. Available: https://maps.nrel.gov/nsrdb-viewer/ 71

[108] H. Ahmadi and J. R. Martı, "Linear current flow equations with application to distribution systems reconfiguration," *IEEE Transactions on Power Systems*, vol. 30, no. 4, pp. 2073–2080, 2014. 92

[109] C. Kielas-Jensen and V. Cichella, "Bernstein polynomial-based transcription method for solving optimal trajectory generation problems," *arXiv preprint arXiv:2010.09992*, 2020. 119

[110] P. Mohajerin Esfahani and D. Kuhn, "Data-driven distributionally robust optimization using the wasserstein metric: Performance guarantees and tractable reformulations," *Mathematical Programming*, vol. 171, no. 1, pp. 115–166, 2018. 121

[111] M. R. Feizi, M. E. Khodayar, and J. Li, "Data-driven distributionally robust unbalanced operation of distribution networks with high penetration of photovoltaic generation and electric vehicles," *Electric Power Systems Research*, vol. 210, p. 108001, 2022. 130, 131

[112] M. Bazrafshan, N. Gatsis, and E. Dall'Anese, "Placement and sizing of inverter-based renewable systems in multi-phase distribution networks," *IEEE Transactions on Power Systems*, vol. 34, no. 2, pp. 918–930, 2018. 131

[113] G. Muñoz-Delgado, J. Contreras, and J. M. Arroyo, "Multistage generation and network expansion planning in distribution systems considering uncertainty and reliability," *IEEE Transactions on Power Systems*, vol. 31, no. 5, pp. 3715–3728, 2015.

[114] M. R. Feizi, M. Khodayar, and B. Chen, "Feasible dispatch limits of pv generation with uncertain interconnection of evs in the unbalanced distribution network," *IEEE Transactions on Vehicular Technology*, 2021.

[115] M. R. Feizi and M. E. Khodayar, "Dispatchability limits for pv generation in unbalanced distribution networks with evs," in *2020 IEEE Power & Energy Society General Meeting (PESGM)*. IEEE, 2020, pp. 1–5.